MXene-based materials as adsorbents, photocatalysts, membranes and sensors for detection and removal of emerging and gaseous pollutants: A comprehensive review

Mohammad Hadi Dehghani [a,b,*], Nadeem Hussain Solangi [c], Nabisab Mujawar Mubarak [d,e,n,*], Natarajan Rajamohan [f], Subrajit Bosu [f], Amina Othmani [g], Md. Ahmaruzzaman [h], Soumya Ranjan Mishra [h], Baishali Bhattacharjee [h], Vishal Gadore [h], Talib Hussain Banglani [i], Nawab Waris [i], Ali hyder [i], Ayaz Ali Memon [i], Khalid Hussain Thebo [j], Payal Joshi [k], Grzegorz Boczkaj [l,m], Rama Rao Karri [d,*]

[a] Department of Environmental Health Engineering, School of Public Health, Tehran University of Medical Sciences, Tehran, Iran
[b] Center for Solid Waste Research, Institute for Environmental Research, Tehran University of Medical Sciences, Tehran, Iran
[c] State Key Laboratory of Chemical Resource Engineering and College of Chemistry, Beijing University of Chemical Technology, P. Box 98, Beisanhuan East Road 15, Beijing 100029, PR China
[d] Petroleum and Chemical Engineering, Faculty of Engineering, Universiti Teknologi Brunei, Bandar Seri Begawan BE1410, Brunei Darussalam
[e] Department of Chemistry, School of Chemical Engineering and Physical Sciences, Lovely Professional University, Jalandhar, Punjab, India
[f] Chemical Engineering section, Faculty of Engineering, Sohar University, Sohar P C-311, Oman
[g] Faculty of Sciences of Monastir, University of Monastir, Avenue of the Environment, 5019 Monastir, Tunisia
[h] Department of Chemistry, National Institute of Technology, Silchar, Assam 788010, India
[i] National Centre of Excellence in Analytical Chemistry, University of Sindh, Jamshoro 76080, Pakistan
[j] Institute of Metal Research (IMR), Chinese Academy of Science, 2 Wenhua Rood, Shenyang, China
[k] Operations and Method Development, Shefali Research Laboratories, Ambernath (East)-421501, Maharashtra, India
[l] Gdansk University of Technology, Faculty of Civil and Environmental Engineering, Department of Sanitary Engineering, 80-233 Gdansk, G Narutowicza St 11/12, Poland
[m] School of Civil, Environmental, and Architectural Engineering, College of Engineering, Korea University, 145 Anam-ro, Seongbuk-gu, Seoul 02841, Republic of Korea
[n] Centre for Research Impact & Outcome, Chitkara University Institute of Engineering and Technology, Chitkara University, Rajpura 140401, Punjab, India

ARTICLE INFO

ABSTRACT

2D materials have garnered significant attention as potential solutions to various environmental challenges. Graphene, molybdenum disulfide, MXenes, and boron nitride have emerged as the most popular candidates among these materials. This article presents a comprehensive review and discussion on the emerging applications of MXenes in environmental engineering. MXenes have demonstrated immense potential as future materials for adsorption purposes. They have proven to be highly effective in removing emerging pollutants (heavy metals and organic pollutants) through the adsorption phenomenon. The effectiveness of MXenes in removing lead (Pb^{2+}), chromium (Cr^{6+}), copper (Cu^{2+}), uranium (U^{6+}), and mercury (Hg^{2+}) has been confirmed, with a sorption capacity ranging from 100 to 250 mg g^{-1}. Furthermore, MXenes have effectively removed several radionuclides, including uranium, europium, strontium, barium, and thorium. MXenes have proven to be highly efficient in treating water through adsorption in emerging organic pollutants, even for various organic dyes such as methylene blue, acid blue, congo red, methyl orange, and rhodamine B (RhB). Additionally, MXenes exhibit high treatment performance in adsorbing several pharmaceuticals like cloxacillin (CLX), ampicillin (AMP), amoxicillin (AMX), ciprofloxacin (CPX), amitriptyline (AMT), verapamil (VRP), carbamazepine (CBM), 17 α-ethinyl estradiol, ibuprofen (IBP), and diclofenac (DCF). Overall, MXenes offer several advantages, such as good conductivity, thermal performance, high surface area, and selectivity of intermolecular interactions. However, their application requires thoroughly evaluating their environmental impact and life cycle assessment.

* Corresponding authors at: Department of Environmental Health Engineering, School of Public Health, Tehran University of Medical Sciences, Tehran, Iran (M.H. Dehghani). Petroleum and Chemical Engineering, Faculty of Engineering, Universiti Teknologi Brunei, Bandar Seri Begawan BE1410, Brunei Darussalam (N.M. Mubarak and R. RaoKarri).

E-mail addresses: hdehghani@tums.ac.ir (M.H. Dehghani), mubarak.yaseen@gmail.com (N.M. Mubarak), karri.rao@utb.edu.bn (R.R. Karri).

Nomenclature

AOPs	Advanced Oxidation Processes
2D	Two-dimensional
3D	Three-dimensional
XRD	X-ray diffraction
SEM	Scanning electron microscopy
TEM	Transmission electron microscopy
DRS	Differential reflectance spectroscopy
XPS	X-ray photoelectron spectroscopy
AMP	ampicillin
AMT	amitriptyline
CBM	carbamazepine
DCF	diclofenac
EDX	Energy dispersive X-ray
UV–Vis	UV–visible spectroscopy
DFT	Density functional theory
TGA	Thermogravimetric analysis
CV	Cyclic voltammetry
VSM	Vibrating-sample magnetometry
DTGA	Derivative thermogravimetric analysis
CLSM	Confocal laser scanning microscopy
TEMA	Tunnelling electron microscopic analysis
PXRD	Powder X-ray diffraction
TMOs	Transition metal oxides
TMDs	Transition metal dichalcogenides
g-C$_3$N$_4$	Graphitic carbon nitride
HPLC	High-performance liquid chromatography
EPR	Electron paramagnetic resonance
HAADF-STEM	High-angle annular dark-field scanning transmission electron microscopy
SA	sodium alginate
MCE	mixed cellulose ester
TMDs	Transition metal dichalcogenides
DPASV	Differential pulse anodic stripping voltammetry
BPA	Bisphenol A
DPV	Differential pulse voltammetry
CT	Catechol
LOD	limit of detection
MOF	Metal-organic frameworks
EHL	Enzymatic Hydrolysis Lignin
CR	Congo red
MB	Methylene blue
MO	Methyl orange
MG	Malachite Green
RhB	rhodamine B
FTIR	Fourier transmission electron microscopy
CLX	cloxacillin
AMX	amoxicillin
VRP	verapamil
IBP	ibuprofen
EMT	1-Ethyl-3-methylimidazolium tetrafluoroborate
EA	Elemental analysis
FESEM	Field emission transmission electron microscopy
BET	Brunauer-Emmett-Teller
EIS	Electrochemical impedance spectroscopy
HRTEM	High-resolution transmission electron microscopy
ZPA	Zeta potential analysis
AFM	Atomic force microscopy
RS	Raman spectroscopy
SAED	Selected area electron diffraction
SSA	Specific Surface area
LDH	Layered double hydroxides
NDMA	nitrosamine dimethylamine
DRS	Differential reflectance spectroscopy
ESR	Electron spin resonance
DSC	Differential scanning calorimetry
ICP-OES	Inductively coupled plasma atomic emission spectrometry
GO	Graphene oxide
BN	Boron nitride
SWAV	square wave anodic stripping voltammetry
SWASV	Square wave anodic stripping voltammetry
GCE	Glassy carbon electrode
HQ	Hydroquinone
TBZ	Thiabendazole
CBZ	Carbendazim
OPs	Organophosphorus pesticides

1. Introduction

Discharging untreated wastewater into rivers, lakes, and seas adversely affects the planet and the creatures inhabiting these ecosystems. Wastewater comprises several harmful substances, including heavy metals, dyes, pesticides, plastics, volatile organic compounds, pharmaceuticals, and pathogenic microbes (Karri et al., 2021; Dehghani et al., 2010). Complex carbon-based compounds are poisonous but can be less harmful via microbial or chemical reactions. The peril of these contaminants is contingent upon their toxicity and the extent of their accumulation in the environment throughout time. Consequently, it is imperative to devise and implement efficient methods for eliminating these contaminants to maintain a clean and safe atmosphere. Recently, researchers have concentrated on developing novel materials with customizable properties to enhance water treatment and monitoring. Nanomaterials with unique characteristics exhibit significant promise for detecting and remedying environmental contaminants (Kulkarni et al., 2024; Koduru et al., 2023; Karri et al., 2023; Umar et al., 2022). These include quantum dots, metallic or polymeric nanoparticles, nanocomposites, carbon nanotubes, and metal–organic frameworks (Kulkarni et al., 2024; Khan et al., 2021; Khan et al., 2022; Mubarak et al., 2024). Advancements in materials such as covalent organic frameworks (COFs) and metal–organic frameworks (MOFs) enable

researchers to fabricate novel nanostructures with diverse applications (Gopalram et al., 2023; Ahmaruzzaman, 2022; Solangi et al., 2024; Solangi et al., 2024). Utilizing carefully engineered nanoparticles can enhance sensitivity, precision, and overall efficacy in new-generation adsorbents for purifying emerging and gaseous pollutants removal applications.

MXenes present a large family of two-dimensional transition metal carbides, nitrides, and carbonitrides with highly controllable structure, composition, and surface chemistry to synthesize for various applications (Pazniak et al., 2021; Solangi et al., 2024). Fig. 1 shows the timeline of development of the synthesizing routes of MXene from 2011 to 2024. These materials have gained great interest due to their high conductivity and excellent properties, allowing them to be used in various applications, particularly for environmental applications (Jun et al., 2019; Liu et al., 2020; Li et al., 2022; Jatoi et al., 2022). The interest in two-dimensional (2D) materials has recently exploded because of their shape-based features, and they exhibit enhanced properties, including a large surface area and many sites for interaction with other materials (Taghipour et al., 2024; Karri et al., 2024; Sani et al., 2023; Solangi et al., 2021). Because of the higher number of sites, their activity with different materials is also high and has higher functionality and capacity (Fondamentales et al., 2017; Gogotsi and Anasori, 2019; Raheem et al., 2023).

MXene is a newly discovered 2D transition material in the field of nanotechnology (Algaradah, 2024; Solangi et al., 2023; Solangi et al., 2023). However, as far as the applications are concerned, it is in a leading position among 2D materials (Anasori and Gogotsi, 2022). Building upon these features, 2D materials have various applications in diverse fields as they possess active sites, high surface area, better functionalization, high conductivity, hydrophilicity, and biocompatibility, thus making them of interest as environmental remediation agents for pollutant extraction as well as for purposes such as catalysis, and sensors (Tunesi et al., 2022; Solangi et al., 2022; Solangi et al., 2024). In addition, MXenes combined a high electrical conductivity and mechanical properties of transition metal carbides/nitrides; functionalized surfaces that make them hydrophilic and ready to bond to various species. They also have high negative zeta potential, enabling stable colloidal solutions in water; and efficient absorption of electromagnetic waves, which have led to many applications (Karri et al., 2024; Gogotsi and Anasori, 2019; Solangi et al., 2023). These transition metals were synthesized from three-dimensional nano lamellar materials called MAX phases, a family currently containing more than 150 members, making it possible to envisage the production of numerous 2D materials with very versatile chemistry. Thus, since the discovery of the first titanium-based MXene, around 30 different MXenes have already been synthesized, and the existence of several others has been theoretically predicted (Solangi et al., 2023; Rasool et al., 2019). A detailed insight into the MXenes family with various precursors and etching methods used to develop 2D MXene is shown in Fig. 2.

Several synthesis and characterization methods have been developed to open new avenues in MXene research. Researchers are developing new synthesis techniques to prepare novel MXenes with unique properties (Zhong et al., 2021; Solangi et al., 2023; Solangi et al., 2023). For example, chemical etching of MAX phases under different conditions can result in MXenes forming with varying surface chemistry, morphology, and properties (Lei et al., 2015; Solangi et al., 2023). The periodic elements synthesize the MAX phase and MXene (Fig. 3). Generally, there are three types of MXene synthesis techniques: Etching, top-down, and bottom-up. In the etching method, the "*A*" elements from the MAX phases of the parent three-dimensional (3D) layer result in the MXenes layered structure. Table 1 presents some methods used for the synthesis of MXenes. Due to the synthesis process, MXenes are functionalized on the surface by different end groups "*T*" (T = −O, −F, −OH), which significantly affect their properties and give them a hydrophilic nature, facilitating their shape (Fondamentales et al., 2017; Solangi et al., 2023). MXenes in disordered solid solutions or organized formations that contain two or more transition metals. The behavior of MXenes is greatly influenced by the diversity, homogeneity, and compositional control of Tx surface groups, which now go beyond −O, −OH, and −F to include other halogens (−Cl, −Br, –I), chalcogens (−S, −Se, −Te), imido (−NH) groups (Azadmanjiri et al., 2023; Li et al., 2020; Nie et al., 2022).

This review offers a comprehensive and up-to-date analysis of MXene-based materials, focusing on their role as next-generation adsorbents for the purification of emerging and gaseous pollutants, and energy-related applications. Unlike previous reviews, this paper not only compiles existing knowledge but also critically evaluates recent advancements in MXene synthesis, functionalization, and their application across diverse environmental domains. The manuscript highlights the unique properties of MXenes, such as their tunable surface chemistry, large surface area, and excellent adsorption capacities, which make them highly effective in pollutant removal. Moreover, the review identifies the gaps in current research, such as the need for deeper investigation into MXene toxicity and environmental safety, while also outlining future directions. These significant insights into the environmental applications of MXenes provide a robust foundation for future studies, marking this review as a valuable resource for researchers in materials science and environmental engineering.

2. Removal of emerging pollutants by MXene-based materials using adsorption mechanism

Emerging pollutants (EPs), including heavy metals, dyes, pharmaceuticals, personal care products, endocrine-disrupting chemicals, pesticides, and present a growing threat to water quality. Common
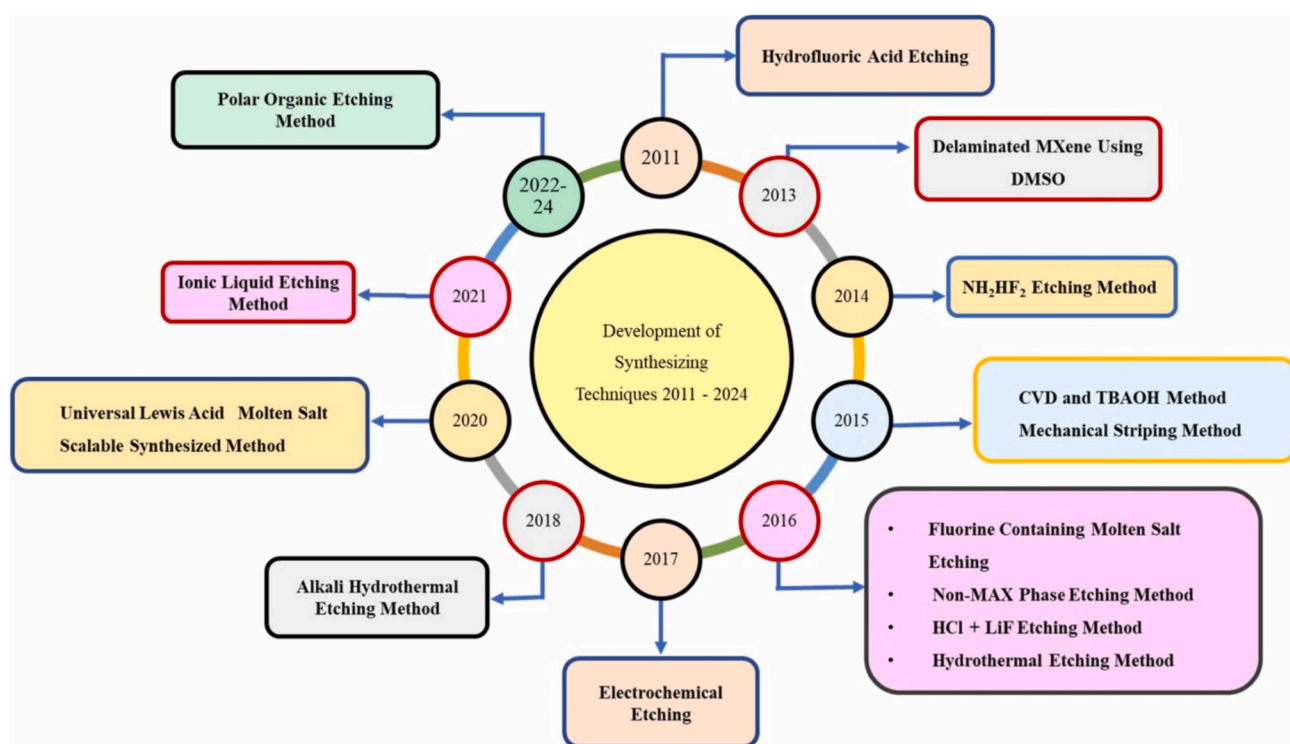

Fig. 1. Development of the synthesizing routes of MXene from 2011 to 2024 (Solangi et al., 2024).
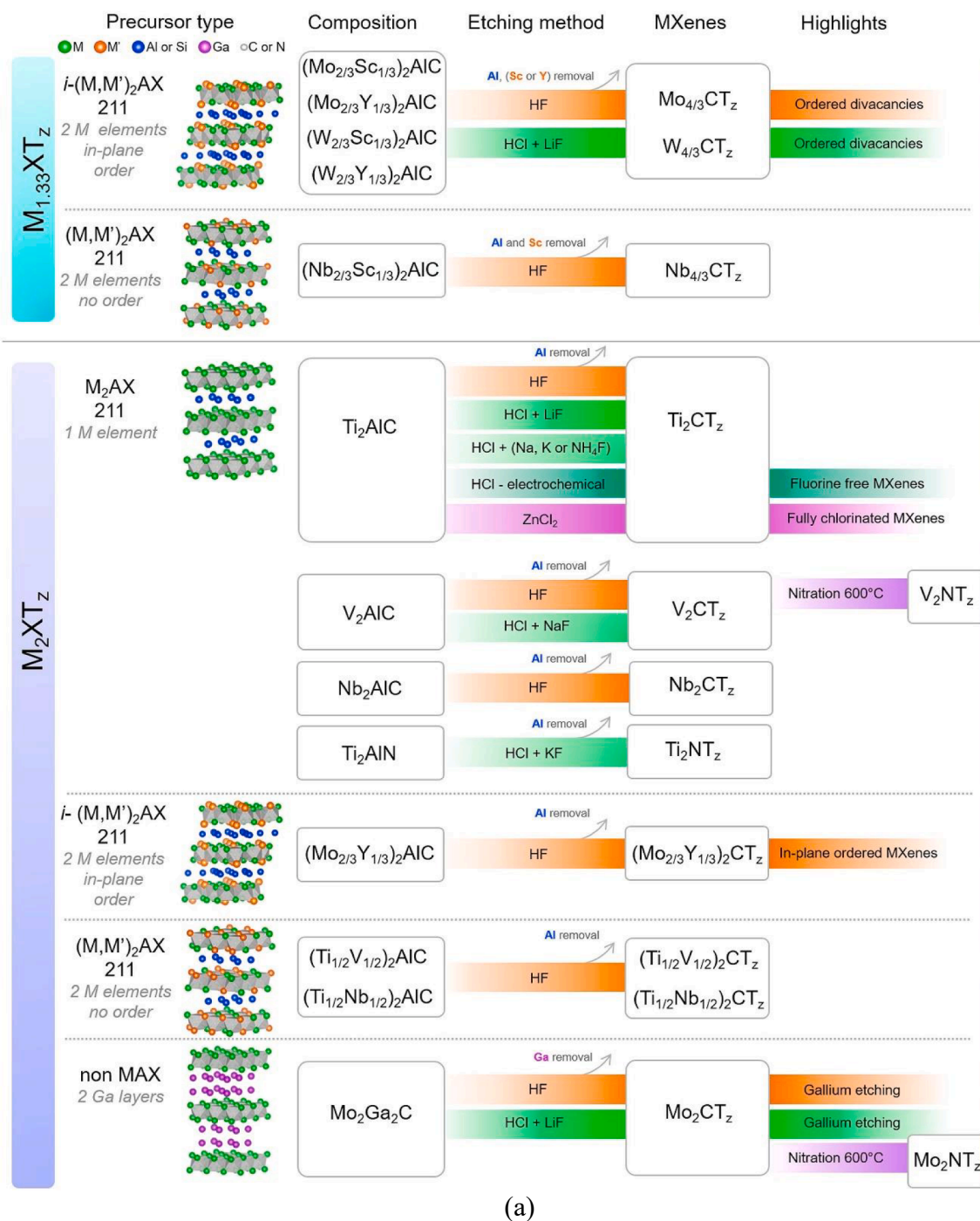
Fig. 2. (a) Summary of MXenes in their family, etching methods used to develop this 2D MXene, (b) Summary of MXenes family with different precursors, etching methods used to develop 2D MXene (Verger et al., 2019).

emerging pollutants are shown in Fig. 4. These pollutants can have harmful effects on ecosystems and human health. MXene-based materials have garnered significant attention for their potential in environmental remediation, particularly for removing emerging pollutants through adsorption.

2.1. Heavy metal ions

The functionalities available on the external surface of MXene have a beneficial impact on the adsorption of heavy metals. For the adsorption of heavy metal ions such as copper, lead, chromium, nickel, cesium, and

uranium, Ti_3C_2Tx represents the most studied MXene (Sheth et al., 2022). The heavy metal ion adsorption mechanism using MXene is presented in Fig. 5 (Pouramini et al., 2023). The performance of various MXene-based adsorbents for removing heavy metals is shown in Table 2. Tang et al. (Tang et al., 2018) synthesized the Ti_3C_2Tx MXene-based adsorbent for the adsorption of Cr^{+6} by utilizing the HF etching technique by eliminating the Al form Ti_3AlC_2. After synthesizing MXene, various characterization techniques like XRD, SEM, TEM, and DRS have been used for their characterization. The synthesized MXene possessed higher adsorption capacity than its parent material, Ti_3AlC_2, because of the successful exfoliation. The synthesized adsorbent has an adsorption
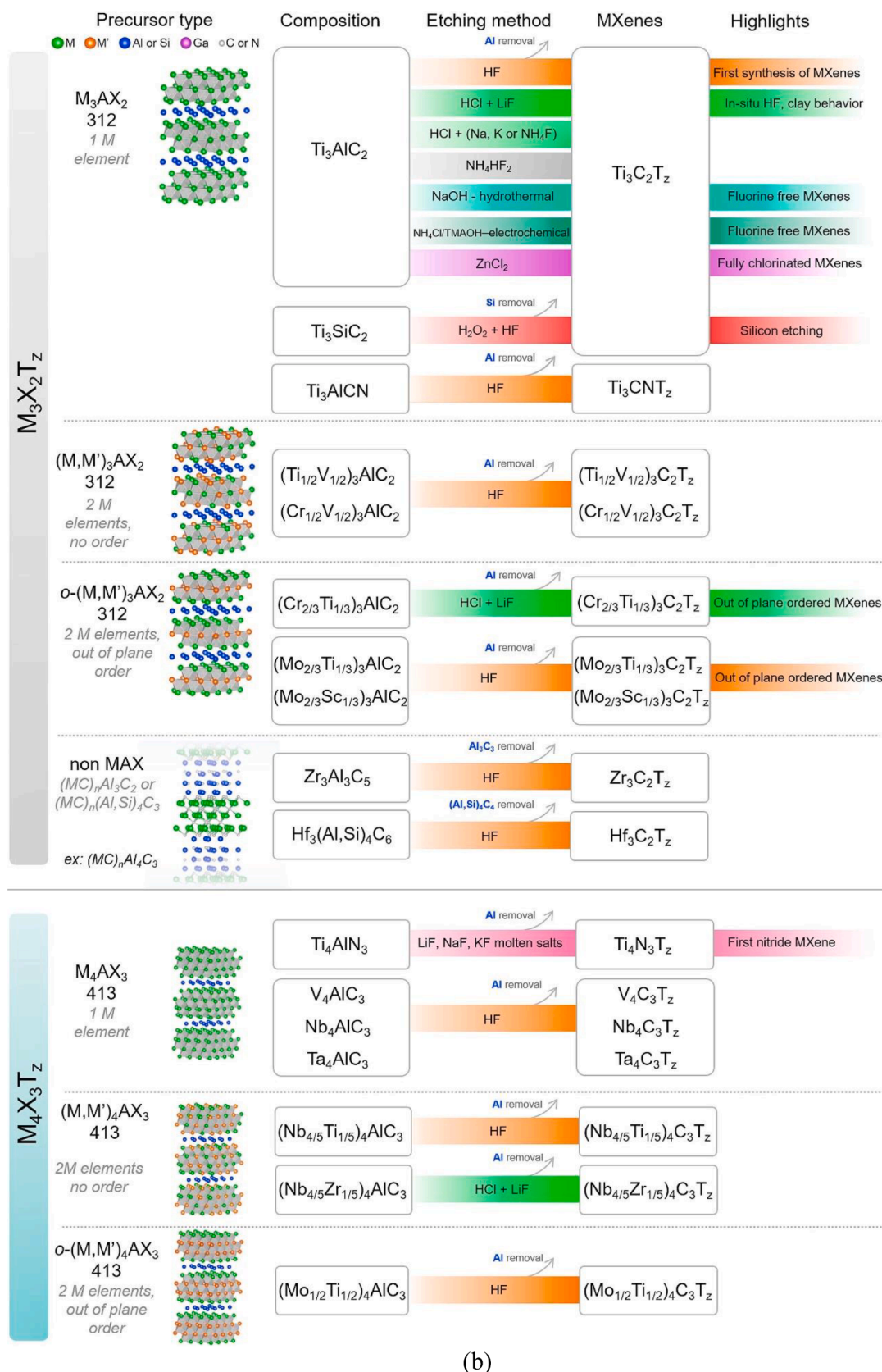
(b)

Fig. 2. (*continued*).

capability of up to 80 mg g^{-1}. They used intercalation and sonication techniques to enhance their adsorption capacity during the experiment. The experimental results show that both modification techniques have a meaningful impact on the adsorption capability of the adsorbent.

Zhan et al. (Zhan et al., 2020) utilized the environmentally friendly alkalization-grafting modification technique to synthesize the

Fig. 3. Periodic elements synthesize the MAX phase and MXene (Solangi et al., 2024).

alkMXene-NH$_2$ nanocomposites for the adsorption of lead (Pb^{2+}). The synthesized MXene has an adsorption capacity of Pb^{2+} heavy metal 187.5 mg g^{-1}. The remarkable adsorption capacity of the synthesized MXene is because of their excellent SSA area of 129.21 m^2.g^{-1} and the availability of the active functionalities on their surface. Some other factors are also discussed during the investigation and have a tremendous impact on the adsorbent's performance. The adsorption temperature, reaction time, adsorbent dose, pH of the system, and pressure also have little effect on the adsorption of Pb^{2+}. These characteristics suggest that MXene-based adsorbents that have been amino-functionalized will make good options for use in the industry.

Mercury emissions substantially harm the natural balance and biological security of flue gas from coal-fired power stations. Acid gases (SO$_2$, NO) frequently present in flue gas will significantly impact (negatively) the mercury adsorbent's effectiveness. Xu et al. (Xu et al., 2022) utilized a cost-effective and environmentally friendly technique to develop CuS/Ti$_3$C$_2$ for the environment's safety and human health. The experimental findings show that the pristine MXene has less adsorption capacity and reusability than the CuS/Ti$_3$C$_2$-based composites which is approximately 20 mg g^{-1}. According to the findings, the reactivity of the pure Ti$_3$C$_2$ interface is increased by CuS dosing. This research thus confirms that CuS/Ti$_3$C$_2$ is an attractive source for eliminating mercury from coal-fired power stations and broadens the MXene's practical applicability.

Liu et al. (Liu et al., 2023) utilized the environmentally friendly electrostatic self-assembly technique to synthesize the Ti$_3$C$_2$@FeS-PDA/PEI nanocomposite. Various analytical methods were used to properly assess all as-prepared substances and evaluate the development of species with the specified structure and characteristics. Findings showed that the novel chemical composition of MXenes enhanced the FeS nanomaterials distribution and prevented their aggregation. Various cations and anions in the synthesized composite have no significant impact on the rejection capacity of the adsorbent. They also specified the endothermic process type. DFT analysis shows the strong chemical bond between FeS and active functionalities present on the layer of Ti$_3$C$_2$@FeS-PDA/PE; that is responsible for effective adsorption. The Ti$_3$C$_2$@FeS-PDA/PEI nanocomposite's adsorption capacity for removal of U^{6+} is 88.5 mg g^{-1}. The schematic illustration of U^{+6}/Cr^{+6} removal pathways on Ti$_3$C$_2$@FeS-PDA-PEI is presented in Fig. 6.

According to Zhang et al. (Zhang et al., 2022), when enzymatic hydrolysis lignin (EHL) reacts with 2D Ti$_3$C$_2$Tx MXene to synthesize the functionalized 2D Ti$_3$C$_2$Tx (TN-EHL) adsorbent for the removal of Cu^{2+} heavy metal. The introduction of EHL into Ti$_3$C$_2$T$_x$ cannot disturb the availability of active functionalities on the surface of Ti$_3$C$_2$Tx, and their addition reduces the chance of oxidation. This role enhances the adsorption capacity of Ti$_3$C$_2$Tx. So, the adsorption capability of TN-EHL for Cu^{2+} is 293.7 mg g^{-1}. The reaction of Cu^{2+} adsorption is endothermic and uncontrolled. During the adsorption of Cu^{2+} on the surface of the developed composite, Cu^{2+} ions are converted to Cu$_2$O and CuO particles to reduce the concentration of Cu^{2+} ions.

2.2. Dyes

Because of the economic disadvantages of conventional adsorbent materials, MXene offers a superior alternative to clear effluent tainted with dye. Studies were reported on removing toxic dyes like methylene blue and acid blue using 2-D MXene by adsorption. These nanomaterials outperformed other 2D substances regarding adsorption. Concerning several conventional adsorbents, the adsorption rate of MXene-based adsorbents for removing various dyes-based contaminants, like Congo red, Methylene blue, and Methyl orange, was competitive (Liu et al., 2023). A comparison of adsorption conditions and performance of removal of various dyes by different MXene-based adsorbents is shown in Table 3.

Ibrahim et al. (Ibrahim et al., 2022) have used the ability of raw and modified MXenes to have high surface area and surface terminations for the adsorption of methylene blue (MB) and acid blue 80 (AB80). They have shown that they create many active sites for direct ion exchange and reductive-adsorptive removal of dyes and cations. For example, various salt-based Ti$_3$C$_2$Tx adsorbent was used to remove MB and AB80 dye from the aqueous solution. The adsorption capacity of MB reached about 39 mg g^{-1}. The adsorption capacity of NaOH-Ti$_3$C$_2$Tx (189 mg g^{-1}) was higher than LiOH- Ti$_3$C$_2$Tx (121 mg g^{-1}), Ti$_3$C$_2$Tx (100 mg g^{-1}), and KOH-Ti$_3$C$_2$Tx (75 mg g^{-1}). They have shown that Ti$_3$C$_2$Tx

Table 1

Review of the main Synthetic methods used to produce MXenes and their applications (Solangi et al., 2024; Gogotsi and Anasori, 2019).

Synthetic methods	Specific properties	Main applications
The etching process includes hydrofluoric acid (HF), electrochemical etching, and Alkali etching. Halogen etching, Lewis's acid molten salt etching	High electrical conductivity, Tuneable Tx towards selective adsorption of analyte, Hydrophilicity, and solution processability	Energy storage and catalytic conversion
HF etching	High electrical conductivity, large surface area, High mechanical stability, Hydrophilicity, and solution processability	Electromagnetic and electronic
HF etching	High electrical conductivity, Hydrophilicity, and solution processability, Tuneable Tx towards selective adsorption of analyte	Environmental and sensing
HF etching, Electrochemical etching	Hydrophilicity and solution processability	Biomedical
Alkali etching Halogen etching Lewis's acid molten salt etching. HF etching	Tuneable Tx towards varying lubrication or stiffness Controllable MXene thickness Minimal defects, large surface area	Mechanical Tribology (stiffness, adhesion, lubrication) Mechanical composites
Alkali etching	Tuneable Tx towards selective adsorption of analyte, large surface area	Antimicrobial, antibacterial Biosensors, cancer theragnostic, Drug delivery Adsorption
Chemical vapor deposition (CVD)	The smoothness and homogeneity of MXene layers can be enhanced using the CVD method.	A polished, flawless surface improves electrical conductivity and surface area, crucial for sensors and electromagnetic interference shielding applications.
Hydrothermal etching	Hydrothermal etching significantly enhances the surface chemistry, structural characteristics, and electrochemical efficiency of MXenes.	This technique makes MXenes appealing for various uses encompassing energy storage, catalysis, electronics, and environmental cleanup.

presents a higher adsorption capacity for MB than AB80, which is due to strong electrostatic interaction with MB. Based on their outcomes, it can be concluded that MXenes present an attractive option for the removal, adsorption, and degradation of numerous dyes like AB80, MB, and others in a variety of composites, membranes, sorbents, photo-catalysts, and electrodes.

To develop an MXene-based nanocomposite (PA-MXene) to extract MB from untreated wastewater, Cai et al. (Cai et al., 2020) employed environmentally friendly and inexpensive hydrothermal procedures. Fig. 7 provides a graphic representation of the PA-MXene nanocomposites created using hydrothermal and dye adsorption processes. The PA was not chemically bonded with MXene, as it was a physical coating of PA on the surface of MXene. The adsorption performance of the MXene-based adsorbent was excellent, up to 85 % after 12 cycles. The variety of characterization approaches is consistent with its excellent efficiency and chemical and thermal stability. The adsorption power of MXene-based adsorbent for removing MB and RhB was 106.7 mg.g^{-1} and 72.4 mg.g^{-1}, respectively. This research offered new information for creating and enhancing MXene-based nanomaterials for various adsorption processes.
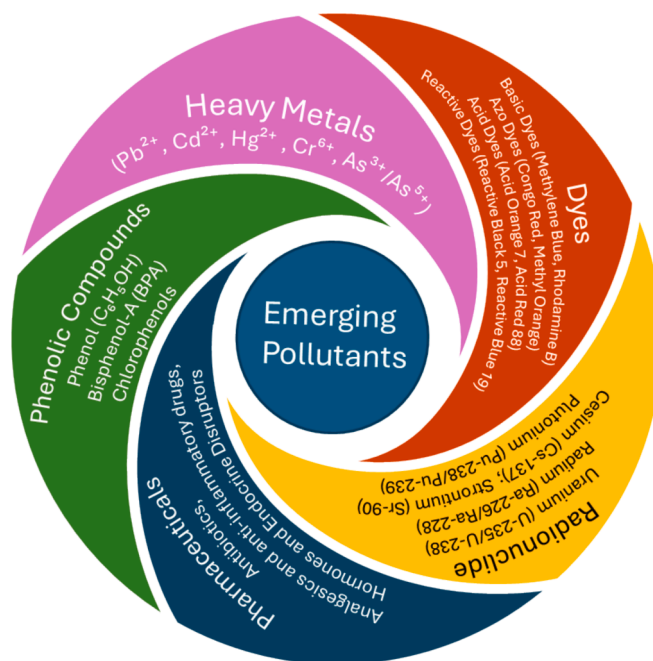

Fig. 4. Common emerging pollutants such as heavy metals, dyes, radionuclides, pharmaceuticals, and phenolic compounds.

Anionic azo dye methyl orange (MO) has been widely utilized in the textile sector for a long time to give orange-like colors to clothing. Sun et al. (Sun et al., 2021) used etching to eliminate the Al layer from their Ti$_2$AlC to synthesize the Ti$_2$CTx MXene-based nano-adsorbent. The various characterization techniques have been utilized to provide an extensive understanding of Ti$_2$CTx MXene via XPS, SEM, XRD, and FTIR techniques. The synthesized MXene-based adsorbent performance was evaluated at different pH levels, contact times, adsorbent concentrations, temperatures, and surrounding ions. The synthetic Ti$_2$CTx layer is positively charged and exhibits good MO adsorption properties. The adsorption efficiency of the adsorbent was 122.6 mg.g^{-1} at reaction conditions (T = 298 °C, t = 24 min, pH = 6.0). Ti$_2$CTx offers outstanding recyclability for eliminating MO, as evidenced by its excellent rejection performance after four cycles. The results of this study demonstrate that members of the MXene family can be employed as adsorbents to remove anionic azo dye methyl orange contaminants from sewage.

To minimize Malachite Green (MG), particularly from effluent discharge, and to protect aquatic life, Wang et al. (Wang et al., 2023) created the alk-MXene/CoFe$_2$O$_4$/CS nanomaterials using an eco-friendly hydrothermal and self-assembly method. Specifically, it is found that etching for 24 h improves the composite's capacity for adsorption throughout the synthesis process. Under ideal experimental conditions, the alk-MXene/CoFe$_2$O$_4$/CS nanostructure can adsorb 537.6 mg of MG per gram of surface area. The dye concentration significantly influences the adsorption rate and capacity of the adsorbent in the water; the adsorption capacity and rate were high at high concentrations of MG and vice versa. The functions on the adsorbent's interfaces can be considerably increased by adding CoFe$_2$O$_4$/CS to the alk-MXene interlayer and surface, providing different active sites for dye adsorption. The MG dye and the SO$_3$ polar group in MG are easily attracted to the outer layer of the produced adsorbent nanostructure due to electrostatic interactions, the availability of functionalities, and positive charges. The ease of access of the H-bond on the adsorbent and dyes is also helpful for the adsorption of MG dyes. After five working cycles, it had reached a very high removal efficiency of about 80 %.

Rhodamine B (RhB) dye is largely used in the paper and textile industries for coloring. A luminous cationic RhB dye is employed in distemper paintings, inks, leather, wood stains, cosmetics, and shoe polish.
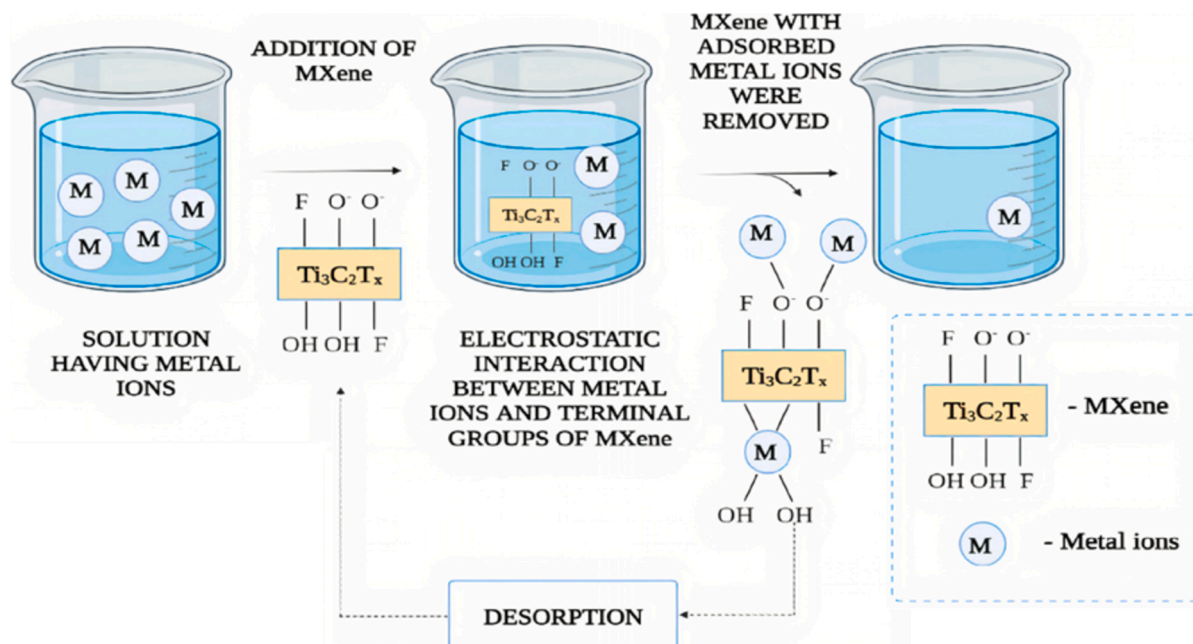
Fig. 5. Mechanism of the adsorption of the metal ions on MXene-based adsorbent (Pouramini et al., 2023).

Rethinasabapathy et al. (Rethinasabapathy et al., 2022) used the magnetic stirring technique to develop the Ti_2CTx/Fe_3O_4 nanostructure by mixing MXene and Fe_3O_4 at 353 K under an argon atmosphere to eliminate RhB organic dyes, especially from textile waste. The designed MXene-based adsorbent had excellent discharge ability of RhB up to 86 mg g^{-1} even when it was just 45. The proposed composite demonstrated great reusability after four cycles with good workability due to magnetic Fe_3O_4 particles. According to their hypothesis, the outstanding RhB rejection effectiveness of Ti_2CTx/Fe_3O_4 is due to the synergistic relationship of electrostatic forces and H bonds between the active functionalities of Ti_2CTx/Fe_3O_4 and lone-pair electrons of the N group of RhB. Moreover, the excellent selectivity of cationic dyes in coexistence was 88 %. The Ti_2CT_x/Fe_3O_4 nanostructure might have been a desirable option for removing harmful cationic dyes from aqueous solutions because of its remarkable sorption.

Wang et al. (Wang et al., 2023) utilized the environmentally friendly hydrothermal and self-assembly approach to synthesize the alk-MXene/$CoFe_2O_4$/CS nanostructure to reduce Congo Red (CR), especially from industrial effluent, to save aquatic life. It has been determined that 24 h is the best etching period to enhance the composite's adsorption capability throughout the synthesis method. The dye concentration in the water also plays a key role in the adsorption rate and capacity of the adsorbent; the adsorption capacity and rate were high at high concentrations of CR and vice versa. Finally, it was discovered that adding $CoFe_2O_4$/CS to the alk-MXene interlayer and surface can significantly increase the functionalities on the adsorbent's interface and offer additional active sites for dye adsorption. Furthermore, the extensive availability of the H-bond on the adsorbent and dyes is advantageous for the adsorption of CR dyes. Contemporary science research presents a novel idea for synthesizing MXene-based magnetic adsorbent materials with an enhanced ability to remove different colors from aqueous pollutants. The synthesis process of the alk-MXene/$CoFe_2O_4$/CS nanostructure is shown in Fig. 8.

2.3. Pharmaceuticals

MXenes have been investigated as potential drug molecule adsorbents in medicinal applications (Ahmaruzzaman, 2022). On the other hand, drug molecules are attracted to the surface of the MXene material during the adsorption process, which can result in more effective medication delivery and tailored therapy. In Table 4, the adsorption of pharmaceuticals by fabricated MXenes is presented. Khatami and Iravani (Khatami and Iravani, 2021) has demonstrated that MXenes can successfully adsorb various medicinal molecules, such as antibiotics, anticancer medications, and anti-inflammatory drugs. The surface chemistry of the MXene material, the kind of drug molecule, and the ambient circumstances all affect how MXenes adsorb these substances. Overall, MXenes are a promising family of materials for pharmaceutical adsorption applications, and additional study is required to maximize their efficacy and promise for therapeutic drug delivery (Khatami and Iravani, 2021; Miri-Jahromi et al., 2022).

Researchers reviewed 2D MXenes, which have a large surface area and are chemically stable enough to be used as adsorption components for CLX, AMP, and AMX (Khatami and Iravani, 2021). Among Mn_2C, Ti_2C, and V_2C, the fabricated Ti_2C had a 100 % adsorption efficiency for cloxacillin. The increased effectiveness was ascribed to the functionalization of MXene with hydroxyl and amine groups, which increased the affinity of antibiotic molecules to the adsorbent surface. The electrostatic attraction between cloxacillin and functionalized Ti_2C is boosted by including the functional group, as shown in Fig. 9(Miri-Jahromi et al., 2022). Analysis of how three different kinds of MXenes interact with pharmaceuticals was conducted using molecular dynamic simulations (MD). MD offers a potent approach for investigating atomic-level intermolecular interactions and characteristics. This part of the study revealed that compared to AMX and AMP, the solution with CLX had greater negative adsorption energy, making adsorption easier for the MXenes (Ti_2C, V_2C, and Mn_2C). It was discovered that Ti_2C absorbed 100 % of CLX while V_2C and Mn_2C adsorbed only 66 % and 55 % of CLX, respectively. Ti exhibited the least negativity compared to V and Mn, even though the pore size of all three MXenes was the same. As a result, the Ti_2C structure had the maximum charge density. Increased charge density enhances the interaction of MXene with the antibiotics, increasing Ti_2C's capacity for adsorption. Hydrogen bonding was chosen as a useful index to evaluate the characteristics of antibiotic adsorption; the stronger the interaction between MXene and the antibiotics, the weaker the H-bonding of MXene with the H_2O molecule. This investigation revealed that CLX had the highest interaction with the MXene surface due to its low H-bond in an aqueous solution.

Ghani et al. (Bhuyan and Ahmaruzzaman, 2023) removed ciprofloxacin (CPX) by producing 2D MXene by intercalating Na ions using a

Table 2

Operating conditions, adsorbent performance, and adsorption mechanisms of various MXene-based adsorbent performance for removal of diverse heavy metals.

MXene-based adsorbent	heavy metals	Operating Conditions					Adsorbent Performance			Adsorption mechanism	Ref.
		Conc. mg.L^{-1}	Time (h)	Adsorbent Dosage (g)	Temperature (K)	pH	Capacity mg g^{-1}	Removal percentage %	Working cycles		
Ti$_3$C$_2$Tx / PmPD	Cr^{6+}	100	–	0.1	303	2.0	540.5	92	5	Reduction; chelation; electrostatic interaction	(Jin et al., 2020)
Fe$_3$O$_4$@Ti$_3$C$_2$-NH2-PT	Cr^{+6}	10	24	0.005	298	5.0	104.9	80	3.0	Electrostatic interaction and adsorption-reduction process	(Liu et al., 2022)
Ti$_3$C$_2$Tx	Cr^{+6}	100	14	0.1	298	6.8	80	80	–	Chemical adsorption	(Tang et al., 2018)
Ti$_3$C$_2$Tx	Cr^{+6}	100	0.6	2.0	303	2.0	103.56	93.2	5	Electrostatic adsorption; ion exchange complexation; surface interactions	(Karthikeyan et al., 2021)
Ti$_3$C$_2$Tx/TiO$_2$	Cr^{+6}	50	1.8	0.05	298	5.0	–	99.35	–	ion exchange; inner-sphere complexation	(Wang et al., 2020)
Ti$_3$C$_2$-Imidazole hybrid composite	Cr^{+6}	30	1.3	0.01	298	2.0	183.8	95	5	Physical adsorption through electrostatic interaction.	(Yang et al., 2021)
Amine functionalized Ti$_3$C$_2$Tx	Cr^{+6}	100	3.0	0.05	298	2.5	107.4	–	6	Electrostatic interaction	(Kong et al., 2021)
Ti$_3$C$_2$Tx-Alginate	Pb^{2+}	0.07	0.25	0.02	298	5.0	383	86.7	10	Electrostatic adsorption	(Dong et al., 2019)
Ti$_3$C$_2$Tx	Pb^{2+}	0.05	2.0	0.5	293	6.0	36.6	–	4	ion exchange; inner-sphere complexation	(Jun et al., 2020)
Ti$_3$C$_2$Tx /10 % KH570	Pb^{2+}	50	1.8	0.05	303	5.0	147.97	99.9	4	Electrostatic interaction	(Du et al., 2019)
Alk-Ti$_3$C$_2$Tx–NH$_2$	Pb^{2+}	25	0.3	0.1	298	6.3	384.6	100	3	Complexation; van der Waals forces;	(Zhang et al., 2020)
MX	Hg^{2+}	100	3.33	0.01	303	5.0	1057.3	100	–	Electrostatic interaction; Chemical adsorption	(Hu et al., 2021)
MoS$_2$/ Ti$_3$C$_2$Tx	Hg^{2+}	100	0.03	0.01	298	6.5	1446.26	77	5	Surface complexation	(Shahzad et al., 2020)
CuS/Ti$_3$C$_2$	Hg^{2+}	100	2.0	0.1	298	4.9	20.467	–	5	Electrostatic interaction	(Xu et al., 2022)
Ti$_3$C$_2$Tx-Alginate Core Shel	Hg^{2+}	25	1.0	–	298	7–10	932.84	100	–	Inner-surface complexation; ion exchange; electrostatic interaction	(Shahzad et al., 2019)
Ti$_3$C$_2$@FeS-PDA/ PEI	U^{+6}	100	0.2	0.2	333	8.0	115	95	–	Adsorption-Reduction process	(Liu et al., 2023)
Carboxy functionalized Ti$_3$C$_2$Tx	U^{+6}	50	0.003	0.0002	298	5.0	344.8	99	–	Physical adsorption through electrostatic interaction.	(Zhang et al., 2020)
Zero valent Fe/ Alk- Ti$_3$C$_2$Tx	U^{+6}	200	24	0.08	298	3.5	1315	–	–	Reduction precipitate, surface complexation, hydrolysis precipitation	(Wang et al., 2021)
MXene/graphene	U^{+6}	100	1.0	0.1	298	6.0	1003.5	95	8	Reduction-induced immobilization and Complexation	(Li et al., 2022)
Fe$_3$O$_4$@Ti$_3$C$_2$-NH$_2$-PT	U^{+6}	10	24	0.005	298	5.0	104.9	80	3.0	Electrostatic interaction and adsorption-reduction process	(Liu et al., 2022)
Ti$_3$C$_2$Tx-PDOPA	Cu^{2+}	30	1.0	0.01	298	11.0	65.126	–	–	Physical adsorption	(Gan et al., 2020)
Ti$_3$C$_2$Tx-Alginate	Cu^{2+}	95.3	0.25	0.01	298	5	87.6	63.5	10	Ion exchange; chemical coordination	(Dong et al., 2019)
TN-EHL50,	Cu^{2+}	50	24	1.6	303	2.0	293.7	88.7	10	ion exchange; electrostatic interaction	(Zhang et al., 2022)
SA/MXene/ CFO	Cu^{2+}	100	48	0.0045	298	5.5	234.3	80	5	Surface complexation	(Ren et al., 2021)
DL-Ti$_3$C$_2$Tx	Cu^{2+}	25	0.03		298	5.0	78.5	80	3	Ion exchange; Inner sphere complexation	(Shahzad et al., 2017)
alk MXene/ LDH	Ni^{2+}	100	2.0	0.05	298	7.0	222.7	97.35	8	Surface Complexation	(Feng et al., 2020)

batch experimentation method. Intercalation has the advantage of accelerating the spacing and surface terminations between layers of SI-MXene, which improves adsorption capacity and reaction rate. The as-fabricated nanocomposite was regenerated Using an electrochemical method in about 5 min. The elimination rate of ciprofloxacin after successive reuse of the nanocomposite is 99.7 %, indicating that the produced materials are highly efficient. After intercalation, SI-Ti$_3$C$_2$Tx MXene's CPX removal rate was twice as high as pure Ti$_3$C$_2$T$_x$ MXene.

Kim et al. (Kim et al., 2021) fabricated Ti$_3$C$_2$Tx-MXene to adsorb amitriptyline (AMT), verapamil (VRP), carbamazepine (CBM), 17 α-ethinyl estradiol, ibuprofen (IBP), and diclofenac (DCF) from aqueous solution, with AMT showing highest adsorption with a capacity of 58.7
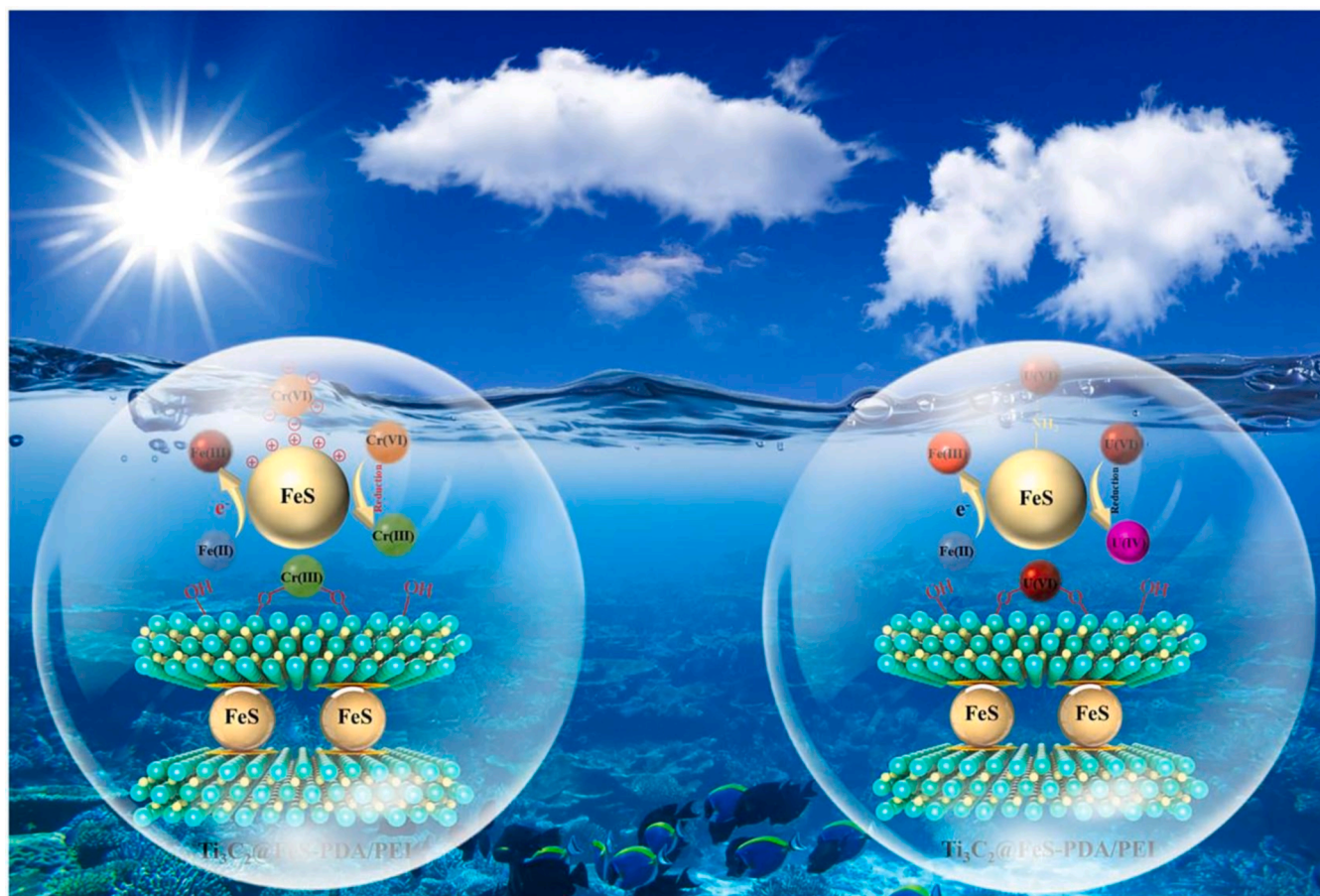
Fig. 6. Schematic illustration of U^{+6}/Cr^{+6} removal pathways on Ti_3C_2@FeS-PDA-PEI (Liu et al., 2023).

Table 3

Adsorption conditions, performance of removal of various dyes by different MXene-based adsorbents.

MXene-based adsorbent material	Pollutant removal	Adsorption conditions					Adsorption Performance		Ref
		Conc. (mg/L)	Dosage (g)	Temp. [K]	Time [h]	pH	Sorption capacity [mg g^{-1}]	Percent removal [%]	
PA-MXene	MB	12	0.01	298	3	–	106.7	97	(Cai et al., 2020)
MXene/MOF	MB	25	0.20	310	1.8	9.0	140.0	95	(Jun et al., 2020)
PA-MXene	MB	12	0.01	298	2.0	7.0	42.0	98	(Cai et al., 2020)
MXene-CMC	MB	75	0.80	298	3.0	2–10	75.0	100	(Zhang et al., 2020)
$Ti_3C_2T_x$	MB	47	0.05	298	2.0	–	39.0	21	(Mashtalir et al., 2014)
lk-MXene/ $CoFe_2O_4$/CS	CR	50	0.1	298	3.0	6.0	2095.9	97	(Liu et al., 2023)
AA-alk-MXene	CR	75	0.2	298	1.5	7.0	264.46	–	(Zhao et al., 2022)
Ti_2CTx	MO	25	0.01	308	24	6.0	2460.9	–	(Sun et al., 2021)
$Ti_3C_2T_x$	MO	40	0.02	303	0.4	3.0	94.8	82	(Karthikeyan et al., 2021)
Nb_2CT_x	MO	20	0.4	298	2.0	5.0	500	–	(Yan et al., 2021)
Peroxo-functionalized $Ti_3C_2T_x$	MO	50	0.10	298	3.0	5.6	292.6	–	(Solangi et al., 2023)
lk-MXene/ $CoFe_2O_4$/CS	MG	20	0.04	298	2.0	6.0	537.6	97	(Liu et al., 2023)
$Ti_3C_2T_x$ MXene	MG	25	0.05	298	3.0	2–10	–	94.1	(Kadhom et al., 2022)
$Ti_3C_2T_x$ /Fe_3O_4	RhB	10	0.01	298	0.45	11.0	86	88	(Rethinasabapathy et al., 2022)
PA-MXene	RhB	6	0.006	298	2.0	7.0	72.4	98	(Cai et al., 2020)
Peroxo-functionalized $Ti_3C_2T_x$	RhB	–	0.02	298	3.0	5.6	1333.9	–	(Li et al., 2022)
lk-MXene/ $CoFe_2O_4$/CS	RhB	10	–	298	2.0	6.0	1333.9	98	(Liu et al., 2023)

mg.g^{-1}. The effect of pH was studied from 3 to 11 by the researchers. Because MXenes have terminal –OH, –O, and –F groups, their surface charge alters with rising pH and becomes negatively charged. The VRP and AMT showed the best performance at pH 7, and the low negative charge of MXene may be responsible for the restricted adsorption at pH

3.5. AMT and VRP are neutralized when the pH value is higher than 10. The impact of pH is minimal with CBM because it cannot be ionizable at any pH. The researchers concluded that at pH levels greater than their pK$_a$ values, electrostatic attraction between negatively charged MXene and ionizable medicines decreased adsorption affinity. Also, to compare
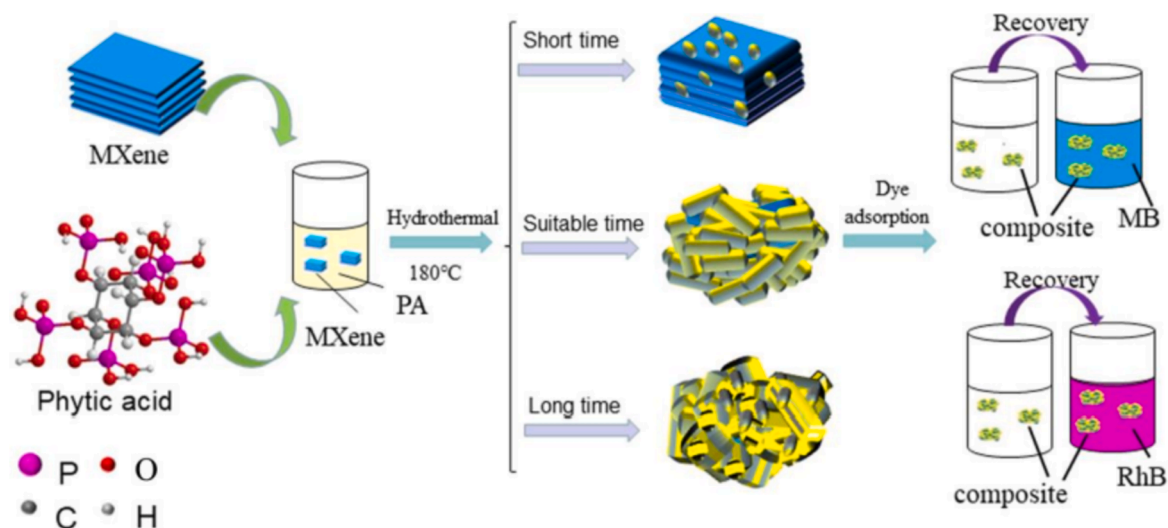
Fig. 7. Schematic representation of the PA-MXene composites fabricated using a dye adsorption procedure and a hydrothermal method (Cai et al., 2020).
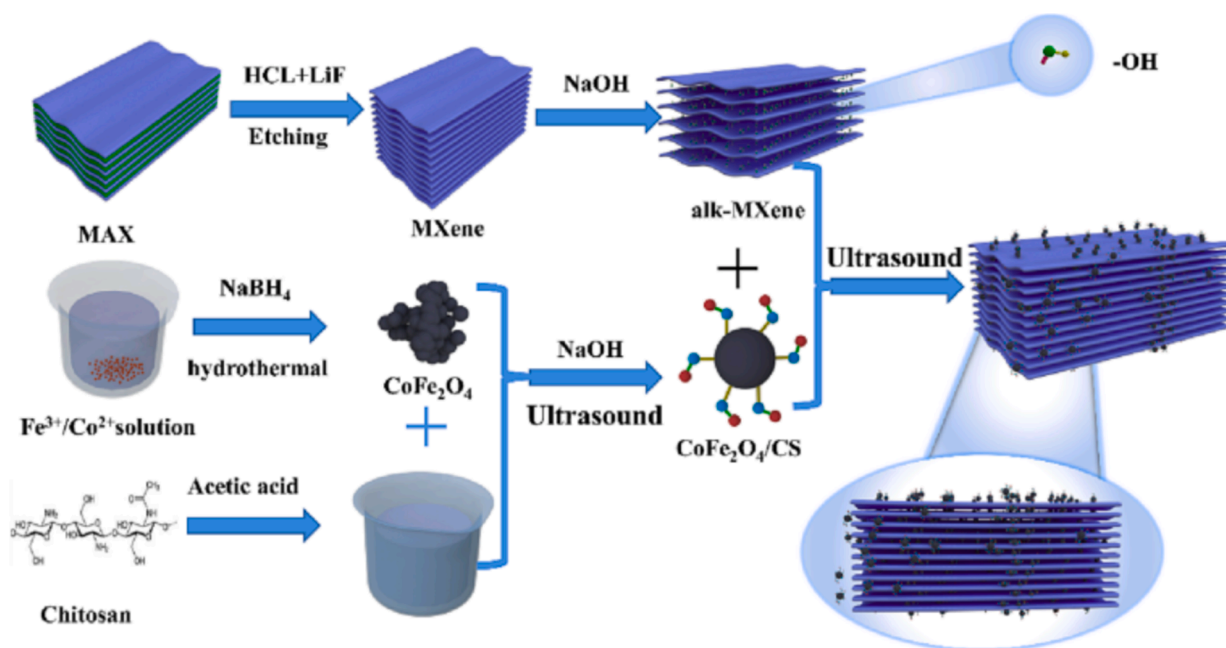

Fig. 8. The alk-MXene/CoFe$_2$O$_4$/CS synthesizing via hydrothermal techniques (Wang et al., 2023).

Table 4
Adsorption of pharmaceuticals by fabricated MXenes.

Adsorbent	Pharmaceutical compound	Adsorption Mechanism	pH	Time (hr)	Adsorption capacity (mg/g)	Removal efficiency (%)	Ref.
Ti$_2$C	Cloxacillin	Electrostatic Interaction: Hydrogen bond	–	–	–	100	(Miri-Jahromi et al., 2022)
SI-MXene	Ciprofloxacin	Electrostatic Interaction	5.5	2	208.2	~99.7	(Ghani et al., 2021)
Ti$_3$C$_2$TX-MXene	Amitriptyline	Electrostatic Interaction	7	0.33	58.7 214 (sonicated)	–	(Kim et al., 2021)

AMT adsorption performance with pure MXene, the authors produced two sonicated MXenes at 28 and 580 kHz. In sonicated MXene, smaller, evenly dispersed particles with a high oxygen-functionalized group and hydrodynamic diameter were found. Better performance and an increased elimination rate were obtained thanks to the sonicated MXene increased adsorption capacity of 214 mg/g for AMT adsorption. This is because sonication-induced cavitation bubbles can produce MXene that

is well-dispersed and can even create oxygenated functional groups on MXene. In particular, the best performance was demonstrated at lower frequencies by producing larger cavitation bubbles. In addition, using sonicated MXene, it was determined how different ions affected the effectiveness of adsorption on pharmaceutical substances because there are several ions in real aquatic habitats.

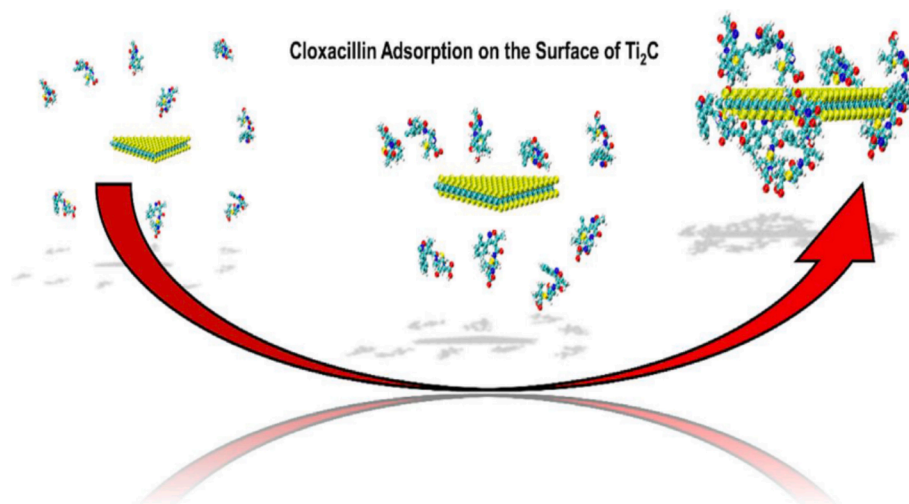Most inorganic contaminants and a small number of organic

Fig. 9. Adsorption of Cloxacillin on hydroxyl and amine groups functionalized Ti_2C (Miri-Jahromi et al., 2022).

pollutants, such as pharmaceuticals, are the focus of MXene adsorbent application. Even fewer findings are based on their ability to remove pharmaceutical substances through adsorption. The use of MXenes to treat pharmaceutical compounds is still in its infancy and requires more research (Bhuyan and Ahmaruzzaman, 2023).

2.4. Radionuclides

Removing radionuclides by adsorption has gained worldwide interest due to its simple procedure, low cost, excellent reliability, and availability of a wide range of adsorbents. A summary of radionuclides adsorption by MXene-based adsorbents is given in Table 5. From nuclear waste management's inception, various inorganic, organic, and organic–inorganic adsorbents have been investigated for radioactive extraction (Ahmaruzzaman, 2022; Wang et al., 2017; Fard et al., 2017; Li et al., 2019; Lai et al., 2018; Yan et al., 2022; Jun et al., 2020; Yu et al., 2015). However, these adsorbents suffer from low adsorption capacity, slow kinetics, and low selectivity. Various 2D layered materials are reported in the literature for the adsorptive removal of radionuclides. Among them, MXene has been extensively explored due to its high selectivity, high thermal and chemical stability, larger surface area, tunable structure, and presence of surface functional groups (Zhang et al., 2018).

Fard et al. (Fard et al., 2017) used Ti_3C_2Tx MXene synthesized by the intercalation followed by exfoliation using HF of MAX phase Ti_3AlC_2 for the first time in the literature. The authors claimed 100 % removal of Ba ions with a maximum adsorption capacity of 9.3 mg/g. About 90 % removal of barium was achieved within 10 min with high selectivity compared to other co-existing ions in the solution. Fig. 10 shows the adsorption mechanism of barium ions by alkali-treated Ti_3C_2Tx MXene. The adsorption of Ba ions was found to be physisorption on the surface in addition to the chemosorption by ion exchange with the surface functional groups according to the reactions: $Ba^{2+} + 2OH^- \rightarrow Ba(OH)_2$; $Ba^{2+} + 2F^- \rightarrow BaF_2$. However, a low adsorption capacity limits its practical use.

Furthermore, Mu et al. (Mu et al., 2018) tried to improve the barium adsorption capacity of Ti_3C_2Tx MXene by surface modification and basic metal intercalation using NaOH. The XRD and TEM studies showed that the Na^+ ions are readily intercalated within the Ti_3C_2Tx; causing an increase in the c-lattice parameter, which increased the interaction affinity of barium ions with the surface functional groups of MXene, resulting in improved removal efficiency. A maximum adsorption capacity of 46.5 mg/g could be achieved by alkali-treated Ti_3C_2Tx MXene, which is about three times higher than untreated MXene and higher than previously reported studies. Therefore, alkali activation of MXene could be an effective way to increase the adsorption capacity of MXenes.

Recently, Jun et al. (Jun et al., 2020) investigated the adsorption

Table 5
Summary of adsorption of various radionuclides by MXene-based adsorbents.

| Adsorbent	Radionuclide	Mechanism	pH	Time (h)	Adsorption capacity (mg/g)	Removal efficiency (%)	Ref.
Ti_3C_2Tx	Sr^{2+}	Ion exchange, electrostatic interactions, and complexation	7	0.5	172	100	(Rethinasabapathy et al., 2021)
Ti_3C_2Tx	Cs^+	Ion exchange, electrostatic interactions	6	0.016	25.4	75	(Khan et al., 2019)
Ti_3C_2Tx	Cs^+	Ion exchange	7	1	148	85	(Jun et al., 2020)
$Ti_3C_2(OH)_2$	U^{6+}	Surface complexation, hydrogen bonding, and chemosorption	–	–	595	–	(Zhang et al., 2016)
V_2CTx	U^{6+}	Inner-sphere complexation	5	50	175	–	(Wang et al., 2016)
Ti_3C_2Tx	U^{6+}	Heterogenous adsorption	5	–	214	54.5	(Wang et al., 2017)
Ti_3C_2Tx	U^{6+}	Chemosorption	5	2.5	165.43	–	(Xie et al., 2022)
Ti_3C_2-AO-PA	$[UO_2(CO_3)_3]^{4-}$	Surface complexation	8.3	2	81.1	–	(Zhang et al., 2023)
Ti_3C_2@FeS-PDA/PEI	U^{6+}	Complex formation and ion exchange	5	–	88.5	100	(Liu et al., 2023)
Ti_3C_2Tx/PAN	U^{6+}	Chemosorption and surface complexation	6	36	1.32	93	(Xu et al., 2023)
Ti_3C_2Tx	Th^{4+}	Inner-sphere complexation	4	12	213.2	98	(Li et al., 2019)
Fe_3O_4@Ti_3C_2-PDA/OA	Th^{4+}	Chemosorption and increased d-spacing	3	2	203	83	(Lim et al., 2022)
Na-Ti_3C_2Tx K-Ti_3C_2Tx	Eu^{3+}	Hydrogen bonding and electrostatic interactions	12	4	222 203	95	(He et al., 2019)
Ti_3C_2Tx	Eu^{3+}	Ion exchange	6	3	118	97	(Yan et al., 2022)
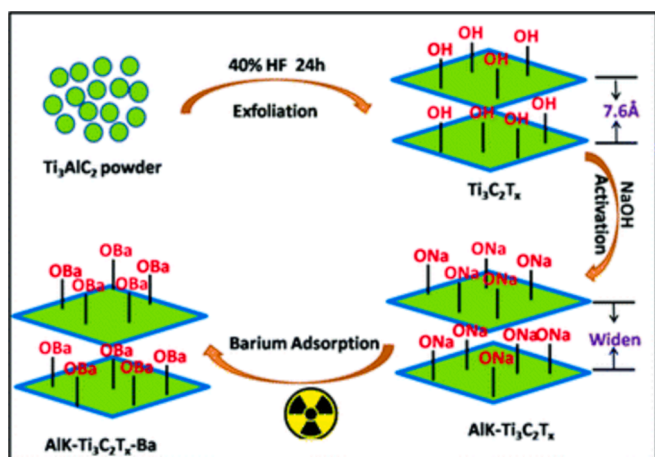
Fig. 10. Schematic illustration of the adsorption of barium ions (Mu et al., 2018).

ability of Ti_3C_2Tx MXene to remove Ba^{2+} and Sr^{2+} ions from model fracking wastewater. The negatively charged MXene surface caused effective bimetallic barium and strontium ion adsorption via electrostatic interactions, with a maximum adsorption capacity reaching 180 and 225 mg.g^{-1} for barium and strontium within 60 min. Additionally, the Ti_3C_2Tx MXene maintained excellent stability and reusability for four consecutive cycles of operations. Recently, a post-intercalation strategy was developed to intercalate POSS-NH$_2$ into Ti_3C_2Tx MXene and was employed to sequester radioactive strontium from wastewater (Rethinasabapathy et al., 2021). The complete removal of Sr^{2+} was achieved within 30 min with an adsorption capacity of 172 mg.g^{-1} following the Freundlich adsorption isotherm.

Additionally, the MXene showed outstanding reusability by maintaining 93 % of its initial adsorption capacity after three cycles. The increased adsorption capacity was attributed to the increased interplanar distance allowing the strontium ions to get adsorbed between the layers, complexing NH$_2$ groups having high affinity for Sr^{2+} ions and the presence of surface functional groups. Thus, POSS-NH$_2$ MXene could be a potential candidate for removing strontium ions from aqueous media. Radioactive cesium (^{137}Cs), having a half-life of more than 30 years, is also one of the most toxic and hazardous radionuclides constantly emitting β and γ rays. Furthermore, Cs$^+$ ions are highly mobile and highly soluble in water. Since the similarity in the hydrated radius of Cs$^+$ and K$^+$ readily replaces K$^+$ ions in the human body's cells. More significantly, it easily penetrates the food chains of humans and animals by ingesting tainted water, meat, fish, and plants, which in turn causes cellular damage and cancer (Shen et al., 2018).

Khan et al. (Khan et al., 2019) investigated the use of Ti_3C_2Tx MXene for the adsorption of Cs$^+$ ions from water samples. The adsorption followed the Freundlich isotherm model. A maximum adsorption capacity of 25.4 mg/g could be achieved within 1 min at room temperature. Here, the surface functional groups played a significant role in the sequestering of cesium ions. The adsorbent accumulated Cs$^+$ ions in its pores and interlayer gaps despite having many competing cations present because of its layered architecture. Recently, Jun et al. (Jun et al., 2020) compared the adsorption capacity of Ti_3C_2Tx and porous activated carbon for the adsorption of Cs$^+$ ions from radioactive waste. Despite having a higher surface area (470 m^2/g), activated carbon showed an adsorption capacity of only 80 mg.g^{-1}. The Ti_3C_2Tx MXene with a low surface area (10 m^2.g^{-1}) showed an outstanding adsorption capacity of 148 mg.g^{-1}. Compared to activated carbon, the enhanced adsorption capacity was attributed to the highly negatively charged MXene surface. According to the findings, the electrostatic interaction between the adsorbent and Cs$^+$ ions was an important factor in determining adsorption capacity. The change in the cesium removal rate in the

presence of other competing ions (K$^+$, Na$^+$, Mg^{2+}, and Ca^{2+}) and organic compounds (oxalic acid, citric acid, and sodium oleate) indicated that the Cs$^+$ ions get adsorbed according to the ion exchange mechanism. Traditional adsorbents, including graphene oxide, activated carbon, and MOF-based materials, have been used to remove uranium (Xie et al., 2022; Yu et al., 2019). However, Zhang et al. (Zhang et al., 2016), for the first time, reported the use of hydroxylated titanium carbide ($Ti_3C_3(OH)_2$) for the adsorption of uranyl with an adsorption capacity of 595 mg g^{-1}, which is the most effective material for removing uranium from the aqueous stream. The results showed that uranium ions preferably get adsorbed over deprotonated oxygen-containing functional groups compared to protonated ones.

Moreover, chemical interactions and hydrogen bonding were reported to be the major interactions between the uranyl ions and the MXene surface. Wang et al. (Wang et al., 2016) investigated using V_2CTx MXene to adsorb uranium from water samples with a significantly higher adsorption capacity of 175 mg.g^{-1}, higher than most previously reported inorganic adsorbents. The DFT study revealed that uranyl ions get attracted to hydroxyl groups present on the surface of V_2CTx MXene via forming a bidentate complex. The authors reported that the presence of functional groups like –OH, −F, and –O and the interfacial spacing are essential factors for uranium adsorption over the MXene surface. In another research, Wang et al. (Wang et al., 2017) reported a method for increasing the interlayer spacing of Ti_3C_2Tx MXene by exposing it to hydrated environments. The MXene soaked in DMSO showed enhanced adsorption capacity for U^{6+} ions with an adsorption capacity of 214 mg/g compared to untreated MXene. Recently, Xie et al. (Xie et al., 2022) synthesized chloroacetic acid-modified Ti_3C_2Tx MXene and investigated its potential for uranium adsorption. The prepared MXene showed an adsorption capacity of 165.43 mg g^{-1} following second-order kinetics following the Langmuir isotherm model, suggesting monolayer-chemisorption. Moreover, the adsorbent maintained an efficiency of 78 % till the fifth cycle, indicating good stability and reusability of the prepared material. Several modifications in the structure and the surface functional groups were also reported to enhance the adsorption capacity of the MXenes (Liu et al., 2023; Zhang et al., 2023; Xu et al., 2023).

Thorium (^{232}Th) is the best alternative nuclear fuel to uranium (^{233}U). Like other radioactive elements, thorium is also harmful to human health and the environment, causes irreversible damage to bone tissues, and is carcinogenic to humans. Therefore, removing thorium from water bodies is a great concern (Meng et al., 2022; Liu et al., 2022). Due to surface functional groups, layered structure, excellent dispersibility, and negatively charged surface, Li et al. (Li et al., 2019) investigated the adsorption of Th^{4+} over Ti_3C_2Tx MXene. The Ti_3C_2Tx MXene was prepared via the lithium salt method under dry and hydrated conditions. The highest adsorption capacity of 213.2 mg g^{-1} was achieved by hydrated Ti_3C_2Tx MXene attributed to the larger interlayer spacing allowing easy incorporation of Th^{4+} ions and inner sphere complexation originated from the interaction of Th^{4+} ions with the surface hydroxyl groups. Recently, Liu et al. (Liu et al., 2022) fabricated magnetically retrievable amidoxime-functionalized Mxene ($Fe_3O_4@Ti_3C_2$-PDA/OA) to effectively remove Th^{4+} ions from the aqueous phase. Fig. 11 illustrates the synthesis mechanism of $Fe_3O_4@Ti_3C_2$-PDA/OA. Similar to other results, a maximum adsorption capacity of 203 mg g^{-1} could be achieved by forming inner-sphere complexation with hydroxyl groups. The results suggested that the MXene could be a potential adsorbent for removing radioactive elements from wastewater.

Trivalent europium (^{152,154}Eu) is the unavoidable by-product of the nuclear fission reaction in the nuclear power plant discharged into the environment, causing major health hazards even at trace levels. As a result, the risks of radioactive contamination sparked research on the adsorptive removal of Eu^{3+} from water samples (Attia et al., 2021). Continuing this vein, Zhang et al. (Zhang et al., 2023) prepared hierarchical titanate nanostructures (HTN) by treating Ti_3C_2Tx with 1 M NaOH/KOH via an in-situ chemical conversion strategy and investigated

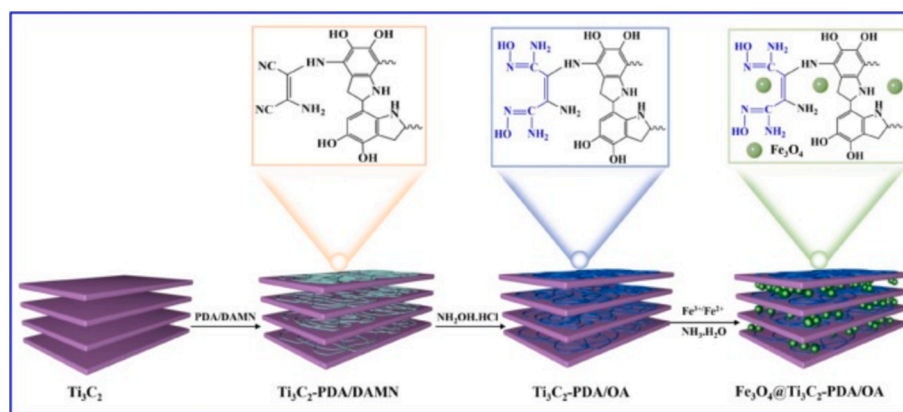**Fig. 11.** Schematic illustration of the synthesis process of Fe_3O_4@Ti_3C_2-PDA/OA MXene (Liu et al., 2022).

the adsorption of europium ions. An enhanced adsorption capacity of 222 mg g^{-1} was shown by Na-HTN compared to K-HTN (203 mg g^{-1}) via an ion ion exchange mechanism through electrostatic interactions and hydrogen bonding. The improved adsorption capacity was attributed to the increased interlayer spacing and a high hydration energy of Na$^+$, resulting in high diffusion and exchange of europium. Recently, Yan et al. (Yan et al., 2022) synthesized alkali-modified Ti_3C_2Tx MXene via a green strategy using citric acid as a surfactant rich in carboxylic and hydroxylic groups for the adsorption of Eu^{3+} ions. The prepared MXene showed an adsorption capacity of 118 mg g^{-1} following pseudo-second-order kinetics and Freundlich adsorption isotherm. Thus, the literature indicates that the MXene and its composites could be a state-of-the-art new-generation heterogeneous adsorbent for the remediation of radionuclides from nuclear waste.

2.5. Phenolic compounds

Organic phenolic pollutants in industrial wastewater cause environmental pollution and physiological damage. Researchers have developed a thermosensitive composite hydrogel made of MXene and PA to remove phenolic pollutants from industrial wastewater. The adsorptive removal of phenolic compounds by MXene-based materials at different conditions is presented in Table 6. MXenes-based composites were obtained via the in-situ polymerization of ionic liquids on their surfaces for superior mechanical strength and adsorption efficiency. A composite hydrogel with ILs is mechanically more efficient than one with MXene/PA composites, in addition to adsorptive properties. MXene flakes are attached to the surface by electrostatic interactions, making MXene more thermally stable and oxidation-resistant. A 45-day aging experiment using modified MXene (MXene-EMT) was insignificant after adding 1-Ethyl-3-methylimidazolium tetrafluoroborate (EMT). P-nitrophenol (4-NP) was very effectively absorbed by the composite hydrogels as prepared, demonstrating exceptional structural characteristics and high uptake efficiency. The highest uptake ability for sorbate was around 200 mg.g^{-1} at 298 K. After five sorption cycles, it continued at 90 % of its starting amount, often because of the presence of EMT. As per the experimental value, Freundlich isotherm and pseudo 2nd order kinetics were used (Lee et al., 2015).

The immobilization of laccase has been achieved using a proprietary ferroelectric 2D hybrid structure of MXene/NiFe-LDH/Fe$_3$O$_4$ (MNLF). MXene nanosheets were co-precipitated with layered double hydroxide (LDH) in situ to achieve surface functional groups. After that, magnetic nanoparticles Fe_3O_4 were introduced, which had excellent biocompatibility and the capacity to separate materials from substrates quickly. The surface of the MNLF was treated with a silane coupling agent. The immobilization of laccase from Trametes-Versicolor was carried out using functionalized MNLF. A 167.9 mg g^{-1} of enzymes were loaded into the nanocomposite (NC) material. The immobilized laccase demonstrated good stability in a wider pH 2–8, temperature range (25–60 °C), and organic solvent concentration 1–4 M range compared to free enzymes. 2, 4-Dichlorophenol exhibited a 55.5 % efficiency after seven cycles of repeated catalysis. Pyrocatechol demonstrated a 70.9 % efficiency after seven cycles. Laccase immobilization carriers are prepared in this study using a radically different strategy. Free laccase at room temperature does not display the same degree of stability as immobilized laccase. MNLF-laccase shows a higher activity at pH > 4 than at pH of 4.0, which is optimal for the free enzyme. In contrast, pH of 5 optimizes the immobilized enzyme (Li et al., 2023).

MXene/poly (N-isopropyl acrylamide) (MP) hydrogel heat-responsive adsorbents were developed to minimize phenolic toxicity and exhibit strong binding performance, superior thermoactive features, and no residual pollution. MXene also exhibited enhanced antioxidative properties and reactive functional groups due to the cyclodextrin fabrication technique. Solvent-based polymerization was used to make a heat-constrained hydrogel, which showed no significant changes after incubation in water for 21 days. 4-NP was removed by the sorbent after five adsorption–desorption cycles at room temperature, removing 82 % of 4-NP in a deionized medium at 308 K following five sorption–desorption cycles. As a result of heterogeneous layer-by-layer uptake and intra-molecular diffusion, the hybrid hydrogel could take up the target material spontaneously selectively. As a consequence of the electrostatic bonding between MXene and the polymer, the breakdown temperature of pure polypropylene acrylamide was increased to 633–723 K, implying that instantaneous dipole interactions between MXene planes and Si-O/Ti-C bonds significantly boosted the thermal stability of the hydrogel (Wang et al., 2022).

Molecular dynamics simulations, coarse-grained simulations, and DFT simulations have been conducted to investigate the adsorption intensity of phenol and chlorophenol on six novel 2D structure nanocomposites. Due to strong instantaneous dipole interactions between the lone pair of amine groups and phenol's p orbital electron cloud, the designed sorbent provides excellent uptake properties. A molecule like chlorophenol has an irregular electron density distribution due to atoms such as chlorine with electronegative properties. Thus, chlorophenol was more strongly attached to the adsorbents than phenols, resulting in bipolar connections. This resulted in greater chlorophenol adsorption by the MXene layers in the sorbents. Increasing the system temperature increases the contact area of sorbate molecules with water, reducing % removal due to a surge in monolayer displacements of MXene and weakening of hydrogen bonds. At room temperature, the experimental isotherm values fit the Freundlich isotherm and possess a maximum sorption capacity of 714.29 mg g^{-1} (Miri-Jahromi et al., 2022).

Table 6
Adsorptive removal of phenolic compounds by MXene-based materials.

Adsorbent	Sorbate	Feedstock	Temperature (K)	Equilibration time (h)	Isotherm	pH	Initial phenolic concentration (mg. L^{-1})	Characterization	Pore size/ μm	Adsorbent dosage (mg)	Sorption capacity (mg g^{-1})	Ref.
Au/g-CN$_x$	4-nitrophenol	Industrial wastewater	298	18	NA	3–6	4.2	TEMA/SAED/EDX/XPS/PXRD/UV-Vis	0.003	5	NA	(Bhowmik et al., 2015)
g-C$_3$N$_4$-Ni$_3$C	p-nitrophenol	Artificial effluent	298	3–12	NA	8	5	XRD/SEM/TEM/XPS/CV/EIS/BET	0.002	5–8	NA	(Liu et al., 2021)
Pd/Ti$_3$C$_2$X$_2$	4-Chlorophenol	Simulated wastewater	298–310	6–24	NA	6–7	25	HRTEM/SEM/TEM/XRD/FTIR/XPS/BET	0.005	4–5	NA	(Fan et al., 2018)
MXene/Poly (N-isopropyl acrylamide)	p-Nitrophenol	Industrial wastewater	298	2–24	Freundlich	5	15	FTIR/TEM/HRTEM /XRD/RS/XPS/SEM	50	2000	200.29	(Lee et al., 2015)
Cyclodextrin-MXene/Poly (N-isopropyl acrylamide)	4-nitrophenol Hydroquinone Phenol	Sewage effluent	308	2–48	Freundlich	6	28	AFM/FTIR/XPS/ZPA/XRD/SEM/DTGA/TGA	150	1000	162.0 62.5 141.0	(Wang et al., 2022)
Ag-Pd/g-C$_3$N$_4$	4-Nitrophenol	Deionized effluent	298	2–10	NA	7	150	SEM/EDX/EA/UV–Vis/XRD/EDX/XPS/TEM/FESEM/FT-IR	0.004	5000	NA	(Saravanakumar et al., 2022)
Ti$_2$C/MXene	Phenol	Simulated effluent	298–328	12	Freundlich	3–8	230	DFT/FESEM/UV-Vis/TGA/XRD/BET	0.019	450	714.29	(Miri-Jahromi et al., 2022)
MXene/NiFe-LDH/Fe$_3$O$_4$	2,4-dichlorophenol Pyrocatechol	Simulated wastewater	303	12	Freundlich	2–7	550–4500	SEM/TEM/BET/FTIR/XRD/XPS/VSM/UV–Vis/ CLSM/ZPA	1.2–2	125	167.9 130.0	(Li et al., 2023)

3. Mxene-based photocatalysts for removal of emerging pollutants

MXene is a strong candidate for a photocatalyst because it has ideal properties such as multiple active sites, outstanding chemical and thermal stability, high interlayer distance, higher electrical and thermal conductivity, and active functional groups compared to traditional 2D materials. The high photocatalytic efficiency of MXene in the degradation of organic contaminants is because of its large surface area (100–103). Because of their one-of-a-kind characteristics, such as high electrical conductivity, broad surface area, and variable surface chemistry, photocatalysts based on MXene have demonstrated tremendous potential for removing developing contaminants. MXene-based composites increase photocatalytic activity when mixed with semiconductors or metals. This is accomplished by enhancing charge separation and increasing the number of active sites to destroy pollutants. These materials are especially effective when exposed to visible light, which enables them to degrade hazardous pollutants such as medicines, dyes, and industrial chemicals in an energy-efficient manner. In addition, MXenes have a high degree of stability and may be reused, which makes them a good candidate for environmentally sustainable cleanup. They can address pollutants that are resistant to the usual water treatment procedures. Table 7 presents the performance of MXene-based photocatalysts for the degradation of heavy metals and various kinds of dyes.

3.1. Heavy metal ions

MXene-based photocatalysts have remarkable efficacy in eliminating heavy metal ions from polluted water, attributable to their superior conductivity, extensive surface area, and abundant surface functional groups. These features facilitate the robust adsorption of heavy metals such as Pb2$^+$, Hg2$^+$, and Cd2$^+$, promoting their photocatalytic reduction or oxidation upon light irradiation. MXenes improve charge separation and augment active sites when integrated with other materials, expediting metal ions' breakdown. Moreover, the stability and recyclability of MXene render it an exemplary choice for removing heavy metal ions in water treatment, providing an environmentally friendly and efficient method for mitigating environmental contamination. Li et al. (Li et al., 2022) utilized the cost-effective and environmentally friendly heat polymerization technique to develop the excellent g-C$_3$N$_4$/Ti$_3$C$_2$ MXene (CN/TC-2) based photocatalyst for the photo catalytical degradation of very intensive heavy metal U^{+6}. The adsorption capacity of the MXene-based composite is 14.05 times greater than the pristine MXene and graphene. Because the pristine MXene and graphene have lower Specific Surface area (SSA) than the g-C$_3$N$_4$/Ti$_3$C$_2$. Ti$_3$C$_2$ addition to CN substantially increased the adsorption selectivity for U^{6+}. Under both dim and bright lighting, they looked at how produced photocatalysts performed regarding photodegradation.

In contrast to dim light, the U^{6+} photodegradation activity was significantly altered by visible light. Researchers concluded that adding cocatalysts to substances like MXenes and TiO$_2$ would enhance the photocatalytic activity of catalysts to destroy U^{6+}. Chen et al. (Chen et al., 2024) effectively synthesized a 2D Ti$_3$C$_2$Tx/g-C$_3$N$_4$ composite utilizing an assembly technique. The substance possesses a stratified architecture, elevated conductivity, and chemical resilience. The amalgamation of MXenes with g-C$_3$N$_4$ enhanced the dispersion of g-C$_3$N$_4$ and inhibited agglomeration. This resulted in exceptional efficacy in eliminating U^{6+} from water, attaining complete removal within 120 min at a high reaction rate. It continued to be effective after five cycles. The material performed effectively at an ideal pH of 6.0 and a U^{6+} concentration of 10 mg/L, exhibiting no chemical alterations post-reaction, thereby demonstrating its stability. The study determined that superoxide radicals (.O$_2^-$) play a crucial role in reducing U^{6+} to U^{4+}. XPS research verified that Ti$_3$C$_2$Tx facilitated the reduction of U^{6+} and functioned as an electron sink, enhancing charge transfer. This work

Table 7

The performance of MXene-based photocatalysts for degrading heavy metals and various kinds of dyes.

MXene − based Photocatalyst		Name of Synthesizing Techniques	Targeted Contaminants		Light Source	Photo- catalytical removal Efficiency (%)	Ref
Name	Dosage (mg)		Pollutant	Conc. (mg.L^{-1})			
g-C$_3$N$_4$/Ti$_3$C$_2$	0.6	Heat polymerization	U^{6+}	0.1 mM	500 W Xe lamp	0.267 min^{-1}	(Li et al., 2022)
Ag/Ti$_3$C$_2$Tx-O	10	Depositing	U^{6+}	100	Visible Light	1257.6 mg g − 1	(Yu et al., 2022)
Bi$_2$MoO$_6$/Ti$_3$C$_2$	–	One-step hydrothermal method	Cr^{6+}	15	50 W white LED	100	(Zhao and Cai, 2020)
Ag/Ag$_3$PO$_4$/Ti$_3$C$_2$	50	Electrostatic Self-Assembly Technique	Cr^{6+}	20	300 W Xe lamp	61.0	(Zhao and Cai, 2020)
Ti$_3$C$_2$Tx/GO/EY	10	Depositing	Cr^{6+}	10	300 W Xe arc lamp	99.3	(Tunesi et al., 2021)
Bi$_2$WO$_6$/Nb$_2$CT$_x$	50	Hydrothermal	MB	15	500 W Xe lamp	92.7	(Cui et al., 2020)
TiO$_2$/Carbon	10	High-energy ball milling	MB	20	500 W Mercury lamp	85.7	(Li et al., 2018)
AgNPs/TiO$_2$/Ti$_3$C$_2$T$_x$	10	Hydrothermal	MB	10	simulated solar light	96	(Othman et al., 2021)
MXene/g-C$_3$N$_4$	500	wet impregnation method	MB	10	500 W halogen lamp	69.4	(Nasri et al., 2022)
handmade MXene (Ti$_3$C$_2$) MX-H	2.0	kitchen blender technique	MB	–	300 W visible light	98	(Pérez-Álvarez et al., 2022)
TiO$_2$/Ti$_3$C$_2$T$_x$	50	In-situ solvothermal	MO	10	500 W Hg lamp	90.5	(Chen et al., 2020)
TiO$_2$/Ti$_3$C$_2$T$_x$	20	In-situ solvothermal	MO	–	500 W Hg lamp	92	(Chen et al., 2020)
BPQDs/Ti$_3$C$_2$@TiO$_2$	50	Hydrothermal	MO	10	visible light irradiation	93	(Yao et al., 2020)
Ti$_3$C$_2$/TiO$_2$/CuO	100	Calcination	MO	20	300 W Xenon lamp	99	(Lu et al., 2017)
Ag/Ag$_3$PO$_4$/Ti$_3$C$_2$	50	Electrostatic Self-Assembly Technique	MO	20	300 W Xe lamp	93	(Sun et al., 2021)
TiO2/Ti$_3$C$_2$ heterostructure	40	Hydrothermal, Ion exchange, and Calcination	RhB	20	visible light irradiation	95	(Tran et al., 2021)
CdSQDs/BiO	20	Two-step precipitation deposition method	RhB	–	Solar light and visible light irradiation	82	(Kandi et al., 2017)
TiO$_2$/mp-Ti$_3$C$_2$T$_x$	–	In-situ solvothermal	RhB	–	500 W Xenon lamp	96	(Cheng et al., 2018)
TiO$_2$/Ti$_3$C$_2$T$_x$	5	In-situ solvothermal	RhB	15	300 W Hg lamp	80	(Miao et al., 2020)
C-TiO$_2$/ Bi$_4$NbO$_8$Cl	40	Calcination	RhB	10	300 W Xenon lamp	97.2	(Jiang et al., 2020)

presents innovative concepts for developing efficient photocatalysts for environmental remediation.

Zhao et al. (Zhao and Cai, 2020) combined Bismuth molybdate (Bi$_2$MoO$_6$) and Ti$_3$C$_2$ MXene by hydrothermal technique to synthesize the MXene-based Bi$_2$MoO$_6$/Ti$_3$C$_2$ nanostructure for the photocatalytic breaking of toxic environmental pollutant Cr^{6+} from wastewater that Cr^{6+} contaminated water. The enhanced photocatalytic performance of the Bi$_2$MoO$_6$/Ti$_3$C$_2$ nanostructure in pure Bi$_2$MoO$_6$ was explained using various characterization techniques, including HRTEM, BET, XRD, EDS, PL, EIS, EPR, TEM, SEM, and DRS. Under sunlight, the higher degradation efficiency of the synthetic MXene-based photocatalyst reached 100 % in 60 min. The photocatalytic degradation effectiveness of the Bi$_2$MoO$_6$/Ti$_3$C$_2$ photocatalyst is 11.2 times more than that of pure Bi$_2$MoO$_6$, based on a scientific study. This finding creates new opportunities for researching low-cost photocatalysts that work well.

3.2. Dyes

MXene-based photocatalysts exhibit remarkable efficacy in eliminating dye ions from wastewater, attributed to their superior conductivity, extensive surface area, and capacity to promote efficient charge separation. MXene-based composites, when integrated with other semiconductor materials, augment photocatalytic degradation by facilitating the decomposition of dye molecules under visible light. These compounds can adsorb and decompose many hazardous dyes, including methylene blue, rhodamine B, and crystal violet, frequently present in industrial effluent. MXenes have distinctive characteristics, including elevated electron mobility and diverse surface chemistry. These facilitate rapid degradation and enhanced stability throughout numerous cycles, rendering them advantageous for sustained dye removal in water

treatment applications. Cui et al. (Cui et al., 2020) synthesized the extremely thin Bi$_2$WO$_6$/Nb$_2$CTx nanoparticles using an environmentally friendly hydrothermal procedure to treat RhB and RhB from wastewater. The architectural functionality of Nb$_2$CTx, Bi$_2$WO$_6$, and Bi$_2$WO$_6$/Nb$_2$CTx nanostructures has been assessed using a variety of characterization approaches, including lateral size, zeta potential, XRD spectra, and mechanical integrity.

Because of its outstanding thermal, chemical, and photostability, bismuth tungstate (Bi$_2$WO$_6$) is one of the most popular photocatalysts for dye degradation. Due to "their slow dissociation of photogenerated electron-hole pairs, its employment is severely constrained by their poor photodegradation ability. One of the strongest ingredients for accelerating the dissociation of photogenerated electron-hole pairs is MXene. Thus, relative to Bi$_2$WO$_6$, Bi$_2$WO$_6$/Nb$_2$CTx photocatalysts demonstrated remarkable photodegradation efficiency for MB, 92.7 %, when Bi$_2$WO$_6$ and Nb$_2$CTx created a composite to change their photocatalytic features. Compared to pristine Bi$_2$WO, the photocatalysis kinetics of Bi$_2$WO$_6$ mixed with two weight percent Nb$_2$CTx for MB appear to be the value of 0.0285 min^{-1}, which is twice as high. This research showed that 2D Nb$_2$CTx is a useful co-catalyst for enhancing photocatalyst photocatalytic degradation performance and producing an efficient photocatalyst with 2D/2D nanomaterials.

Tran et al. (Tran et al., 2021) synthesized the MXene-based TiO$_2$/Ti$_3$C$_2$ heterostructure for the photocatalytic degradation of RhB synthetic dye to treat wastewater and save humans and aquatic animals. TiO$_2$/Ti$_3$C$_2$ nanostructure nanorods were used in a novel way to create microscale safflowers. Beginning with 2D Ti$_3$C$_2$Tx MXene, a sequential in-body transition was used to create this one-of-a-kind architecture. Ion exchange, heat treatment, hydrothermal oxidation, and alkalization were intricately coupled stepwise for the conversion. After those

procedures, TiO_2/Ti_3C_2 nanostructures developed laterally from the layer-structured MXene sheets broken into nanomaterials. It was discovered that the heat treatment conditions significantly impacted the heterostructures' geometry, structural elements, and characteristics. The catalytical photo activity of synthesized MXene-based TiO_2/Ti_3C_2 photocatalyst was 95 %. The TiO_2/Ti_3C_2 heterostructures produced under ideal conditions exhibited semiconductor-like behavior, in contrast to Ti_3C_2Tx MXene. The excellent heterostructure photocatalytic activity was also exhibited. Chen et al. (Chen et al., 2020) synthesized the TiO_2/MXene heterostructure by employing the low price and echoloving in-situ solvothermal procedure for the photo-catalytical degradation of MO in textile-contaminated water. Ti_3C_2Tx is used as a cocatalyst to increase the photocatalytic degradation ability of TiO_2 by capturing the photoexcited. By employing C_3H_8O molecules, the findings from experiments show that TiO_2 NPs are uniformly distributed over the Ti_3C_2Tx surface. The maximal photocatalytic activity of the TiO_2/ Ti_3C_2Tx- C_3H_8O nanostructure was 90.5 % during 75 min of Hg illumination, which is 57.9 % higher than the capacity of the pure Tio_2 nanoparticles. Due to the synergistic effects of $Ti_3C_2T_x$ and TiO_2, the maximum photocatalytic lowering capability was attained. First, they synthesized the MXene Ti_3C_2Tx from the original material Ti_3AlTx by removing Al via echo enemy chemical-based HF etching procedure. After synthesizing MXene, they employed a friendly solvothermal procedure to synthesize the TiO_2/MXene heterostructure for MO adsorption, as shown in Fig. 12.

This section concludes that MXene-based photocatalysts are successful in dye degradation, emphasizing improving photocatalytic performance by integrating MXenes with other semiconductor materials. Research indicated that incorporating MXenes, namely Ti_3C_2Tx, markedly enhanced electron-hole separation, thus increasing photocatalytic efficiency. This improvement was apparent in degrading dyes such as methylene blue and rhodamine. The production of new heterostructures, including Bi_2WO_6/Nb_2CTx and TiO_2/Ti_3C_2, demonstrated enhanced photodegradation performance relative to their pristine counterparts, achieving up to 95 % degradation efficiencies. The findings highlight the function of MXenes as co-catalysts that improve photocatalyst efficiency through their distinctive 2D architecture, elevated conductivity, and interactions with other substances. The findings suggest that MXenes possess significant promise for efficiently eliminating dye contaminants in water treatment applications.
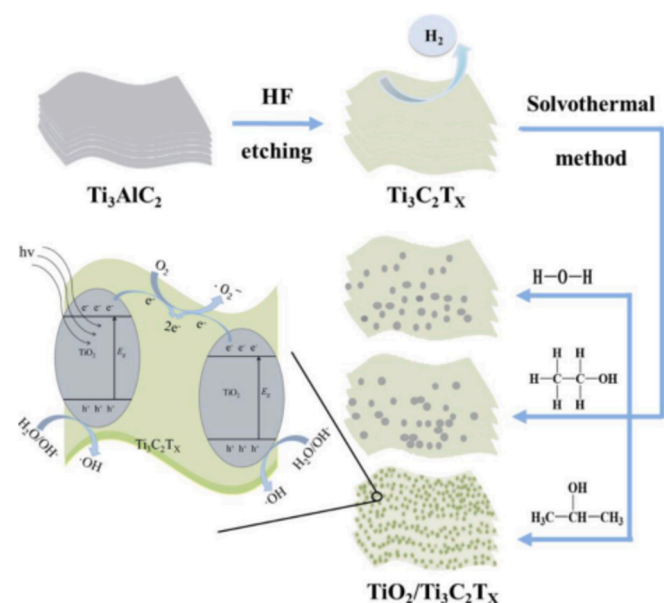

Fig. 12. Synthesizing of TiO2/MXene procedure and MO photodegradation procedure (Chen et al., 2020).

3.3. Pharmaceuticals

For the photocatalytic removal of pharmaceutical compounds from the water, many 2D nanomaterials are available. However, after a thorough review of the literature, we can conclude that MXene-based nanomaterials have superior properties to all other 2D nanomaterials such as layered double hydroxides (LDH), transition metal oxides (TMOs), graphene and transition metal dichalcogenides (TMDs) (Kemp et al., 2013; Bhattacharjee et al., 2022). MXene-based photocatalysts for the photo-catalytic degradation of various pharmaceutical compounds are presented in Table 8.

To improve the photocatalytic properties of MXenes, they may be hybridized with other substances such as MOFs, polymers, metal oxide, graphene, etc. Because of their interesting properties, such as adjustable band gap (0.92–1.75 eV), high structural stability, non-toxicity, high interlayer spacing, and hydrophilicity, MXene-based photocatalysts are used for the removal of a variety of pharmaceutical compounds and antibiotics from the aqueous system. MXenes can potentially increase the photo-catalytic efficiency of their composites when used as co-catalysts due to their distinctive lamellar nanostructures and excellent conductivity (Feng et al., 2021; Javaid et al., 2022).

In recent work, a multi-functional adsorbent photo-catalyst MXene-TiO_2 composite was synthesized using a rapid microwave hydrothermal method to remove enrofloxacin from water (Sukidpaneenid et al., 2023). Moreover, the layered structure of MXene improves photocatalytic efficiency by increasing the charge carrier separation and acting as a robust support (Kuang et al., 2020). MXenes showed great potential in the photodegradation of several pharmaceutical compounds and antibiotics. MXenes may also be utilized as a host substance to improve the catalytic activity of certain co-catalysts. Pharmaceuticals have been successfully degraded using MXene-based photo-catalysts synthesized using various techniques, including chemical vapor deposition, sol-hydrothermal method, anodization, and in-situ reductive deposition method (Ihsanullah, 2022).

For the degradation of tetracycline hydrochloride (TC-HCl), NH_2-MIL-125(Ti)(TiO_2)/Ti_3C_2 dual heterojunction exhibited 11.5 times higher degradation efficiency than pristine MIL-125-NH_2 under the irradiation of visible light (Wu et al., 2020). The enhancement in the photocatalytic activity of the heterojunction is due to the incorporation of Ti_3C_2, which increased the charge transfer. When NH_2-MIL-125 (Ti) is used, the TC-HCl degradation process comprises the generation of ˙OH by water oxidation, and electrons are excited from the valence band ‐ to the conduction band. Similarly, electron migration occurs across the hetero-junction from the NH_2-MIL-125 (Ti) CB to the TiO_2 CB and subsequently from TiO_2 to Ti_3C_2. The Schottky junction captures the photoinduced electrons transported to the Ti_3C_2 surface for electron-oxygen reduction (Ihsanullah, 2022; Wu et al., 2020).

The advanced oxidation process is also used to remove pharmaceuticals using MXene-based nanocomposite. Ranitidine is a toxic pharmaceutical compound, the nitrosamine dimethylamine (NDMA) source. Novel Ti_3C_2-based MXene nanosheets adorned with zero-valent iron particles ($nZVIPs@Ti_3C_2$ nanosheets) were synthesized by Ma et al. (Ma et al., 2021) to increase the catalytic activity of peroxymonosufate. This synthesized Ti_3C_2-based nanosheet exhibited notable degradation efficiency for quickly removing ranitidine by an advanced oxidation process under mild reaction conditions. The high stability of the catalyst is mostly due to the fast transfer of charge between the electron-rich active centers (Fe and Ti), with ranitidine degradation being carried out by $SO_4^{\cdot-}$ and OH⁻ derived from PMS activation, with $SO_4^{\cdot-}$ being the predominant contributor. Another study reported the synthesis of a highly photoactive Z–scheme of graphene layers anchored TiO_2/g–C_3N_4 (GTOCN) photocatalyst by a step-in-situ calcination process. It is used for photocatalytic degradation of two pharmaceutical compounds, ciprofloxacin and tetracycline (Wu et al., 2020). This MXene-based photocatalyst exhibited a degradation efficiency of 83.5 % of tetracycline

Table 8

Photocatalytic degradation of the MXene-based photocatalyst for the degradation of the pharmaceutical compounds.

MXene based photocatalyst	Pharmaceutical compounds	Light source	Degradation efficiency	Reactive species	Time (min)	Ref.
NH_2-MIL-125(Ti)(TiO_2)/Ti_3C_2	Tetracycline hydrochloride (TC-HCl)	Visible light ($\lambda > 420$ nm)	82.80 %	$\cdot OH$ and H^+	60	(Wu et al., 2020)
nZVIPs@Ti_3C_2 nanosheets	Ranitidine	–	–	$SO_4^{\cdot-}$ and OH^-	–	(Ma et al., 2021)
graphene layers anchored TiO_2/g–C_3N_4	Tetracycline Ciprofloxacin	Visible light	83.5 % 61.7 %	$O_2^{\cdot-}$ and OH^-	80 60	(Wu et al., 2020)
2D/2D/2D CuO-MXene-OCN S-scheme heterojunction	Tetracycline hydrochloride Metoprolol Diclofenac	Solar light	98.2 % 75.6 % 92.6 %	$\cdot O_2^-$ and $\cdot OH$	60	(Dai et al., 2022)
$CuFe_2O_4$/MXene	Sulfamethazine	Visible light	59.4 %	$\cdot OH$	60 min	(Cao et al., 2020)
Few-layer MXene/alkaline g-C_3N_4	Tetracycline (TC-HCl)	Visible light ($\lambda > 420$ nm)	77 %	$\cdot O_2^-$, $\cdot OH$, h^+, and e^-	60	(Yi et al., 2020)
MXene-Ti_3C_2/MoS_2	Ranitidine	LED lamp (25 W, Trusttech PLS-SXE 300	88.4 %	h^+, $\cdot OH$ and $\cdot O_2^-$	60	(Zou et al., 2021)
Ti_3C_2/TiO_2/BiOCl	Tetracycline	500 W Xe lamp	100 %	$\cdot OH$ and $\cdot O_2^-$	120	(Liu et al., 2020)
Ti_3C_2/g-C_3N_4	Levofloxacin	300 W Xe lamp	72 %	–	30	(Liu et al., 2021)
ZnO/TiO_2-nanorod MXene	Ceftriaxone sodium	Solar light	99.4 %	–	–	(Abbas et al., 2022)
g-C_3N_4/BiOBr/MXene	Tetracycline hydrochloride	Visible light	99 %	h^+, $\cdot O_2^-$, $^1O_2$ and $\cdot OH$	–	(Gao et al., 2023)

within 80 min of visible light irradiation and 61.7 % of ciprofloxacin within 60 min of visible light irradiation. The electron spin resonance and free radical experiments confirmed that the active radicals responsible for the degradation of pharmaceuticals are $O_2^{\cdot-}$ and OH^-. Schematic of the photocatalytic process for organic pollutants degradation over Z-scheme heterojunction of GTOCN3 under visible light irradiation, as shown in Fig. 13. Dai et al. (Dai et al., 2022) synthesized 2D CuO nanosheets by drip method. They introduced the layered MXenes as the charge transfer bridges into CuO and O-doped g-C_3N_4 nanosheets to

prepare a 2D/2D/2D CuO-MXene-OCN S-scheme heterojunction. The CuO-MXene-OCN heterojunction exhibited higher photocatalytic efficiency than the CuO-OCN heterojunction because of the close interaction between the interfaces. This MXene-based photocatalyst exhibited a degradation efficiency of 98.2 % for tetracycline hydrochloride, 75.6 % for metoprolol, and 92.6 % diclofenac within 60 min of solar light irradiation.

Cao et al. (Cao et al., 2020) reported the use of novel $CuFe_2O_4$/ MXene hierarchical heterostructure for the photocatalytic degradation
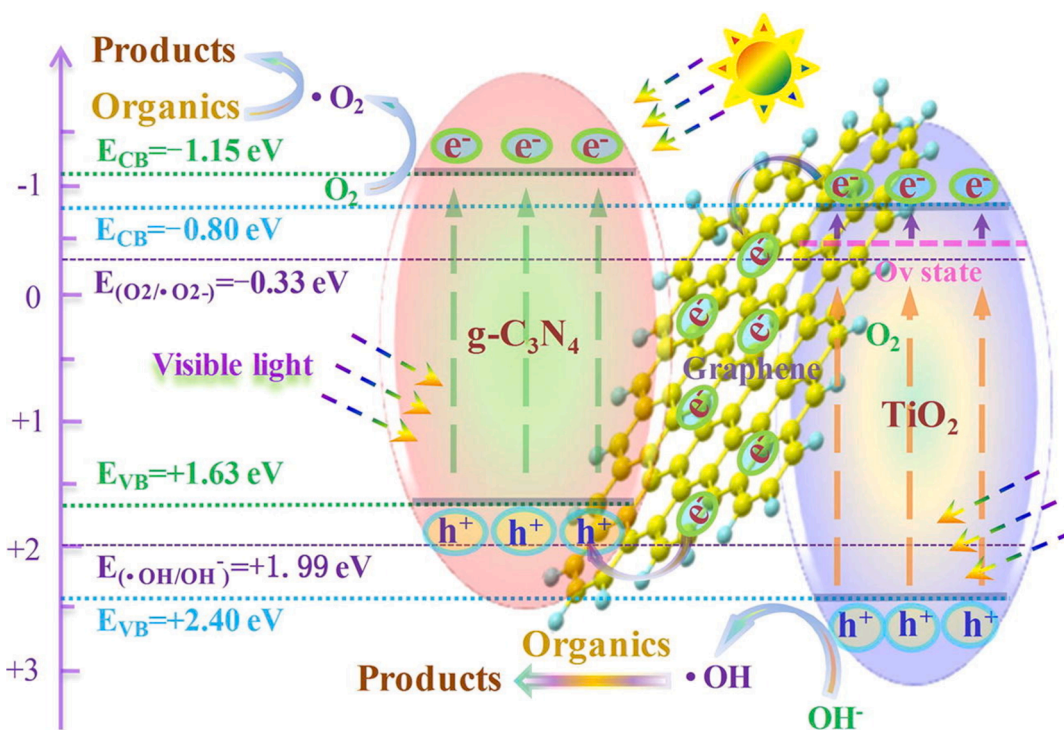

Fig. 13. Schematic of the photocatalytic process for organic pollutants degradation over Z-scheme heterojunction of GTOCN$_3$ under visible light irradiation (Wu et al., 2020).

of the antibiotic sulfamethazine (SMZ) up to 59.4 % under the irradiation of visible light, which is attributed to the increased lifespan of carriers and charge transfer in the composite. The visible light activates the $CuFe_2O_4$ (CFO) photocatalyst with a band gap of 1.43 eV. The electrons are excited from the valence band to the conduction band. The photo-generated electrons are shifted from the $CuFe_2O_4$ to the 2D Ti_3C_2. However, many electrons emerge at the Fermi level in the Ti_3C_2 flakes. Moreover, because of its substantial specific surface area, Ti_3C_2 may provide many active adsorption sites. Furthermore, during photocatalysis, the active material may potentially adsorb the sulfamethazine, a toxic antibiotic.

3.4. Radionuclides

Several methods have been used to remove radioactive nuclides from wastewater and aqueous solutions, such as adsorption, chemical precipitation, electrochemical treatment, membrane filtration, reverse osmosis, and photodegradation (Zhang et al., 2019; Rana et al., 2013). In practical applications, conventional adsorption and ion exchange methods using nanomaterials have several drawbacks, such as poor interaction with radionuclides. However, most published reduction techniques involve high reagent usage and readily produce secondary waste. A novel solution to the problems mentioned above is semiconductor photocatalysis. This green method uses semiconductor photocatalysts under solar light irradiation to reduce toxic heavy metals (Lu et al., 2017). However, very little work has been reported on the photoreduction of toxic radionuclides using MXene-based nanomaterials. A unique and effective method of U^{+6} transformation is the photocatalytic reduction of U^{+6}, in which the free U^{+6} will first attach to the surface of the photocatalysts. Then, the generated photoelectrons reduce the U^{+6} to U^{+4}. Yu et al. (Yu et al., 2022) synthesized an MXene-based photocatalyst by the deposition of Ag nanoparticles on $Ti_3C_2T_x$ with profuse binding sites for U(VI) ($Ag/Ti_3C_2T_x$-O). Many characterization techniques were used to comprehend the physicochemical characteristics of the synthesized MXene-based composite. The photocatalytic activity of $Ag/Ti_3C_2T_x$-O photocatalyst for the photoreduction of U^{+6} was found to be 1257.6 mg g^{-1} in 2 h of the treatment process, which is 11 times higher compared to conditions with the absence of light. This research advances our knowledge of the mechanism behind U^{+6} reduction. It proposes a strategy for developing efficient catalysts for U^{+6} photocatalytic reduction.

Li et al. (Li et al., 2022) developed an MXene-based photocatalyst by modifying g-C_3N_4 with oxidized MXene (Ti_3C_2). Modification of graphitic carbon nitride (g-C_3N_4) with MXene (Ti_3C_2) enhances the adsorption capacity for U^{+6}, separation efficacy of photo-generated e$^-$/h$^+$, and optical absorptivity which results in the enhancement of photoreduction of U^{+6}. The reaction constant for reducing U^{+6} to U^{+4} using the g-C_3N_4/MXene (0.267 min^{-1}) is 14.05 times higher than the pristine g-C_3N_4 (0.019 min^{-1}). TiO_2 was formed on the surface of Ti_3C_2, and a Z-scheme heterojunction was developed. This heterojunction helps effectively separate charge carriers and improves the photocatalytic activity of the g-C_3N_4 composite. Reduction of U^{+6} to U^{+4}

occurs during the photocatalytic reaction, generating deposits of UO_{2+x} (x < 0.25) with $^{\cdot}O_2^-$ serving as the primary reduction species (Fig. 14(a)).

A novel $Ti_3C_2/SrTiO_3$ heterostructure was synthesized by partial oxidation of multi-layered Ti_3C_2 precursor depending on the simple crystallography. It was used as a photocatalyst for the photocatalytic reduction of U^{+6} (Solangi et al., 2023). This MXene-based composite showed an excellent photocatalytic efficiency of 77 % for removing UO_2^{2+} ions, which is 38 times higher than pure $SrTiO_3$ (Fig. 14(b)). The multi-layered Ti_3C_2 improved charge transfer while preventing electron recombination in the conduction band. This study revealed the alluring possibility of generating doped perovskite oxide materials based on MXene (Ti_3C_2) and using sunlight.

3.5. Phenolic compounds

Phenol, which is frequently utilized in industries such as the chemical and pharmaceutical industries, poses significant threats to both the environment and human health when it is released into water because it is poisonous and resistant to breakdown via microbes. One of the most important things is to achieve its complete mineralization using procedures that are energy efficient. Co-catalyst modification, which involves using metals such as platinum, gold, cobalt, or manganese, improves charge transfer and redox kinetics, increasing the effectiveness of photocatalytic reactions. Conventional co-catalysts, on the other hand, are either expensive, difficult to manufacture, or unstable. Ti_2C_2 MXene, on the other hand, is a two-dimensional material with great conductivity and exposed active sites. It has garnered interest due to its capacity to increase photocatalysis. The combination of semiconductors with MXene improves charge separation and raises photocatalytic efficiency, making it a potentially useful option for phenol degradation.

Zhang et al. (Zhang et al., 2024:) synthesized the BT composite photocatalysts with different Ti_3C_2 mass loadings by a hydrothermal technique to improve the separation of photogenerated carriers and phenol degradation. Characterization experiments validated the successful synthesis of a $BiVO_4/Ti_3C_2$ composite exhibiting good shape and carrier separation, particularly in the BT-3 sample. Studies on the breakdown of phenol demonstrated that PMS activation and Ti_3C_2 doping markedly enhanced efficacy, with BT-3 attaining an 87.2 % degradation rate within 60 min (rate constant k = 0.02537 min^{-1}). Elevated PMS dosage improved decomposition; however, increased starting phenol concentrations diminished effectiveness, with neutral pH being best. The catalysts exhibited commendable stability over ten cycles. Experiments on free radical capture indicated $SO_4^{\cdot-}$ as the paramount species in the breakdown of phenol. This study presents novel approaches for developing effective photocatalysts to degrade persistent organic pollutants such as phenol.

Hussain et al. (Hussain et al., 2024) synthesized pure $CdAl_2O_4$ and Ag–$CdAl_2O_4$ employing coprecipitation and Ag–$CdAl_2O_4$/MXene-based composite material via ultrasonication. The photocatalytic efficacy of these substances was evaluated by degrading contaminants such as crystal violet and phenol. The composite demonstrated markedly improved performance, decomposing approximately 95 % of crystal
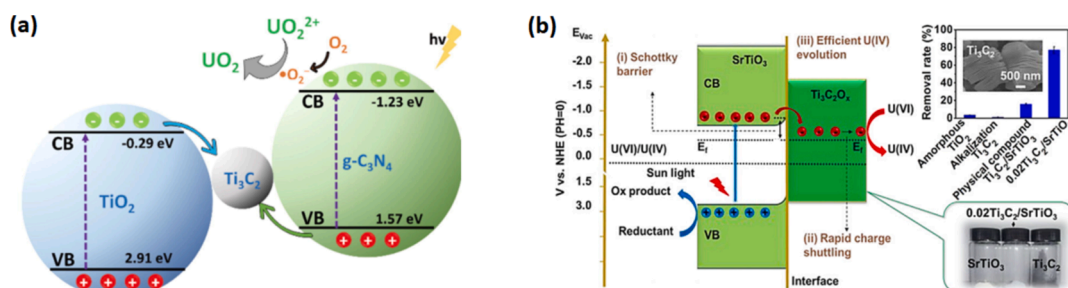

Fig. 14. Mechanism of photocatalytic reduction of U^{+6} by (a) g-C_3N_4/Ti_3C_2 heterojunction, (b) Ti_3C_2/$SrTiO_3$ heterostructure (Li et al., 2022).

violet and around 84.6 % of phenol. The enhancement results from the interaction between silver doping and the MXene-based composite, which improves visible light absorption and charge carrier separation. Scavenging tests found active species responsible for pollutant degradation, and the process adhered to first-order kinetics. The findings underscore the composite's significant potential for decomposing organic contaminants.

In-situ preparation of composite photocatalysts using MXene − $Ti_3C_2T_x$ was carried out using decahedral anatase particles and titanium carbide. Magnetron sputtering was employed to prepare Fe-modified composites containing decahedral anatase particles coupled with Ti_3C_2, which were applied to the photocatalytic degradation of phenol. UV–VIS light was used to evaluate photocatalytic activity during phenol decomposition. 20 mg/dm^3 of phenol was applied at an initial pH of 6.8. In an air-supplied quartz reactor, photodegradation reactions were conducted. After introducing the photocatalyst to the reactor, an aqueous phenol solution was introduced and stirred continuously for 30 min. The reaction was kept in the dark for 30 min to achieve equilibrium before exposure to UV light. The irradiation source was an Xe lamp of 300 W. Aliquots of samples were collected at 0, 20, 40, and 60 min after irradiation. This experiment used 0.2 m syringe filters to separate photocatalyst particles from the solution. Phenol photodegradation progress and intermediate concentrations were analyzed through reverse-phase high-performance liquid chromatography. Tert-butanol was added to investigate the sorbent's capability to remediate free radicals and detect surface structural changes (Grzegórska et al., 2021).

An electrostatically driven self-assembly strategy successfully synthesized an Ag_3PO_4/Ti_3C_2 MXene Schottky catalyst. In the etching solution used for fabricating Ti_3C_2 MXene, Ti_3AlC_2 was immersed in Ti_3C_2. HCl solution of 20 mL was mixed with 3.35 g NaF and kept at 60 °C for 12 h with continuous stirring to prepare the etching solution. In the following steps, the residue was washed repeatedly with diluted hydrochloric acid, ethanol, and deionized water before centrifugation was performed to separate them. A vacuum at 80 °C was used to dry the obtained MXene powder. 2,4 DNP was photodegraded with visible photons under a given interval, and 1 mL of the suspension was centrifuged to separate it from the suspension. Schottky contact results show electron transfer from Ag_3PO_4 to the Ti_3C_2 surface by XPS. The Mott-Schottky measurements indicate that Ag_3PO_4 has a higher Fermi level than Ti_3C_2. Therefore, energies flow from Ag_3PO_4 to Ti_3C_2 because of the Fermi level difference between Ti_3C_2 and Ag_3PO_4, which leads to band bending and Schottky junctions. Furthermore, the efficient photocatalytic reduction of Cr^{6+} was achieved in an AgI/Ti_3C_2 system, demonstrating Ti_3C_2's versatility as an electron sink in various environments (Cai et al., 2018). The band theory was employed to elucidate the interaction between Ti_3C_2 and Ag_3PO_4 at their contact. The Fermi level, indicative of the energy state of electrons, is elevated in Ag_3PO_4 relative to Ti_3C_2. Due to this disparity, electrons transfer from Ag_3PO_4 to Ti_3C_2 until their Fermi levels equilibrate. This movement induces the bending of energy bands, forming a Schottky junction, a specific type of interface between a metal and a semiconductor. A Schottky junction is established at the interface of Ag_3PO_4 to Ti_3C_2, facilitating unidirectional electron flow. Ti_3C_2 functions as an "electron sink," signifying its ability to capture electrons. The built-in electric field generated at the junction enables this phenomenon. Consequently, the electrons and holes (carriers) produced during the photocatalytic process are more efficiently segregated, inhibiting their recombination. This enhanced separation improves photocatalytic efficiency by facilitating greater electron involvement in processes such as pollutant breakdown. The detailed mechanism of the degradation of the phenol by the Ag_3PO_4/Ti_3C_2 MXene Schottky catalyst is presented in Fig. 15. Table 9 shows the degradation of phenolic compounds by MXene-based photocatalysts.

In a nutshell, MXene-based photocatalysts exhibit significant potential for eliminating phenolic compounds owing to their superior conductivity, extensive surface area, and capacity to improve charge separation. MXene-based composites demonstrate markedly enhanced photocatalytic activity under visible light when integrated with other materials, as discussed above. These composites effectively decompose phenolic chemicals, leveraging improved light absorption and the inhibition of charge recombination, rendering them extremely suitable for environmental remediation.

4. Mxene-based membranes for removal of emerging pollutants

Membrane separation has drawn much interest as a prospective water treatment method because of its reduced energy consumption, low running costs, environmental friendliness, and combined capabilities. Numerous advantages of membrane technology exist, including production uniformity and a lower carbon footprint (Raheem et al., 2022).

4.1. Heavy metal ions

MXene can efficiently collect heavy metal ions like mercury Hg^{2+}, copper Cu^{2+}, lead Pb^{2+}, etc. The specific pollutants are also absorbed by MXene when its surface groups interact with impurities (Bai and Guan, 2023). The functionalization of MXenes can increase stability while simultaneously promoting sustainability and the elimination of heavy metals from water and wastewater. The hydrothermal process effectively synthesizes the magnetic $Ti_3C_2T_x$ MXene (MGMX) composite. Table 10 presents the synthesizing techniques for reacting parameters and the refection performance of MXene-based membranes.

$Ti_3C_2T_x$ composite has a maximal Hg^{2+} adsorption capacity of 1128.41 mg/g, and lead can be successfully removed throughout a wide pH range (Fu et al., 2020). After five desorption/ adsorption operations, high extraction efficiency was maintained, and MGMX nanomaterials were successfully reused. Likewise, Hg^{2+} removal is accomplished using 2D $Ti_3C_2T_x$ MXene core–shell sodium alginate (SA) aerogel spheres (MX-SA) (II). The primary methods are ion exchange, electrostatic interaction, and complex formation. MX-SA has a saturation adsorption capability of 932.84 mg/g for Hg^{2+} (Fu et al., 2020). Removing Hg^{2+} out of an aqueous phase requires the synthesis of a multidimensional oxygen-functionalized Ti_3C_2 (MTi_3C_2) nanostructure. Fig. 16 shows that M demonstrated strong selectivity- Ti_3C_2, particularly a highly effective removal rate to Hg^{2+} of 4806 mg g^{-1}. In addition, it also displayed a pH range of 3–12. The MoS$_2$/MXene nanostructures had outstanding Hg^{2+} extraction capability, demonstrating that the elimination efficiency of MXene may be enhanced through manufacturing, functionalization with suitable materials, and structural modification. As a result, it can be used to rehabilitate the ecosystem successfully (Shahzad et al., 2020).

Unique architectures and a wealth of MXene-based compounds have stimulated adsorbents to eliminate Cu^{2+} from wastewater. Delaminated (DL)-$Ti_3C_2T_x$ exhibits strong capability for removing Cu^{2+}; the sorption

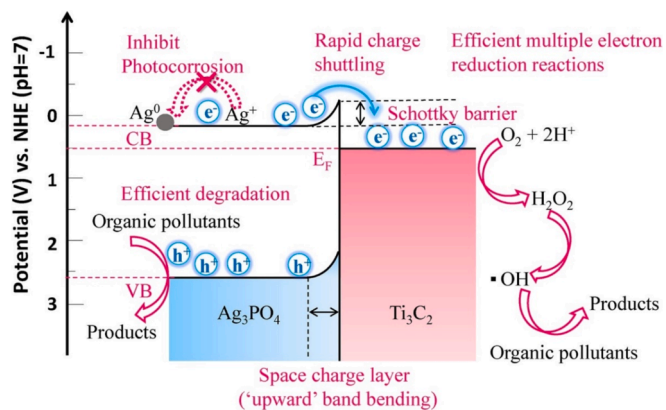**Fig. 15.** Photocatalytic degradation of phenolic compounds by the Ag_3PO_4/Ti_3C_2 MXene-based Schottky catalyst MXene (Cai et al., 2018).

Table 9
Degradation of phenolic compounds by MXene-based photocatalysts.

Sorbent	Sorbate	Characterization	Temperature (K)	Photocatalyst amount (mg. L^{-1})	Irradiation time (h)	Initial phenol concentration (mg. L^{-1})	pH	Radiation source	Removal %	Ref.
C_3N_4	4-Chlorophenol	XRD/UV–Vis/DRS/TEM/ESR/HPLC	298	40	0.5–2	4.09	6–7	300 W Xe lamp	96	(Cui et al., 2012)
g-C_3N_4	Phenol	XRD/AFM/RS	298	50	15	NA	5–8	LED	20	(Zhang et al., 2015)
Carbon dots/g-C_3N_4	Phenol	TEM/XPS/FTIR/UV–Vis/DRS/ ESR	293	50	2–8	50	4–7	300 W Xe lamp	87	(Zhang et al., 2016)
TiO_2-CdS/g-C_3N_4	Phenol	XRD/AFM/FTIR/TEM/XPS/BET/DRS/UV-is/HPLC	303	50	0.5–6	10	10	500 W Xe lamp	80	(Yao et al., 2017)
Ag/ g-C_3N_4	Phenol	XRD/HRTEM/UV–Vis/DRS/TGA/FETEM/EDX/DSC	293	0.5	60	10	6	300 W xenon lamp	17.4	(Sumathi and Kavipriya, 2017)
Ag_3PO_4/Ti_3C_2	2,4-Dinitrophenol	XRD/XPS/TEM/FESEM/EDX/DRS/UV–Vis/ESRA	293	20	2	25	7	300 W Xe lamp	68–70	(Cai et al., 2018)
g-C_3N_4	Phenol	HPLC/UV–Vis/XRD/SEM/HRTEM/DLS/FTIR	700	5000	0.2–1.0	20	3–8	10 W UV LED	99	(Svoboda et al., 2018)
TiO_2/Ti_3C_2 MXene	Phenol	XRD/SEM/TEM/HRTEM/ESRA/SAED/XPS/UV–Vis	323	50	3	20	5–6	200 W Xe lamp	96	(Huang et al., 2019)
CdS-Ti_3C_2/TiO_2	Phenol	EDX/XRD/XPS/UV–Vis/BET/ EPR	298	50	0.5–15	20–22	5–6	300 mW/cm^2 xenon lamp	4.3	(Liu et al., 2019)
MXene-Ti_3C/TiO_2/Bi_4NbO_8Cl	2,4-dichlorophenol	SEM/XPS/UV–Vis/DRS/XPS	298	10	40	5	2–7	300 W xenon lamp	13	(Jiang et al., 2020)
g-C_3N_4/Bi_2MoO_6	Phenol	DRS/UV–Vis/TEM/SEM/XPS/BET	298	2	80	10	4	300 W xenon lamp	98	(Kumar et al., 2020)
Bi_2WO_6/g-C_3N_4	Phenol	HPLC/TEM/EDS/XRD/FTIR/BET/DRS/ESR/UV–Vis	293	10–100	5	10	5–8	300 W xenon lamp	93.1	(Brunetti et al., 2019)
Ti_3C_2/Fe-anatase	Phenol	XRD/DRS/RS/UV–Vis/ SEM/XPS/TEM/TGA/EIS/EPR	298	20	1–18	20	6–7	300 W Xe lamp	19–69	(Grzegórska et al., 2021)
CoO-TiO_2/MXene	Phenol	XRD/HRTEM/FESEM/EDS/BET/XPS/EIS/HPLC	303	45	0.5–2	15–20	6	300 W Xe lamp	96	(Ding et al., 2021)
g-C_3N_4	Phenol	FTIR/SEM/ZPA/HPLC/TEM/XRD/XPS/UV-VIS/BET	323	150	2–4	35	3–10	430 nm LED lamp	83.8	(Rana and Minceva, 2021)
Fe(Co)/MXene	Phenol	XRD/SEM/XPS/DRS/UV–Vis/RS	313	300	15	20	6–10	Xenon lamp	98	(Zhang et al., 2021)
Alkalized MXene/Fe	4-nitrophenol	PXRD/TEM/EDX/FTIR/UV–Vis/BET/SEM/ HAADF-STEM/ ICP-OES	298	3	0.2–1	15	8	20 W LED lamp	91.3	(Zhang et al., 2022)
Ti_3C_2-PDA/Pd	4-nitrophenol	XRD/FTIR/TGA/HRTEM/BET/SEM/XPS/UV–Vis	293	1	2–10	10	5–8	20 W Sodium lamp	92	(Chen and Liu, 2022)
$BaSnO_3$/MXene	4-nitrophenol	ZPA/XRD/FTIR/HRTEM/XPS/DRS	298	50	20	5	NA	28 W Mercury lamp	98.8	(Chen et al., 2022)
CuO/g-C_3N_4-carbon dots	P-nitrophenol	SEM/TEM/XRD/XPS/UV–Vis/EIS/BET/FTIR/DRS	298	75	0.7–2	25	4–8	20 W LED tube light	99.8	(Wu et al., 2023)

Table 10

The synthesizing techniques, operating conditions and rejection performance of MXene-based membranes.

MXene based Membranes	MXene Synthesizing Techniques	Pollutants	Conditions			Membrane		Pressure (MPa)	Rejection performance %	Ref.
			C_O (mg/L)	Dosage (g)	pH	Pore size (nm)	Thickness (nm)			
MXene/PAO mixed matrix membrane	Simple Phase inversion method	U^{+6}	18	0.0182	6.2	30	550	0.44	76	(Xu et al., 2023)
$Ti_3C_2T_x$-CNT hybrid membrane	Vacuum filtration	Au^{3+}	20	0.02	2.0	–	–	0.1	99.8	(Wang et al., 2020)
β-FeOOH@MXene0.2 membrane	One-step hydrothermal method and vacuum filtration	Hg^{2+}	60	0.052	7.2	–	–	0.1	99.7	(Chen et al., 2022)
Thermal cross-linked 2D MXene membrane	Facile thermal treatment/Vacuum assisted filtration	Pb^{2+}	100	0.1	5.5	–	365	0.1	99	(Fan et al., 2020)
MXene/CNFs membrane	Electrospining technique	Pb^{2+}	1.0	0.001	3.9	40	330	0.5	89	(Mahar et al., 2023)
Hydroxylated MXene membranes	vacuum-assisted filtration	Pb^{2+}	50	0.052	5.7	–	383	0.2	99.43	(Wang et al., 2021)
MXene/CNFs membrane	Electrospining technique	As^{3+}	1.0	0.001	6.9	40	330	0.5	81	(Mahar et al., 2023)
Hydroxylated MXene membranes	vacuum-assisted filtration	Cd^{2+}	50	0.005	3.6	–	383	0.2	93.45	(Wang et al., 2021)
$Ti_3C_2T_x$ MXene@MOF Membrane	Non-induced phase separation process	Cd^{2+}	250	0.25	5.0	1.67	0.83	0.4	95	(Ghanbari et al., 2023)
ZIF-67 modified MXene/sepiolite composite membrane	ultrasonically dispersed Technique	Cu^{2+}	–	–	6.9	160.63	440	–	79.9	(Wang et al., 2022)
PFDTMS-modified hydrophobic 2D d-Ti_3C_2 membrane	Vacuum filtration	Cu^{2+}	–	–	7.8	–	–	–	100	(Ihsanullah and Bilal, 2022)
$Ti_3C_2T_x$ MXene@MOF Membrane	Non-induced phase separation process	Cu^{2+}	250	0.25	9.0	1.67	0.83	0.4	97	(Ghanbari et al., 2023)
Hydroxylated MXene membranes	vacuum-assisted filtration	Cu^{2+}	50	0.05	5.3	–	383	0.2	96.43	(Wang et al., 2021)
$Ti_3C_2T_x$ MXene@MOF Membrane	Non-induced phase separation process	Zn^{2+}	250	0.25	6.2	1.67	0.83	0.4	94	(Ghanbari et al., 2023)
ZIF-67 modified MXene/sepiolite composite membrane	ultrasonically dispersed Technique	Zn^{2+}	–	–	4.9	160.63	440	–	78.26	(Wang et al., 2022)
ZIF-67 modified MXene/sepiolite composite membrane	ultrasonically dispersed Technique	Ni^{2+}	–	–	6.8	160.63	440	–	48.27	(Wang et al., 2022)

rate has reached 80 % in 1 min. To create innovative functionalized $Ti_3C_2T_x$, a facile one-step inspired fabrication process is adopted. As demonstrated in Fig. 17, the carboxyl group of DOPA and catechol groups lead Ti_3C_2Tx to establish a greater removal capability of Cu^{2+}-PDOPA than $Ti_3C_2T_x$. To eliminate Cu^{2+}, MXene-based materials can provide a range of active ligands (Gan et al., 2020). For instance, large oxygen-containing groups were used to generate MXene/alginate composites that demonstrated an improvement in extraction efficiency ($87.6 \ mg.g^{-1}$) and a reduction in equilibrium time (15 min). MXene/alginate composites and Cu^{2+} were bound by two distinct mechanisms: ion exchange and chemical interaction (Dong et al., 2019). For Ti_3C_2Tx to interact with amino acid residues in water, delaminated MXene (d-Ti_3C_2Tx) flakes must first generate rutile phase titanium dioxide (TiO_2). A degradation efficiency rate of 75 % results in the elimination of 94.6 mg g^{-1} of Cu^{2+} in 5 min. The effective elimination of heavy metals from functionalized Ti_3C_2Tx after successful production makes them suitable for solving environmental issues (Elumalai et al., 2020).

4.2. Dyes

The dye industry contributes significantly to the annual emissions of organic pollutants and creates serious environmental risks. The textile sector mostly releases dye. MXene makes it possible to quickly and effectively eliminate dye from wastewater released (Fayyaz et al., 2021). MXene-based membranes were proven to be the best option for removing several harmful dyes from colored water. Table 11 gives an overview of the existing literature on the synthesizing techniques, reacting parameters, and removal performance for different dyes.

Liu et al. (Liu et al., 2020) utilized a modified Hummers approach to synthesize the graphene oxide (GO) and develop $Ti_3C_2T_x$ MXene by eliminating Al from their parent material Ti_3AlC_2 via chemical synthesizing techniques. So, for synthesizing GO/$Ti_3C_2T_x$ MXene-based membranes, the commercial mixed cellulose ester (MCE) membrane techniques were utilized; based on the proportional quantities of GO and MXene, the GO/MXene membrane's distinctive diverse structure displayed a beneficial effect regarding substrate breakdown and permeability. Under comparable experimental conditions, a composite membrane (550 nm) with a GO/MXene mass ratio of 1/4 demonstrated significantly higher water flux ($71.9 \ L.m^{-2}.h^{-1}.bar^{-1}$) than a benchmark GO membrane ($6.5 \ L.m^{-2}.h^{-1}.bar^{-1}$) thanks to its beneficial two-dimensional (2D) interparticle channels and hydrophilicity. The sudden change in the membrane's interlayer distance and the decline in oxygen-based functional groups were primarily responsible for the GO/MXene combination membrane's improved water flow compared to the standard GO membrane. Lin et al. (Lin et al., 2022) produced the raw materials $Bi_2O_2CO_3$ and Ti_3C_2Tx by employing chemical etching and a low-temperature chemical modification process. They created the $Bi_2O_2CO_3/Ti_3C_2Tx$ composite membranes by synthesizing the constituent materials and ultrasonic stirring. The experiment outcomes showed that adding N-doped $Bi_2O_2CO_3$ nanoparticles resulted in an extremely high water flux for the composite membrane ($815.3 \ L.m^{-2}h^{-1}$). The rejection capacities of the MXene-based membranes RhB and CR are
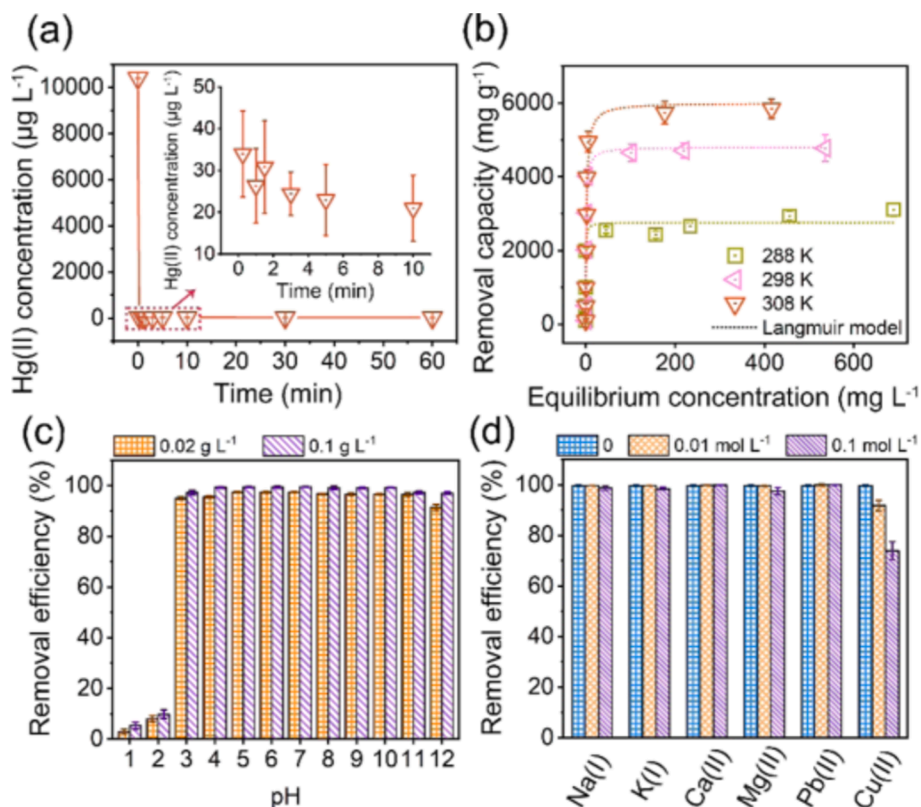
Fig. 16. (a) Adsorption kinetics for Hg^{2+} onto $M-Ti_3C_2$ (b) Adsorption isotherms for different temperatures (from 288 to 308 K) for Hg^{2+} onto $M-Ti_3C_2$ (c) Effect of pH on Hg^{2+} removal (d) Effect of ionic species on Hg^{2+} removal (Fu et al., 2020).

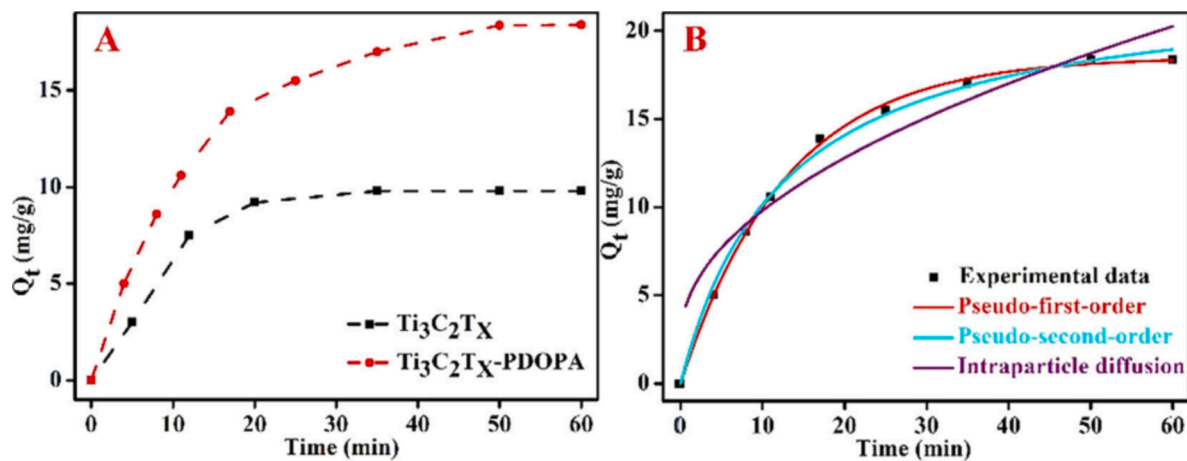**Fig. 17.** (a) The resemblance of the Cu^{2+} sorption, (b) Adsorption kinetics for Cu^{2+} onto Ti_3C_2Tx-PDOPA (Gan et al., 2020).

99.9 % and 98.4 %, respectively. It is crucial to note that the composite membrane kept its constant permeability and selectivity even after five continuous cycles of visible light irradiation. The number of electrons stored close to MXene was decreased due to the efficient extraction of photoexcited electron-hole pairs, which further encouraged the fast mobility of free electrons inside the crystal and of photogenerated charge carriers. In general, the extraction impacts of dyes from water were enhanced by a synergistic interaction between photocatalysts and 2D membrane composites. In contrast to conventional pulverized photocatalysts that lack transport, the photocatalytic membrane may be easily detached from the water without causing additional pollution from photocatalyst powder. The practical goal of lowering the cost of wastewater treatment was achieved by combining photocatalytic technology with membrane separation technology in this work. Gong et al. (Gong et al., 2022) utilized the vacuum filtration technique to synthesize the Ti_3C_2Tx /COF composite membranes to reject MG synthetic dyes for wastewater treatment. These techniques are FTIR, BET, AFM, and XRD for the extensive understanding of morphology and the internal structure of the developed Ti_3C_2Tx/COF composite membranes. The MXene has high instability and low permeability, and the addition of COF improves its stability and permeability to a large extent. Ti_3C_2Tx /COF composite membranes were rejected at 97 %, and the water flux is still as great as 194.5 L m^{-1}. At experimental conditions $C_0 = 250$ mg.L^{-1}, P = 0.01 MPa. The molecular sieving function of the MXene/COF composite membrane is shown in Fig. 18.

Table 11
The synthesizing techniques reacting parameter and refection performance for different dyes.

MXene based Membranes	MXene Synthesizing Techniques	Pollutants	Reacting Parameter					Pressure MPa	Rejection performance %	Ref.
			Dye (mg. L^{-1})	Dosage	pH	Membrane				
						Pore size (nm)	Thickness (nm)			
GO/MXene composite membranes.	Filtration	MB	10	–	–	–	550	0.3	97	(Liu et al., 2020)
MXene$_{(L)}$ −M	Vacuum filtration	MB	–	–	–	552.5	100	0.01	95.6	(Xiang et al., 2022)
MXene$_{(M)}$ −M	Vacuum filtration	MB	–	–	–	397.5	100	0.01	94.7	
MXene$_{(L)}$ −M	Vacuum filtration	MB	–	–	–	281.8	100	0.0195.6	88.3	
Ti$_3$C$_2$Tx MXene	Vacuum-assisted filtration	MB	200	0.25	–	1.07 µm	50	0.4	98.84	(Jin et al., 2021)
Ti$_3$C$_2$Tx MXene	Vacuum-assisted filtration	CR	200	0.3	–	1.07 µm	50	0.4	99.42	(Jin et al., 2021)
Bi$_2$O$_2$CO$_3$/ Ti$_3$C$_2$Tx	Ex-situ photocatalysis	CR	100	0.1	–	–	–	0.01	>95	(Lin et al., 2022)
TA/ Ti$_3$C$_2$Tx	Vacuum filtration	CR	10	0.01	–	–	1.33	0.2	96.6	(Tong et al., 2021)
PESNi@MXene	Wet phase inversion process	CR	50	0.4	–	–	–	0.01	98.35	(Huang et al., 2021)
TA/ Ti$_3$C$_2$Tx	Vacuum filtration	RhB	10	0.02	–	–	1.33	0.2	90	(Tong et al., 2021)
Bi$_2$O$_2$CO$_3$/ Ti$_3$C$_2$Tx	Ex-situ photocatalyst	RhB	10	0.5	–	–	–	0.01	23	(Lin et al., 2022)
Ag@ Ti$_3$C$_2$Tx	Vacuum-assisted filtration	RhB	100	–	–	2.1	470	0.4	81.04	(Pandey et al., 2018)
Ti$_3$C$_2$Tx /cellulose acetate	Phase inversion	RhB	–	–	–	Porosity: 69.7 %		0.01	92.27	(Pandey et al., 2020)
Ti$_3$C$_2$Tx /cellulose acetate	Phase inversion	MG	200	–	–	Porosity: 69.7 %		0.01	100	(Pandey et al., 2020)
Ag@ Ti$_3$C$_2$Tx	Vacuum-assisted filtration	MG	100	–	–	2.1	470	0.4	92.32	(Pandey et al., 2018)
MXene/COF composite	vacuum filtration	MG	250	0.2	11	2.1	–	0.01	97	(Gong et al., 2022)
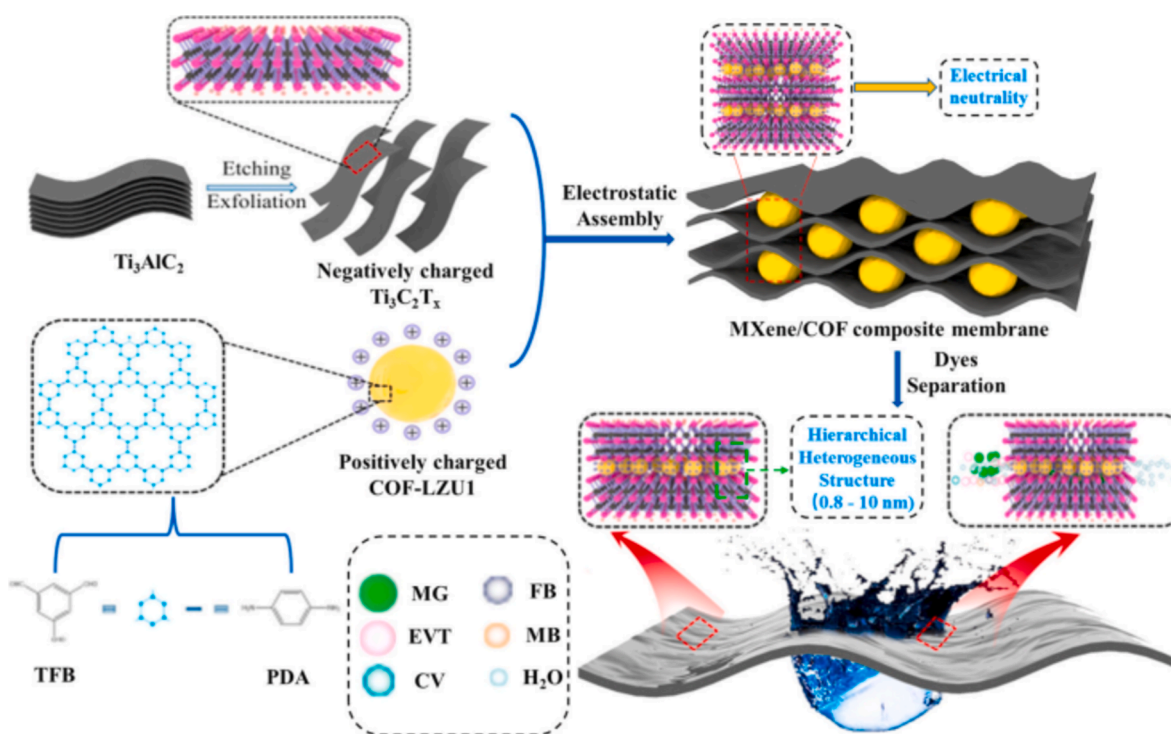
Fig. 18. The molecular sieving function of the MXene/COF composite membrane (Gong et al., 2022).

4.3. Pharmaceutical chemicals

Membrane-based filtration has long been used in the environment and medical and material sciences. However, their uses have been limited and for only removing selected environmental pollutants (Sutariya et al., 2023). Recently, excessive growth has been observed in the design and application of these membranes in environmental remediation. Since synthesizing 2D materials like MXene and its derivatives of titanium oxide, these membranes have been prepared for the selective removal of dyes, drugs, and other pollutants. The MXene-based membrane provides stability selectivity and a large surface area suitable for this purpose (Sutariya et al., 2023). Table 12 shows the MXene-based nanofiltration membranes for the separation of pharmaceutical chemicals.

Yue et al. (Yue and Sun, 2021) experimented with a Co^{2+}/Mxene-based membrane to remove tetracycline in peroxy mono-sulfate. They observed that the drug was removed more than 97 % within 5 min. In the presence of peroxy monosulfate, a higher flux of 52 % was observed compared to 22 % with peroxy monosulfate. They also concluded that sulfate and hydroxyl radicals were actively involved in the degradation. Zhang et al. (Liang et al., 2023) presented the solution to the swelling problem in MXene-based membranes by incorporating carboxylated cellulose nanofibers into the Mxene titanium oxide membrane. They discovered that incorporating these nanofibers greatly reduced the swelling of the membrane. They selected azithromycin to check the membrane application. They found that more than 99 % of azithromycin was filtered, and a very high water permeance of 26 $Lm^{-2}h^{-1}bar^{-1}$ was obtained.

Moreover, Wang et al. (Wang et al., 2023) proposed a greener method for synthesizing fluorine-free titanium carbide MXene. In this study, the degradation impacts of Doxycycline and Oxytetracycline reached about 90 %. Sun et al. (Sun et al., 2022) prepared a hybrid organic–inorganic MXene-pillarene-based membrane. They achieved 88 % rejection for ampicillin and 95 % rejection for bacitracin. Li et al. (Li et al., 2020) prepared a laminated titanium carbide membrane with regular slit-shaped channels. They filtered not only water-based drugs but also organic solvent-based drugs. Devaraj et al. (Devaraj et al., 2022) prepared alginate/MXene/CoFe$_2$O$_4$-based Composite material to enhance the adsorbing properties of MXenes. They observed that this composite material had highly improved absorption rates of 359.76 percent and 371 % respectively, for ciprofloxacin and copper ions; they also observed that using a rotating magnetic field can greatly enhance the adsorbing rate and performance. Kim et al. (Kim et al., 2021) studied the effects of sonication on the adsorption of selected pharmaceuticals added different pH by MXene deselected verapamil carbamazepine, ibuprofen, and diclofenac and used sonication to enhance adsorption by MXene. They observed that increasing the sonication frequency can increase the absorption capacity of MXene material because sonication costs the even distribution dispersion of MXene. Kim et al. (Kim et al., 2022) studied the effects of Ultrasonication on single and multi-layered MXenes. They also analyzed how Ultrasonication affected the adsorption performance of single-layered and multi-layered MXenes off diclofenac and verapamil. They concluded that using ultrasonic treatment can greatly enhance the efficiency of multilayered and single-layer

MXenes. Park et al. (Park et al., 2023) prepared cobalt doped/ZnTiO$_3$ (ZTO)/TiC$_2$ Mxene. They checked the adsorption of tetracycline, a persistent pharmaceutical pollutant, and analyzed the effects of pH, background ions, and temperature; they performed different types of isotherms to study the adsorption of tetracycline by the prepared material. They found that prepared material had greater adsorption capacity than activated carbon and simple MXene. Sukidpaneenid et al. (Sukidpaneenid et al., 2023) observed that incorporating sodium chloride in MXene titanium composite material can greatly enhance the adsorption capacity and photocatalysis activity of the membrane. They found that incorporating sodium chloride greatly increased the absorption of norfloxacin by MXene titanium oxide composites.

5. Mxene-based sensors designated for the detection of emerging pollutants

5.1. Heavy metal ions

Up to date, various 2-D nanomaterials such as graphene, metal oxides, MoS$_2$, layered double hydroxides, transition metal dichalcogenides (TMDs), boron nitride (BN), silicenes and germanene have been exploited as an electrochemical sensor for the detection of heavy metal ions from environmental samples (Su et al., 2018). However, these 2-D materials have some drawbacks, including low electrical conductivity, high hydrophilicity, and difficult surface functionalization. Conversely, MXene-based electrochemical sensors have excellent properties such as ease of functionalization, high electrical conductivity, high hydrophilicity, good ion intercalation behavior, and feasibility for large-scale fabrication (Rizwan et al., 2022). Therefore, these are perfect for developing high-performance electrochemical sensors to determine heavy metal ions from environmental samples. Table 13 summarizes MXene-based electrochemical sensors for detecting heavy metals and phenolic-based pollutant species contaminants.

Zhu et al. (Zhu et al., 2017) have prepared a 2-dimensional accordion-like alk-Ti$_3$C$_2$ composite material through acid etching and alkaline intercalation treatment. The prepared alk-Ti$_3$C$_2$ composite was employed on the surface of a glassy carbon electrode and used for the determination of different heavy metal ions such as Cd^{2+}, Pb^{2+}, Cu^{2+}, and Hg^{2+} using square wave anodic stripping voltammetry (SWAV) mode of the electrochemical workstation. The alk-Ti$_3$C$_2$/GCE modified electrode showed outstanding electrochemical ability compared to the Ti$_3$C$_2$/GCE modified electrode for determining various heavy metal ions. The proposed Ti$_3$C$_2$/GCE sensor exhibited tremendous selectivity and sensitivity towards the target analytes with the linear dynamic range of 1–1.5 μM, and the limit of detection for Cd^{2+}, Pb^{2+}, Cu^{2+}, and Hg^{2+} was found to be as 0.098, 0.041, 0.032 and 0.130 μM respectively. Also, the proposed alk-Ti$_3$C$_2$/GCE sensor exhibits brilliant selectivity in the presence of different interferant species.

Chen et al. (Chen et al., 2023) have synthesized three-dimensional melamine-doped graphene oxide/MXene composite aerogel (3D MGMA) by using the self-assembled method and applied it as a modified sensor for the detection of multiple heavy metal ions like Zn^{2+}, Cd^{2+}, and Pb^{2+} from the environmental samples. Moreover, combining melamine 3-D structure melamine with a 2-D network like MXene and

Table 12
MXene-based nanofiltration membranes for the separation of pharmaceutical chemicals.

Membrane material	Types of Anti-biotic drugs	Rejection %	Water permeance (L m^{-2}h^{-1} bar^{-1})	pH	Temperature	concentration (ppm)	Ref.
Co^{2+}/Mxene (CM) Membrane	Tetracycline	97	–	–	25 ℃	10	(Yue and Sun, 2021)
Ti$_3$C$_2$T$_x$/CNFs	azithromycin	99 %	26	7	25 ℃	250	(Liang et al., 2023)
Ff-Ti$_3$C$_2$T$_x$	Tetracycline	89 %	–	7	25 ℃	20	(Wang et al., 2023)
MXene-pillarene	Ampicillin bacitracin	88 % 95 %	200	1–7	–	200	(Sun et al., 2022)

Table 13

The MXene-based electrochemical sensors for the determination of heavy metals and phenolic-based pollutants species.

Composite Material	Target Analyte(s)	Techniques	Linear Range	Detection Limit (LOD)	Ref
alk-Ti$_3$C$_2$	Cd^{2+}	SWAV	1–1.5 µM	0.098 µM	(Zhu et al., 2017)
	Pb^{2+}			0.04 µM	
	Cu^{2+}			0.03 µM	
	Hg^{2+}			0.13 µM	
3D MGMA	Zn^{2+}	DPAVS	3–900 µg/L	0.48 µg/L	(Chen et al., 2023)
	Cd^{2+}			0.45 µg/L	
	Pb^{2+}			0.3 µg/L	
MXA-CuO/CC	Cd^{2+}	DPAVS	4–800 µg/L	0.3 µg/L	(Wen et al., 2022)
	Pb^{2+}		4–1200 µg/L	0.2 µg/L	
Ti$_3$C$_2$TxR/CNT	Hg^{2+}	DPV	0.01–7.0 µM	5.2 nM	(Liu et al., 2022)
Ti$_3$C$_2$@N-C	Cd^{2+}	SWASV	0.1–4.00 µM,	2.55 nM	(Zhao et al., 2022)
	Pb^{2+}		0.05–2.00 µM	1.10 nM	
PANI-Ti$_3$C$_2$	Hg^{2+}	ASV	0.1–20 µg/L	0.017 µg/L	(Cheng and Yang, 2020)
Au/DNA	Pb^{2+}	DPV	10 nM − 5 µM	4 nM	(Rasheed et al., 2022)
BiNPs/Ti$_3$C$_2$Tx	Cd^{2+}	SWASV	−	10.8 nM	(He et al., 2020)
	Pb^{2+}			12. 4 nM	
Zn-Co-NC/Nb$_2$CTx	4-nitrophenols	DPV	1 µM to 500 µM	0.070 µM	(Huang et al., 2021)
Pt@Ti$_3$C$_2$Tx	Bisphenol A	DPV	50 nM − 5 µM	32 nM	(Rasheed et al., 2021)
D-Ti$_3$C$_2$Tx/GR/GCE	p-Nitrophenol	DPV	1–175 µmolL^{-1}	0.16 µmol L^{-1}	(Wang et al., 2022)
N-Ti$_3$C$_2$/PC	4-aminophenol acetaminophen	DPV	1–150 µM	0.06–0.05 µM	(Liao et al., 2022)
Mo$_2$Ti$_2$AlC$_3$/MWCNT	Bisphenol A	DPV	0.01–8.50 µM	2.7 nM	(Sanko et al., 2022)
Gr/MXene	Bisphenol A	CV	10—180 nM	4.08 nM	(Rajendran et al., 2022)
Lac/Au/MXene	Catechol	CV	0.05–0.15 mM	0.05 mM	(Chandran et al., 2021)
alk- Ti$_3$C$_2$/N-PC	Hydroquinone	DPV	0.5–150 µM	4.8 nM	(Huang et al., 2020)
	Catechol			3.1 nM	
MnMoO$_4$-MXene	Hydroquinone	DPV	5—65 nM	0.26–0.3 nM	(Ranjith et al., 2022)
	Catechol				
V$_2$CTx@NiCoMn-OH	Hydroquinone	DPV	2–1050 µM	0.559 µM	(Yu et al., 2023)
Ti$_3$C$_2$Tx-TiO$_2$	thiabendazole	DPV	0.3–100.0 nM	0.1 nM	(Zhong et al., 2023)
MXene@Ag	carbendazim	DPV	0.3 nM- 10 µM	0.1 nM	(Zhong et al., 2021)
MXene/CNHs/-CD-MOFs	carbendazim	DPV	3.0 nM- 10.0 µM	1.0 nM	(Tu et al., 2020)
MWCNTs-COOH/MXene	benomyl	DPV	10 nM-10 µM	3.0 nM	(Zhong et al., 2022)
SnO$_2$/Nb$_2$CTx MXene	chlorpyrifos	DPV	$5.1 \times 10^{-14} - 5.1 \times 10^{-7}$ M	5.1×10^{-14} M	(Guo et al., 2023)
MXene/AuPt	chlorpyrifos	DPV	$10^{-8} - 10^{-3}$ mg mL^{-1}	1.55 pg mL^{-1}	(Ding et al., 2023)
Ti$_3$C$_2$Tx	methiocarb diethofencarb	DPV	−	0.19 l g/mL	(Sinha et al., 2021)
				0.46 l g/mL^{-1}	
AChE-Chit/MXene/Au NPs/MnO$_2$/ Mn$_3$O$_4$	methamidophos	DPV	10^{-12}–10^{-6} M	1.34×10^{-13} M	(Song et al., 2019)

graphene oxide enhanced the surface area. It improved the electrical conductivity and uptake of the excess heavy metal ions from the environmental samples. Also, the synthesized 3D MGMA/SPCE modified electrode exhibited an outstanding linear dynamic range from 3-900 µg/L with detection limits of 0.48, 0.45, and 0.29 µg/L simultaneously from the environmental samples.

Wen et al. (Wen et al., 2022) fabricated a composite based on the MXene aerogel-CuO/carbon cloth (MXA-CuO/CC) for the sensitive electrochemical determination of Cd^{2+} and Pb^{2+} ions. The fabricated MXA-CuO/CC Modified electrode showed brilliant sensing properties towards target analytes because the oxygen vacancies of CuO have a strong capability for target analytes that promoted the adsorption of heavy metal ions, i.e., Cd^{2+} and Pb^{2+} on the surface of modified electrode. Moreover, the differential pulse anodic stripping voltammetry (DPASV) was exploited for the detection of Cd^{2+} and Pb^{2+} ions with a wide linear range from 4-800 µg/L and 4–1200 µg/L simultaneously with a limit of detections of 0.3 µg/L and 0.2 µg/L respectively. Also, the fabricated MXA-CuO/CC has exceptional anti-interference, good stability, and reproductivity properties.

Xia et al. (Liu et al., 2022) have engineered a novel MXenes nano-ribbons/carbon nanotube (Ti$_3$C$_2$TxR/CNT) heterostructure composite and employed on the glassy carbon electrode surface as a sensing platform for detecting Hg^{2+} ion. The modified Ti$_3$C$_2$TxR/CNT/GCE showed tremendous selectivity and sensitivity towards Hg^{2+} ion with a good wide linearity range from 0.01-7.0 µM with a limit of detection 5.2 nM from real water samples in the presence of different foreign interferants. However, this improvement in the sensitivity and limit of detection is due to the high surface area and electrical conductivity of the MXenes that allow more adsorption sites for the target analytes. Similarly, Zhang

et al. (Zhao et al., 2022) prepared a novel 2-dimensions nitrogen-doped carbon-coated Ti$_3$C$_2$-MXene heterostructure (Ti$_3$C$_2$@N-C) based electrochemical platform for the detection of Cd^{2+} and Pb^{2+} ions from seawater and tap water by using the square wave anodic stripping voltammetry (SWASV) mode. The developed Ti$_3$C$_2$@N-C/GCE demonstrated excellent electrochemical sensing capacity for the Cd^{2+} and Pb^{2+} ions with a wide linear dynamic range of 0.1–4.00 and 0.05–2.00 µM. The limit of detection was found to be 2.55 and 1.10 nM, respectively. The developed sensor showed excellent selectivity for the Cd^{2+} and Pb^{2+} ions in the existence of various metal ions and molecules.

Cheng et al. (Cheng and Yang, 2020) synthesized PANI-Ti$_3$C$_2$ composite for the electrochemical monitoring of Hg^{2+} ions from the natural environment. The synthesized PANI-Ti$_3$C$_2$ composite was employed on the surface of a glass carbon electrode for modification purposes and improved its properties. The developed sensor PANI-Ti$_3$C$_2$/GCE showed admirable electrochemical sensing towards Hg^{2+} ions with a wide range linear range between 0.1–20 µg/L with a limit of detection estimated 0.017 µg/L and the proposed senor also employed for the determination Hg^{2+} ions from tap water.

Rasheed et al. (Rasheed et al., 2022) fabricated the novel Nb$_4$C$_3$Tx (MXene)/Au/DNA composite. They fabricated and used it as an electrochemical sensor for the detection of Pb^{2+} ions from the aqueous system. The Au/DNA decorated sensor showed enhanced sensing ability toward the Pb(II) ions. For the Pb^{2+} sample detection, the proposed sensor displayed a linear response from 10 nM to 5 µM with a limit of detection of 4 nM in the presence of different interferant species. This study provides new ideas for developing stable and reliable electrochemical sensors for monitoring Pb(II) ions in environmental samples. He et al. (He et al., 2020) have reported an electrochemical sensor for

determining Cd^{2+} and Pb^{2+} ions. The Bismuth/MXene (BiNPs/Ti$_3$C$_2$Tx) Nanocomposite showed tremendous electrochemical performance using SWASV mode, with a limit of detection found at 10.8 and 12. 4 nM.

5.2. Phenolic compounds

Synthetic phenolic compounds contain one or more hydroxyl groups than benzene. They may include other groups, which are also created artificially through chemical synthesis. Therefore, detecting these pollutants from the wastewater samples is very important. Huang et al. (Huang et al., 2021) suggested a straightforward self-assembled technique to create a novel heterostructure (MXene/ZIF) made of bimetallic Zn, Co embedded N-doped carbon (Zn-Co-NC) nanocages and derived from Zn-Co-ZIFs and Nb$_2$CTx. When detecting 4-nitrophenols electrochemically, modified Nb$_2$CTx/Zn-Co-NC hybrid electrodes were used. (4-NP). According to SEM pictures, Zn-Co-NC can be successfully inserted to prevent Nb$_2$CTx from restacking. The effective synthesis of a bimetallic Zn, Co co-embedded N-doped carbon nanocage was shown by EDS and XPS. The wide linear range that could be obtained in ideal circumstances ranged from 1 M to 500 M. The high sensitivity of 4.65 A M1 cm^{-2} and low detection limit of 0.070 M was achieved. The Nb$_2$CTx/Zn-Co-NC sensor also possesses exceptional selectivity and durability.

Rasheed et al. (Rasheed et al., 2021) created a nanocomposite of platinum nanoparticles and Ti$_3$C$_2$Tx (Pt@Ti$_3$C$_2$Tx). They did this by using delaminated Ti$_3$C$_2$Tx nanosheets, which served as a reducing agent and a conductive scaffold, to self-reduce Pt salt to Pt nanoparticles. It was discovered that 10 %Pt@Ti$_3$C$_2$Tx had the greatest electrochemical activity in the anodic potential window after they characterized the electrochemical activity of Pt@Ti$_3$C$_2$Tx nanocomposites with varying Pt loading. Using this nanocomposite, they later developed an electrochemical sensor for detecting Bisphenol A (BPA), a prevalent environmental pollutant. Under ideal circumstances, the oxidation peak of BPA had a detection limit of 32 nM. It was proportionate to the analyte concentration from 50 nM to 5 M. The sensor was effectively tested using samples of fresh milk and drinking water.

Wang et al. (Wang et al., 2022) developed a sensor for p-Nitro phenol (p-NP), a significant environmental pollutant, which was quickly detected using a highly sensitive electrochemical sensor. The Ti$_3$C$_2$T$_x$ MXene/graphene composite that served as the sensor's foundation was made using a minimally intensive layer delamination (MILD) technique and a self-assembly procedure. SEM, XRD, AFM, and Raman spectroscopy were all used to characterize the final product. The D-Ti$_3$C$_2$Tx/GR/GCE sensor was made by modifying a glassy carbon electrode (GCE) with the alloy. Chronocoulometry, electrochemical impedance spectroscopy, and cyclic voltammetry were all used to examine the sensor's electrochemical behavior. Due to the abundance of active sites, quick electron transfer, and good electro-catalytic performance of the D-Ti$_3$C$_2$Tx/GR composite, the sensor demonstrated a strong electrochemical response to the p-NP reduction reaction.

Liao et al. (Liao et al., 2022) used in-situ nucleation and conversion of ZIF-8 on 2D hierarchical Ti$_3$C$_2$ MXene nanosheets to effectively synthesize a novel composite, N-Ti3C2/PC. Adding ZIF-8 greatly enhanced the composite's electrochemical properties and stopped the restacking of Ti$_3$C$_2$ nanosheets. The construction of an electrochemical sensor for the combined detection of 4-aminophenol (4-AP) and acetaminophen using the N-Ti$_3$C$_2$/PC composite followed. (ACOP). Because N-Ti$_3$C$_2$ and PC work together to speed up electron transfer on the electrode surface, this sensor showed outstanding electrocatalytic activity for 4-AP and ACOP.

Sanko et al. (Sanko et al., 2022) created an electrochemical sensor using a Mo$_2$Ti$_2$AlC$_3$/MWCNT (multi-walled carbon nanotube) nanocomposite. The Mo$_2$Ti$_2$AlC$_3$ was used to develop the MAX phase of the sensor, and MWCNT was used to increase conductivity and sensitivity. The sensor's electrochemical capabilities were assessed using differential pulse voltammetry (DPV) and cyclic voltammetry. The outcomes demonstrated that the Mo$_2$Ti$_2$AlC$_3$/MWCNT nanocomposite

demonstrated a single, diffusion-controlled, irreversible oxidation process against BPA. The sensor also had a linear working range of 0.01–8.50 M determined from DPV, a LOD of 2.7 nM, and a LOQ of 8.91 nM.

Rajendran et al. (Rajendran et al., 2022) the objective of this study was to create an electrochemical sensor for the detection of BPA, used a top-down approach to create a 2D mixed graphene/Ti$_3$C$_2$Tx nanocomposite (Gr/MXene) to accomplish this. XRD and Raman spectroscopy analysis were used to corroborate the successful formation of Gr sheets with MXene, and HR-SEM was used to confirm the formation of MXene and Gr/MXene nanocomposite. The researchers then used the Gr/MXene nanocomposite-modified GCE for BPA oxidation in 100 mM phosphate buffer solution to create an electrochemical BPA monitor in (PBS). The Gr/MXene/GCE showed linear BPA detection limits of 4.08 nM and 0.35 mM by differential pulse voltammetry (DPV) and a linear range of detection from 10 to 180 nM and 1 to 10 M BPA. Additionally, the sensor demonstrated good repeatability, selectivity, stability, and consistency regarding BPA detection. The researchers effectively used the Gr/MXene modified sensor to detect BPA in contemporary plastic products, with a recovery rate ranging from 99.2 % to 104.5 %. Overall, this study offers an electrochemical sensor that has the potential to be sensitive and specific for the detection of BPA, which could have a big effect on food and environmental safety.

Chandran et al. (Chandran et al., 2021), in their study, a glassy carbon electrode was immobilized with laccase (Lac) on Au/MXene to create a sensing electrode. XRD, SEM, and energy-dispersive X-ray spectroscopy were used to characterize the synthesized Au/MXene substance. The adsorbed enzymes could still function as biological electrocatalysts because the Au nanoparticles enabled the transfer of electrons between the Au surface and the T1 copper site of the electroactive Laccase. With a comparatively high sensitivity of 0.05 mA/mM and a detection limit of 0.05 mM, the Lac/Au/MXene/GCE electrode was used to study the electrochemical oxidation of catechol. This electrode showed a linear amperometric response in the 0.05 to 0.15 mM concentration range. Moreover, the biosensor electrode demonstrated outstanding repeatability, reproducibility, and durability.

Huang et al. (Huang et al., 2020) modified functional groups on the surface of Ti$_3$C$_2$ by alkalization treatment to create new electrode materials. Unfortunately, practical applications face major difficulties when trying to stack Ti$_3$C$_2$ sheets again. To get around this restriction, an innovative self-assembling technique was created to build a heterostructure of MOF and Ti$_3$C$_2$. Alk- Ti$_3$C$_2$ was combined with nitrogen-doped porous carbon (N-PC) produced from MOF-5-NH$_2$ to generate the structure known as alk- Ti$_3$C$_2$/N-PC. The latter was created by treating Ti$_3$C$_2$ with acid etching and alkaline intercalation. This method successfully stopped the Ti$_3$C$_2$ sheets from stacking again, enabling the detection of benzenediol via hydrogen-bond contact. The abundance of OH functional groups on alk- Ti$_3$C$_2$ and the many CeN bonds on N-PC cause this interaction. Using the benzenediol/benzoquinone redox reactions to detect hydroquinone (HQ) and catechol (CT), the alk- Ti$_3$C$_2$/N-PC electrode had good conductivity and surface area. The electrode demonstrated excellent performance with low detection limits of 4.8 nM (S/N = 3) for HQ and CT, respectively, and a broad linear detection range of 0.5–150 M under ideal circumstances. The electrode showed outstanding reproducibility and durability as well. Moreover, the alk-Ti$_3$C$_2$/N-PC electrochemical sensor was used to detect HQ and CT in industrial wastewater, with acceptable recoveries, to evaluate the viability of the electrode for environmental analysis. In conclusion, decorating alk- Ti$_3$C$_2$ with N-PC is a novel technique for developing different alk- Ti$_3$C$_2$-based composites to identify phenolic isomers and examine ecological materials.

Ranjith et al. (Ranjith et al., 2022) created a composite electrochemical sensor with a few-layered exfoliated 2D MXene and 1D MnMoO$_4$ nanofibers. The 1D MnMoO$_4$ and 2D MXene nanoarchitectures were created to improve electrocatalytic activity and synergistic signal enhancement for the oxidation of HQ and CC. The synthesized MnMoO$_4$-

MXene-GCE sensor displayed oxidation potentials of 0.102 V and 0.203 V for HQ and CC, respectively. It also had a distinct and simultaneous sensing range of 0.101 V and a powerful anodic peak current. With low detection limits of 0.26 nM and 0.30 nM, respectively, the 1D-2D hybridized MnMoO$_4$-MXene-GCE developed sensor shows a broad linear response from 5 nM to 65 nM for both HQ and CC.

Additionally, the sensor showed significant stability. The 1D-2D MnMoO$_4$-MXene nanocomposite-based biosensor successfully detected HQ and CC in hazardous water pollutants. Recovery values were obtained using the differential pulse voltammetric method. In conclusion, the hybrid electrochemical sensor created in this study demonstrates promise for real-world analysis and dual HQ and CC detection in wastewater.

Yu et al. (Yu et al., 2023) focused on creating electrode materials that can perform double duty as pollutant monitors and supercapacitors. This research uses the two-step method to successfully synthesize the novel electrode material V2CTx@NiCoMn-OH. Using ZIF-67 as a framework and basic anion exchange, a 3D hollow structure of NiCoMn-OH was first created. The NiCoMn-OH structure was combined with the 2D layered V2CTx MXene in the subsequent phase. The self-accumulation of the MXene nanosheets was successfully constrained by intercalating the NiCoMn-OH structure with the V$_2$CTx MXene, and a 3D cross-linked hollow structure was created. This structure increased the conductivity of NiCoMn-OH, revealed more active sites of V$_2$CTx@NiCoMn-OH, and widened the ion transport channel.

5.3. Pesticides

Due to its sensitivity, selectivity, simplicity, quick response, and cost-effectiveness, electrochemical sensing has emerged as a viable method for detecting pesticides. The foundation of this technique is the measurement of the electrical signals produced by the contact of the pesticide molecules with the electrode surface (Wang et al., 2020). It is possible to detect and measure pesticide residues in various matrices, including water, soil, and food products, using the type and magnitude of these signals. The choice of electrode material is a crucial factor in electrochemical sensing because it greatly impacts how well the sensor works. Metals, metal oxides, carbon-based materials, and conducting polymers are just a few of the materials investigated for constructing electrochemical instruments for pesticide detection. Each of these substances demonstrates unique electrochemical characteristics, which impact the sensor's sensitivity, selectivity, and durability (Wang et al., 2020). Because of their exceptional transmission and biocompatibility, metal electrodes made of gold, silver, and platinum have been used extensively. Their high price and fouling propensity might constrain their practical uses. Metal oxides, like titanium dioxide, zinc oxide, and indium tin oxide, have benefits like improved electron transfer, excellent chemical stability, and adjustable electrocatalytic properties (Umapathi et al., 2022).

The development of electrochemical sensors for pesticide detection using various electrode materials and sensing techniques is the subject of eight recent studies we address in this review. In research (Zhong et al., 2023), the authors created a heterostructure Ti$_3$C$_2$Tx-TiO$_2$ composite electrode to detect thiabendazole (TBZ). The sensor obtained a linear range from 0.3 to 100.0 nM and a limit of detection (LOD) of 0.1 nM by tracking the anodic stripping peak signal change of media Cu^{2+}. The sensor demonstrated outstanding anti-interference, repeatability, stability, and applicability with fruit and water samples. Another study showed an electrochemical ratio metric sensor for detecting carbendazim (CBZ) made of a composite of MXene@Ag nanoclusters and amino-functionalized multi-walled carbon nanotubes. The sensor had a LOD of 0.1 nM and a linear range of 0.3 nM to 10 M. It showed high selectivity, excellent reproducibility, secular stability, and acceptable applicability in vegetable samples.

Tu et al. (Tu et al., 2020) used an electrochemical sensing platform for CBZ detection made of nanoarchitecture of MXene/carbon nanohorns/-cyclodextrins-Metal-organic frameworks (MXene/CNHs/-CD-MOFs). The sensor showed a low LOD of 1.0 nM and a broad linear range of 3.0 nM to 10.0 nM. A tomato sample analysis also revealed high selectivity, reproducibility, long-term stability, and satisfactory applicability (Tu et al., 2020).

Zhong et al. (Zhong et al., 2022) suggested a hierarchical nano-CuO decorated MWCNTs-COOH/MXene composite-based highly sensitive and selective electrochemical sensor for real samples' benomyl (BN) detection. The sensor had a LOD of 3.0 nM and a linear range of 10.0 nM to 10.0 M. It also demonstrated successful application in apple samples, excellent long-term stability, and repeatability. In another study, the researchers developed an acetylcholinesterase (AChE) biosensor based on a SnO$_2$/Nb$_2$CTx MXene nanocomposite for pesticide detection. With a LOD of 5.1 X10^{-14} M, the sensor showed a linear detection range for chlorpyrifos of 5.1 X 10^{-14} – 5.1 X 10^{-7} M. Additionally, another study described the creation of an ultrasensitive AChE-based electrochemical biosensor and the synthesis of MXene/AuPt nanocomposite for chlorpyrifos detection (Ding et al., 2023). The sensor's linear range was 10^8 and 103 mg mL1, and its LOD was 1.55 pg mL^1. In another research, methiocarb, diethofencarb, and carbamate pesticides were quickly electroanalytical screened. The authors used colloidal single/few-layer Ti$_3$C$_2$Tx MXene flakes prepared via the minimally intensive layer delamination (MILD) method. The sensor showed acceptable recoveries in actual samples and detection limits of 0.19 g mL-1 for methiocarb and 0.46 g mL-1 for diethofencarb, respectively (Sinha et al., 2021).

Song et al. (Song et al., 2019) used MnO$_2$/Mn$_3$O$_4$ and Ti$_3$C$_2$ MXene/Au NP composites derived from MOFs to create a novel electrochemical sensing platform for detecting organophosphorus pesticides (OPs). Combining MXene/Au NPs with the 3D MnO$_2$/Mn$_3$O$_4$ hierarchical microcuboids formed from Mn-MOF produced excellent electrochemical performance, good environmental biocompatibility, and a synergistic signal amplification effect. The AChE-Chit/MXene/Au NPs/MnO$_2$/Mn$_3$O$_4$/GCE sensing platform was able to identify methamidophos in a concentration range of 1012–106 M with a low limit of detection (1.34—10^{13} M) and good linearity (R^2 = 0.995). With excellent recoveries (95.2 %–101.3 %), the biosensor effectively detected methamidophos in real samples.

6. Mxene-based materials for removal of gaseous pollutants

Gaseous pollutants are produced due to combustion processes in automobiles, manufacturing, and power plants. Of particular interest are those gaseous pollutants that are volatile, toxic, and released into the air, causing adverse effects on both human health and the environment. The focus of gaseous air pollutants is oxides of carbon (CO, CO$_2$), nitrogen (NO, NO$_x$), sulfur (SO$_2$, H$_2$S), ammonia (NH$_3$), and other VOCs such as hydrocarbons and smoke. Removal of gaseous pollutants has always been the central premise of environmental applications. Ideally, gaseous pollutant removal is perceived with MXenes to act as catalysts, sensory materials, membrane separators, and even as capture materials (Zhang et al., 2017; Cao et al., 2018).

6.1. CO$_2$ reduction

CO$_2$ is a gas analyte of interest, and their capture and reduction using MXene as an adsorbent/catalyst are explored. CO$_2$ reduction over MXene-based composite surfaces is extensively investigated due to their brilliant photocatalytic efficiencies (Zhang et al., 2017). Cao et al. (Cao et al., 2018) discovered that the reduction efficiency of CO$_2$ (0.069 mmol/g) into methane and methanol over Ti$_3$C$_2$/Bi$_2$WO$_6$ nanosheet was 4.6 times that of pristine Bi$_2$WO$_6$. Parui et al. (Parui et al., 2022) described a simulation study (DFT calculations and AIMD-ab initio molecular dynamics) to describe the single-step selective reduction of CO$_2$ to HCOO$^-$ and HCOOH using Ti$_2$C(OH)$_2$ MXene material. To make the material reactive, it transfers electrons to carbon dioxide (CO$_2$), and then CO$_2$ removes protons off the surface of titanium dioxide (Ti$_2$C(OH)$_2$) to

produce these products. The formation of formate or formic acid is determined by how carbon dioxide is connected to the surface. It is possible for moisture to readily repair any surface imperfections that may have been generated throughout the procedure, allowing the reaction to continue. $Ti_2C(OH)_2$ is advantageous because it can donate electrons and protons, enabling it to convert carbon dioxide into compounds of great value effectively. Li et al. (Li et al., 2021) synthesized a novel mesoporous g-C_3N_4/Ti_3C_2Tx MXene photocatalyst and reported a higher yield of methane of about 2.117 μmol $g^{-1}h^{-1}$ on CO_2 reduction due to the contributing factor of Ti_3C_2Tx that allowed greater separation of holes and electrons. Furthermore, the material possesses a structure characterized by numerous minuscule pores, facilitating rapid electron transport and charge separation (electrons and holes), hence enhancing efficiency. MCT generates methane at a rate 2.4 times greater than a comparable material without Ti_3C_2Tx. The extensive surface area and many flaws in MCT offer ample sites for CO_2 adsorption, whereas Ti_3C_2Tx functions as a "capacitor," facilitating efficient electron transport. This combination diminishes electron recombination, enhancing the efficacy of the CO_2 reduction reaction (CO_2RR). The research indicates that materials such as Ti_3C_2Tx may enhance the efficacy of photocatalysts.

6.2. Reduction/removal of other gases

Ngoc et al. (Wang et al., 2019) investigated Sc_2CF_2 MXene monolayer adsorption characteristics for common gaseous analytes using first-principles calculations. They chose Sc_2CF_2 MXene monolayer as a catalyst due to its small bandgap of 1.023 eV, high tunability under electric fields, doping and strain, and higher thermoelectric conductivities. They discovered how these gasses adhere to the material, found the amount of energy that is involved, and discovered how the electrical properties of the material change. The majority of gases have a weak attachment to Sc_2CF_2. Still, when molecules such as oxygen, nitrogen,

and nitrogen dioxide are adsorbed onto the material, they transform it from a non-magnetic to a magnetic state. When nitrogen oxide is linked to the material, it exhibits the behavior of a semimetal, yet its conductivity remains the same for the majority of other gases. According to this, Sc_2CF_2 has the potential to be an effective material for the detection of NO gas. Exploiting Sc_2CF_2 MXene monolayer catalyst, Cheng et al. (Cheng et al., 2022) explored its application as a NO_2 gas sensor. They performed simulation activity to determine the adsorption of 11 gas analytes, such as NH_3, NO_2, SO_2, CO_2, H_2O, H_2S, CO, NO, O_2, N_2, and H_2. They observed a larger charge transfer quantity between the NO_2 analyte and Sc_2CF_2 due to the placement of LUMO (NO_2) between the valence band gap of Sc_2CF_2. This observation substantiated that Sc_2CF_2 can selectively detect NO_2 and thus act as a potential gas sensor. Wang et al. evaluated the selectivity of monolayer- Hf_2CO_2 for ammonia gas using theoretical first-principle calculations. They observed that SO_2, water, and CO_2 enhance ammonia adsorption on the Hf_2CO_2 layer (Wang et al., 2019). Recently, Li et al. (Li et al., 2023) utilized the MXene-Hf_2CO_2 monolayer for SO_2 capture through the adsorption of water molecules. Both the research works are based on first-principles calculations and substantiate that the reabsorption of water molecules before major analytes on MXene layers is due to hydrogen bonding.

6.3. Separation of gases analytes

MXene-based molecular sieving membranes are a lucrative technology with far-reaching implications for separating gaseous pollutants. With facile operations, lower energy consumption, and cost efficiency, MXene-based gas membrane sieves are gaining popularity. They are favoured over polymeric or carbon-based nanomembranes. Ding et al. (Ding et al., 2018) developed exfoliated MXenes nanosheets to selectively obtain laminar membranes to separate gaseous analytes. They demonstrated molecular sieving through MXenes for hydrogen and
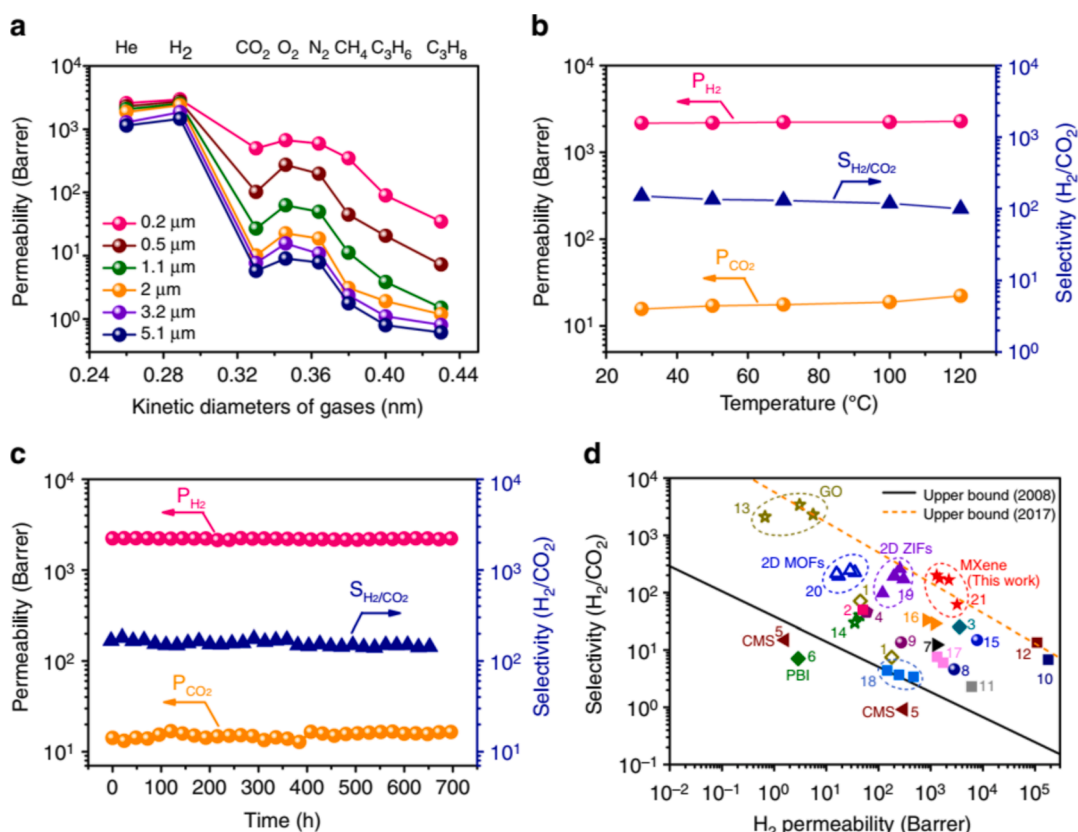

Fig. 19. Gas separation performance of the MXene membranes, MXene molecular sieving membranes for highly efficient gas separation (Ding et al., 2023).

carbon dioxide gases. Fig. 19 shows the gas separation performance of the MXene membranes.

6.4. Gas sensing applications

Due to high electrical conductivity, tunable surface properties, and diverse stacking patterns, MXenes have superseded carbon-based nanomaterials in gas sensing applications. Seminal work on the MXene-gas sensor was performed by Yu et al. (Yu et al., 2015), who described the behavior of NH_3, H_2, O_2, CH_4, CO, CO_2, N_2, and NO_2 on Ti_2CO_2 – MXene. They observed that ammonia was strongly chemisorbed amongst all gases, and the adsorption site was at the nitrogen atom sitting above the titanium atom of Ti_2CO_2. Their studies revealed adsorption energies and charge transfer of – 0.37 eV and 0.174e on ammonia gas in their novel MXene material. Xiao et al. (Xiao et al., 2016) further investigated the reusability of MXenes for ammonia capture and sensing, particularly focused on interactions between gas molecules and O-functionalized M_2CO_2 MXene where M was either Ti, Zr, Sc, and Hf. These reports were based on computational study and needed a practical demonstration to substantiate the data on MXene as potential gas sensors.

Also, MXenes are largely hydrophilic; hence, their sensing capability for non-polar gaseous analytes presents a serious challenge. Of all the gases, hydrogen and methane are nonpolar gas analytes. Various investigations pivoted towards experimental evidence to demonstrate that MXenes are ideal gas separation and sensing materials. Lee et al. (Lee et al., 2019) demonstrated a 2D vanadium carbide MXene gas sensor, illustrating LoD for hydrogen and methane analytes at 2 ppm and 25 ppm at room temperature, respectively. LoD values for V_2CTx-MXene were significantly lower than other nanomaterials and functionalized metal nanoparticles. Hence, these materials are also tunable to sense nonpolar gases, overcoming a major limitation to MXene applications.

7. Challenges and future research

MXenes hold great potential for environmental protection and engineering applications. However, as with any emerging technology, several challenges and areas of future research need to be addressed to ensure their safe and effective utilization. One of the key challenges is understanding the potential toxicity of MXenes. While MXenes have shown low toxicity in preliminary studies, further research is needed to assess their full impact on human health and the environment. Toxicity studies should investigate the potential release of metal ions, degradation products, and their long-term effects on living organisms. It is crucial to determine the safe exposure limits and develop appropriate regulations to protect human health and the environment. MXenes are often used in water treatment applications, where they come into direct contact with water. The leaching of MXenes can lead to the contamination of water sources, potentially causing adverse effects on aquatic ecosystems and human health. Future research should focus on understanding the leaching behavior of MXenes under different environmental conditions (including different pH conditions and the possibility of bioleaching caused by bacteria or yeast) and develop strategies to minimize their release into water systems.

Regarding MXene utilization, ongoing research is on activating oxidants like hydrogen peroxide, persulfates, and percarbonate for enhanced environmental remediation. These oxidants, such as dyes and pharmaceuticals, can be used with MXenes to degrade organic pollutants in water and soil. However, further investigation is needed to optimize the MXene-oxidant systems, including understanding the kinetics, reaction mechanisms, and the influence of MXene properties on the overall performance. This research can contribute to the development of efficient and sustainable remediation technologies.

The future of MXene research in environmental engineering and protection also involves exploring their potential applications beyond current knowledge. MXenes possess remarkable properties such as high surface area and tunable surface chemistry, which can be utilized to prepare functionalized fit-to-the-purpose materials with high selectivity. For example, MXenes could be utilized in advanced sensors for environmental monitoring, efficient renewable energy conversion catalysts, and novel pollutant capture materials. Additionally, efforts should be made to develop scalable and cost-effective synthesis methods for MXenes. Currently, most MXene production methods are conducted in small-scale laboratory settings, limiting their practical application. Scaling up the synthesis process while maintaining the quality and properties of MXenes is a crucial step to facilitate their integration into real-world environmental engineering solutions. Furthermore, exploring the environmental fate and transport of MXenes is essential. Understanding how MXenes interact with different environmental matrices, such as soil and sediments, is crucial to predicting their behavior, potential accumulation, and long-term impacts. This knowledge can guide the safe handling, disposal, and potential reuse of MXenes, ensuring their sustainability in environmental applications.

8. Conclusions

MXene, an innovative material composed of metal carbides and nitrides, is attracting interest for its possible environmental protection capabilities. MXene possesses exceptional properties, including strong conductivity, chemical stability, and a substantial surface area, rendering it advantageous for various environmental applications. One of its primary applications is in water purification. MXene-based membranes are effective for desalination, facilitating the removal of salts, organic contaminants, and microbes from water. These membranes are efficient because of their high permeability, selectivity, and stability. MXenes function as adsorbents, capturing and eliminating heavy metals, medicines, and radioactive substances from water, with a significant sorption capacity of 10–200 mg/g. They have shown particularly adept at eliminating pharmaceuticals such as antibiotics and analgesics, including ibuprofen and diclofenac, from water. In addition to water treatment, MXene can be utilized in environmental monitoring via sensors. These sensors can identify and quantify pollution levels, harmful chemicals, and air quality by selectively absorbing specific molecules or ions. MXene-based sensors offer immediate data, facilitating the prompt identification and management of pollutants. MXene is advantageous in photocatalysis, a technique in which light facilitates chemical processes. It can decompose contaminants in water and air, converting dangerous compounds into less toxic variants. This renders it advantageous for air purification and wastewater treatment. Nonetheless, there are apprehensions regarding the environmental ramifications of MXene, encompassing the possible release of metals and erosion, which could generate minuscule particles that may pose a threat. Notwithstanding these apprehensions, the adaptability of MXene renders it a viable material for addressing environmental difficulties, including water purification, pollution monitoring, and facilitating sustainable development. Continued research may further reveal its possibilities for a more sustainable and environmentally friendly future.

CRediT authorship contribution statement

Mohammad Hadi Dehghani: Writing – review & editing, Writing – original draft, Supervision. **Nadeem Hussain Solangi:** Conceptualization. **Nabisab Mujawar Mubarak:** Data curation. **Natarajan Rajamohan:** Formal analysis. **Subrajit Bosua:** Formal analysis. **Amina Othmani:** Investigation. **Md. Ahmaruzzaman:** Methodology. **Soumya Ranjan Mishra:** Data curation. **Baishali Bhattacharjee:** Methodology. **Vishal Gadore:** Data curation. **Talib Hussain Banglani:** Methodology. **Nawab Waris:** Investigation. **Ali hyder:** Data curation. **Ayaz Ali Memon:** Conceptualization. **Khalid Hussain Thebo:** Software. **Payal Joshi:** Software, Writing – review & editing. **Grzegorz Boczkaj:** Validation, Writing – review & editing. **Rama Rao Karri:** Visualization, Validation.

Funding

No funding.

References

Abbas, K.K., AbdulkadhimAl-Ghaban, A.M., Rdewi, E.H., 2022. Synthesis of a novel ZnO/TiO2-nanorod MXene heterostructured nanophotocatalyst for the removal pharmaceutical ceftriaxone sodium from aqueous solution under simulated sunlight. Journal of Environmental Chemical Engineering 10 (4), 108111.

Ahmaruzzaman, M., 2022. MXene-based novel nanomaterials for remediation of aqueous environmental pollutants. Inorganic Chemistry Communications, 109705.

Ahmaruzzaman, M., 2022. MXenes based advanced next generation materials for sequestration of metals and radionuclides from aqueous stream. Journal of Environmental Chemical Engineering, 108371.

Ahmaruzzaman, M., 2022. MXenes and MXene-supported nanocomposites: a novel materials for aqueous environmental remediation. RSC Advances 12 (53), 34766–34789. https://doi.org/10.1039/D2RA05530A.

Algaradah, M.M., 2024. MXene-based adsorbent materials for pollutants removal from water: Current challenges and future prospects. Inorganic Chemistry Communications 161, 112113. https://doi.org/10.1016/j.inoche.2024.112113.

Anasori, B., Gogotsi, Y., 2022. MXenes: Trends, growth, and future directions. Graphene and 2D Materials 1–5.

Attia, L.A., Youssef, M., Abdel Moamen, O., 2021. Feasibility of radioactive cesium and europium sorption using valorized punica granatum peel: kinetic and equilibrium aspects. Separation Science and Technology 56 (2), 217–232.

Azadmanjiri, J., Roy, P.K., Děkanovský, L., Sofer, Z.J.N., 2023. Chalcogen (S, Se, and Te), Decorated Few-Layered Ti3C2Tx MXene Hybrids: Modulation of Properties through Covalent Bonding. Nanoscale 15 (8), 4033–4044.

Bai, X., Guan, J., 2023. Applications of MXene-Based Single-Atom Catalysts. Small Structures 2200354.

Bhattacharjee, B., Ahmaruzzaman, M., Djellabi, R., Elimian, E., Rtimi, S., 2022. Advances in 2D MXenes-based materials for water purification and disinfection: Synthesis approaches and photocatalytic mechanistic pathways. Journal of Environmental Management 324, 116387.

Bhowmik, T., Kundu, M.K., Barman, S., 2015. Ultra small gold nanoparticles–graphitic carbon nitride composite: an efficient catalyst for ultrafast reduction of 4-nitrophenol and removal of organic dyes from water. RSC Advances 5 (48), 38760–38773.

Bhuyan, A., Ahmaruzzaman, M., 2023. Recent advances in new generation nanocomposite materials for adsorption of pharmaceuticals from aqueous environment. Environmental Science and Pollution Research 1–41.

Brunetti, A., Pomilla, F.R., Marcì, G., Garcia-Lopez, E.I., Fontananova, E., Palmisano, L., Barbieri, G., 2019. CO2 reduction by C3N4-TiO2 Nafion photocatalytic membrane reactor as a promising environmental pathway to solar fuels. Applied Catalysis b: Environmental 255, 117779.

Cai, T., Wang, L., Liu, Y., Zhang, S., Dong, W., Chen, H., Yi, X., Yuan, J., Xia, X., Liu, C., Luo, S., 2018. Ag3PO4/Ti3C2 MXene interface materials as a Schottky catalyst with enhanced photocatalytic activities and anti-photocorrosion performance. Applied Catalysis b: Environmental 239, 545–554. https://doi.org/10.1016/j.apcatb.2018.08.053.

Cai, C., Wang, R., Liu, S., Yan, X., Zhang, L., Wang, M., Tong, Q., Jiao, T., 2020. Synthesis of self-assembled phytic acid-MXene nanocomposites via a facile hydrothermal approach with elevated dye adsorption capacities. Colloids and Surfaces a: Physicochemical and Engineering Aspects 589, 124468.

Cao, Y., Fang, Y., Lei, X., Tan, B., Hu, X., Liu, B., Chen, Q., 2020. Fabrication of novel CuFe2O4/MXene hierarchical heterostructures for enhanced photocatalytic degradation of sulfonamides under visible light. Journal of Hazardous Materials 387, 122021.

Cao, S., Shen, B., Tong, T., Fu, J., Yu, J., 2018. 2D/2D heterojunction of ultrathin MXene/Bi2WO6 nanosheets for improved photocatalytic CO2 reduction. Advanced Functional Materials 28 (21), 1800136.

Chandran, M., Aswathy, E., Shamna, I., Vinoba, M., Kottappara, R., Bhagiyalakshmi, M., 2021. Laccase immobilized on Au confined MXene based electrode for electrochemical detection of catechol. Materials Today: Proceedings 46, 3136–3143.

Chen, G., Cheng, W., Wang, Y., Luo, C., Guo, W., Wang, G., Qiu, M., 2024. Enhanced photoreduction of U(VI) in solution by Ti3C2Tx/g-C3N4 composites. Journal of Environmental Chemical Engineering 12 (3), 112818. https://doi.org/10.1016/j.jece.2024.112818.

Chen, S., Liu, R., Kuai, Z., Li, X., Lian, S., Jiang, D., Tang, J., Li, L., Wu, R., Peng, C., 2022. Facile synthesis of a novel BaSnO3/MXene nanocomposite by electrostatic self-

assembly for efficient photodegradation of 4-nitrophenol. Environmental Research 204, 111949.

Chen, S., Liu, H., 2022. Self-reductive palladium nanoparticles loaded on polydopamine-modified MXene for highly efficient and quickly catalytic reduction of nitroaromatics and dyes. Colloids and Surfaces a: Physicochemical and Engineering Aspects 635, 128038.

Chen, X., Tong, X., Gao, J., Yang, L., Ren, J., Yang, W., Liu, S., Qi, M., Crittenden, J., Hao, R., 2022. Simultaneous nitrite resourcing and mercury ion removal using mxene-anchored goethite heterogeneous fenton composite. Environmental Science & Technology 56 (7), 4542–4552.

Chen, Y., Zhao, P., Liang, Y., Ma, Y., Liu, Y., Zhao, J., Hou, J., Hou, C., Huo, D., 2023. A sensitive electrochemical sensor based on 3D porous melamine-doped rGO/MXene composite aerogel for the detection of heavy metal ions in the environment. Talanta 256, 124294.

Chen, J., Zheng, H., Zhao, Y., Que, M., Wang, W., Lei, X., 2020. Morphology and photocatalytic activity of TiO2/MXene composites by in-situ solvothermal method. Ceramics International 46 (12), 20088–20096.

Chen, J., Zheng, H., Zhao, Y., Que, M., Lei, X., Zhang, K., Luo, Y., 2020. Preparation of facet exposed TiO2/Ti3C2Tx composites with enhanced photocatalytic activity. Journal of Physics and Chemistry of Solids 145, 109565.

Cheng, K., Wang, M., Wang, S., Liu, N., Xu, J., Wang, H., Su, Y., 2022. Monolayer Sc2CF2 as a Potential Selective and Sensitive NO2 Sensor: Insight from First-Principles Calculations. ACS Omega 7 (11), 9267–9275.

Cheng, H., Yang, J., 2020. Preparation of Ti3C2-PANI composite as sensor for electrochemical determination of mercury ions in water. Int. J. Electrochem. Sci 15, 2295–2306.

Cheng, X., Zu, L., Jiang, Y., Shi, D., Cai, X., Ni, Y., Lin, S., Qin, Y., 2018. A titanium-based photo-Fenton bifunctional catalyst of mp-MXene/TiO 2−x nanodots for dramatic enhancement of catalytic efficiency in advanced oxidation processes. Chemical Communications 54 (82), 11622–11625.

Cui, C., Guo, R., Xiao, H., Ren, E., Song, Q., Xiang, C., Lai, X., Lan, J., Jiang, S., 2020. Bi2WO6/Nb2CTx MXene hybrid nanosheets with enhanced visible-light-driven photocatalytic activity for organic pollutants degradation. Applied Surface Science 505, 144595.

Cui, Y., Huang, J., Fu, X., Wang, X., 2012. Metal-free photocatalytic degradation of 4-chlorophenol in water by mesoporous carbon nitride semiconductors. Catalysis Science & Technology 2 (7), 1396–1402.

Dai, S., Wang, Y., Xiao, L., Hao, G., Hu, Y., Zhang, G., Jiang, W., 2022. 2D/2D/2D CuO-MXene-OCN heterojunction with enhanced photocatalytic removal of pharmaceuticals and personal care products: Characterization, efficiency and mechanism. Journal of Alloys and Compounds 919, 165873.

Dehghani, M.H., Najafpoor, A.A., Azam, K., 2010. Using sonochemical reactor for degradation of LAS from effluent of wastewater treatment plant. 2010. Desalination 250, 82–86.

Devaraj, M., Rajendran, S., Hoang, T.K., Soto-Moscoso, M., 2022. A review on MXene and its nanocomposites for the detection of toxic inorganic gases. Chemosphere 302, 134933.

Ding, M., Ao, W., Xu, H., Chen, W., Tao, L., Shen, Z., Liu, H., Lu, C., Xie, Z., 2021. Facile construction of dual heterojunction CoO@ TiO2/MXene hybrid with efficient and stable catalytic activity for phenol degradation with peroxymonosulfate under visible light irradiation. Journal of Hazardous Materials 420, 126686.

Ding, J., Condon, A., Shah, S.P., 2018. Interpretable dimensionality reduction of single cell transcriptome data with deep generative models. Nature Communications 9 (1), 2002.

Ding, L., Y. Wei, L. Li, T. Zhang, H. Wang, J. Xue, L.-X. Ding, S. Wang, J. Caro, and Y. Gogotsi, MXene molecular sieving membranes for highly efficient gas separation, in MXenes. 2023, Jenny Stanford Publishing. p. 853-873.

Ding, R., Jiang, W., Ma, Y., Yang, Q., Han, X., Hou, X., 2023. A highly sensitive MXene/AuPt/AChE-based electrochemical platform for the detection of chlorpyrifos. Microchemical Journal, 108425.

Dong, Y., Sang, D., He, C., Sheng, X., Lei, L., 2019. Mxene/alginate composites for lead and copper ion removal from aqueous solutions. RSC Advances 9 (50), 29015–29022. https://doi.org/10.1039/c9ra05251h.

Du, Y., Yu, B., Wei, L., Wang, Y., Zhang, X., Ye, S., 2019. Efficient removal of Pb (II) by Ti3C2T x powder modified with a silane coupling agent. Journal of Materials Science 54 (20), 13283–13297.

Elumalai, S., Yoshimura, M., Ogawa, M., 2020. Simultaneous delamination and rutile formation on the surface of Ti3C2Tx MXene for copper adsorption. Chemistry–an Asian Journal 15 (7), 1044–1051.

Fan, G., Li, X., Xu, C., Jiang, W., Zhang, Y., Gao, D., Bi, J., Wang, Y., 2018. Palladium supported on titanium carbide: A highly efficient, durable, and recyclable bifunctional catalyst for the transformation of 4-chlorophenol and 4-nitrophenol. Nanomaterials 8 (3), 141.

Fan, Y., Li, J., Wang, S., Meng, X., Zhang, W., Jin, Y., Yang, N., Tan, X., Li, J., Liu, S., 2020. Voltage-enhanced ion sieving and rejection of Pb2+ through a thermally cross-linked two-dimensional MXene membrane. Chemical Engineering Journal 401, 126073.

Fard, A.K., Mckay, G., Chamoun, R., Rhadfi, T., Preud'Homme, H., Atieh, M.A., 2017. Barium removal from synthetic natural and produced water using MXene as two dimensional (2-D) nanosheet adsorbent. Chemical Engineering Journal 317, 331–342.

Fayyaz, A., Saravanakumar, K., Talukdar, K., Kim, Y., Yoon, Y., Park, C.M., 2021. Catalytic oxidation of naproxen in cobalt spinel ferrite decorated Ti3C2Tx MXene activated persulfate system: Mechanisms and pathways. Chemical Engineering Journal 407, 127842.

Feng, X., Yu, Z., Long, R., Li, X., Shao, L., Zeng, H., Zeng, G., Zuo, Y., 2020. Self-assembling 2D/2D (MXene/LDH) materials achieve ultra-high adsorption of heavy metals Ni2+ through terminal group modification. Separation and Purification Technology 253, 117525.

Feng, X., Yu, Z., Sun, Y., Long, R., Shan, M., Li, X., Liu, Y., Liu, J., 2021. Review MXenes as a new type of nanomaterial for environmental applications in the photocatalytic degradation of water pollutants. Ceramics International 47 (6), 7321–7343.

Fondamentales, S., Poitiers, U.D., Brunet, M., Batiment, B., 2017. Les MXènes : une large famille de matériaux 2D - De la fonctionnalisation aux propriétés. Mauchamp 23, 235428.

Fu, K., Liu, X., Yu, D., Luo, J., Wang, Z., Crittenden, J.C., 2020. Highly efficient and selective Hg (II) removal from water using multilayered Ti3C2O x MXene via adsorption coupled with catalytic reduction mechanism. Environmental Science & Technology 54 (24), 16212–16220.

Gan, D., Huang, Q., Dou, J., Huang, H., Chen, J., Liu, M., Wen, Y., Yang, Z., Zhang, X., Wei, Y., 2020. Bioinspired functionalization of MXenes (Ti3C2Tx) with amino acids for efficient removal of heavy metal ions. Applied Surface Science 504, 144603.

Gao, K., Hou, L.-A., An, X., Huang, D., Yang, Y., 2023. BiOBr/MXene/gC3N4 Z-scheme heterostructure photocatalysts mediated by oxygen vacancies and MXene quantum dots for tetracycline degradation: Process, mechanism and toxicity analysis. Applied Catalysis b: Environmental 323, 122150.

Ghanbari, R., Nazarzadeh Zare, E., Paiva-Santos, A.C., Rabiee, N., 2023. Ti3C2Tx MXene@MOF decorated polyvinylidene fluoride membrane for the remediation of heavy metals ions and desalination. Chemosphere 311, 137191. https://doi.org/10.1016/j.chemosphere.2022.137191.

Ghani, A.A., Shahzad, A., Moztahida, M., Tahir, K., Jeon, H., Kim, B., Lee, D.S., 2021. Adsorption and electrochemical regeneration of intercalated Ti3C2Tx MXene for the removal of ciprofloxacin from wastewater. Chemical Engineering Journal 421, 127780.

Gogotsi, Y., Anasori, B., 2019. The Rise of MXenes. ACS Nano 13 (8), 8491–8494. https://doi.org/10.1021/acsnano.9b06394.

Gong, X., Zhang, G., Dong, H., Wang, H., Nie, J., Ma, G., 2022. Self-assembled hierarchical heterogeneous MXene/COF membranes for efficient dye separations. Journal of Membrane Science 657, 120667.

Gopalram, K., Kapoor, A., Kumar, P.S., Sunil, A., Rangasamy, G., 2023. MXenes and MXene-Based Materials for Removal and Detection of Water Contaminants: A Review. Industrial & Engineering Chemistry Research 62 (17), 6559–6583. https://doi.org/10.1021/acs.iecr.3c00595.

Grzegórska, A., Głuchowski, P., Karczewski, J., Ryl, J., Wysocka, I., Siuzdak, K., Trykowski, G., Grochowska, K., Zielińska-Jurek, A., 2021. Enhanced photocatalytic activity of accordion-like layered Ti3C2 (MXene) coupled with Fe-modified decahedral anatase particles exposing 1 0 1 and 0 0 1 facets. Chemical Engineering Journal 426, 130801.

Guo, W., Liang, L., Zhao, Y., Zhao, C., Lu, X., Cao, Y., Gao, F., 2023. In-situ growth of SnO2 nanoparticles on Nb2CTx nanosheets as highly sensitive electrochemical sensing platform for organophosphorus pesticide detection. Biointerfaces, Colloids and Surfaces B, p. 113238.

He, Y., Ma, L., Zhou, L., Liu, G., Jiang, Y., Gao, J., 2020. Preparation and application of bismuth/MXene nano-composite as electrochemical sensor for heavy metal ions detection. Nanomaterials 10 (5), 866.

He, B., Man, P., Zhang, Q., Fu, H., Zhou, Z., Li, C., Li, Q., Wei, L., Yao, Y.-J.-N.-M.-L., 2019. All Binder-Free Electrodes for High-Performance Wearable Aqueous Rechargeable Sodium-Ion Batteries. Nano-Micro Letters 11, 101.

Hu, X., Chen, C., Zhang, D., Xue, Y., 2021. Kinetics, isotherm and chemical speciation analysis of Hg(II) adsorption over oxygen-containing MXene adsorbent. Chemosphere 278, 130206. https://doi.org/10.1016/j.chemosphere.2021.130206.

Huang, L., Ding, L., Wang, H., 2021. MXene-Based Membranes for Separation Applications. Small Science 1 (7), 2100013.

Huang, R., Liao, D., Chen, S., Yu, J., Jiang, X., 2020. A strategy for effective electrochemical detection of hydroquinone and catechol: Decoration of alkalization-intercalated Ti3C2 with MOF-derived N-doped porous carbon. Sensors and Actuators b: Chemical 320, 128386.

Huang, R., Liao, D., Liu, Z., Yu, J., Jiang, X., 2021. Electrostatically assembling 2D hierarchical Nb2CTx and zifs-derivatives into Zn-Co-NC nanocage for the electrochemical detection of 4-nitrophenol. Sensors and Actuators b: Chemical 338, 129828.

Huang, H., Song, Y., Li, N., Chen, D., Xu, Q., Li, H., He, J., Lu, J., 2019. One-step in-situ preparation of N-doped TiO2@ C derived from Ti3C2 MXene for enhanced visible-light driven photodegradation. Applied Catalysis b: Environmental 251, 154–161.

Hussain, M., Mahmoud, M., Rasheed, A., El Azab, I.H., Anwar, M., El-Bahy, Z.M.J.O.M., 2024. Silver-Doped Cadmium Aluminate and Its MXene Based Composite for Visible-Light Driven Photocatalytic Degradation of Organic Pollutants. 155, 115824.

Ibrahim, Y., Meslam, M., Eid, K., Salah, B., Abdullah, A.M., Ozoemena, K.I., Elzatahry, A., Sharaf, M.A., Sillanpää, M., 2022. A review of MXenes as emergent materials for dye removal from wastewater. Separation and Purification Technology 282, 120083.

Ihsanullah, I., 2022. MXenes as next-generation materials for the photocatalytic degradation of pharmaceuticals in water. Journal of Environmental. Chemical Engineering, 107381.

Ihsanullah, I., Bilal, M., 2022. Potential of MXene-based membranes in water treatment and desalination: A critical review. Chemosphere 303, 135234. https://doi.org/10.1016/j.chemosphere.2022.135234.

Jatoi, A.S., Mubarak, N.M., Hashmi, Z., Solangi, N.H., Karri, R.R., Hua, T.Y., Mazari, S.A., Koduru, J.R., Alfantazi, A., 2022. New insights into MXene applications for sustainable environmental remediation. Chemosphere, 137497. https://doi.org/10.1016/j.chemosphere.2022.137497.

Javaid, A., Latif, S., Imran, M., Hussain, N., Bilal, M., Iqbal, H.M., 2022. MXene-based hybrid composites as photocatalyst for the mitigation of pharmaceuticals. Chemosphere 291, 133062.

Jiang, D., Sun, X., Wu, X., Zhang, S., Qu, X., Shi, L., Zhang, Y., Du, F., 2020. MXene-Ti3C2 assisted one-step synthesis of carbon-supported TiO2/Bi4NbO8Cl heterostructures for enhanced photocatalytic water decontamination. Nanophotonics 9 (7), 2077–2088.

Jin, L., Chai, L., Yang, W., Wang, H., Zhang, L., 2020. Two-dimensional titanium carbides (Ti3C2Tx) functionalized by poly (m-phenylenediamine) for efficient adsorption and reduction of hexavalent chromium. International Journal of Environmental Research and Public Health 17 (1), 167.

Jin, Y., Fan, Y., Meng, X., Li, J., Li, C., Sunarso, J., Yang, N., Meng, B., Zhang, W., 2021. Modeling of hydrated cations transport through 2D MXene (Ti3C2Tx) membranes for water purification. Journal of Membrane Science 631, 119346. https://doi.org/10.1016/j.memsci.2021.119346.

Jun, B.-M., Kim, S., Heo, J., Park, C.M., Her, N., Jang, M., Huang, Y., Han, J., Yoon, Y., 2019. Review of MXenes as new nanomaterials for energy storage/delivery and selected environmental applications. Nano Research 12, 471–487.

Jun, B.-M., Jang, M., Park, C.M., Han, J., Yoon, Y., 2020. Selective adsorption of Cs+ by MXene (Ti3C2Tx) from model low-level radioactive wastewater. Nuclear Engineering and Technology 52 (6), 1201–1207.

Jun, B.-M., Her, N., Park, C.M., Yoon, Y., 2020. Effective removal of Pb (ii) from synthetic wastewater using Ti 3 C 2 T x MXene. Environmental Science: Water Research & Technology 6 (1), 173–180.

Jun, B.-M., Heo, J., Taheri-Qazvini, N., Park, C.M., Yoon, Y., 2020. Adsorption of selected dyes on Ti3C2Tx MXene and Al-based metal-organic framework. Ceramics International 46 (3), 2960–2968.

Jun, B.-M., Park, C.M., Heo, J., Yoon, Y., 2020. Adsorption of Ba2+ and Sr2+ on Ti3C2Tx MXene in model fracking wastewater. Journal of Environmental Management 256, 109940.

Kadhom, M., Kalash, K., Al-Furaiji, M., 2022. Performance of 2D MXene as an adsorbent for malachite green removal. Chemosphere 290, 133256. https://doi.org/10.1016/j.chemosphere.2021.133256.

Kandi, D., Martha, S., Thirumurugan, A., Parida, K., 2017. Modification of BiOI microplates with CdS QDs for enhancing stability, optical property, electronic behavior toward rhodamine B decolorization, and photocatalytic hydrogen evolution. The Journal of Physical Chemistry C 121 (9), 4834–4849.

Karri, R.R., Ravindran, G., Dehghani, M.H., 2021. Wastewater—Sources, Toxicity, and Their Consequences to Human Health, in Soft Computing Techniques in Solid Waste and Wastewater. Management. Elsevier, 3–33. https://doi.org/10.1016/B978-0-12-824463-0.00001-X.

Karri, R.R., Mubarak, N.M., Koduru, J.R., Lingamdinne, L.P., Dehghani, M.H., Jatoi, A.S., Mazari, S.A., 2023. Role of hybrid nanomaterials for a sustainable environment, in Hybrid Nanomaterials for Sustainable Applications. Case Studies and Applications. Elsevier, 1–24. https://doi.org/10.1016/B978-0-323-98371-6.00017-3.

Karri, R.R., Solangi, N.H., Mubarak, N.M., Jatoi, A.S., Lingamdinne, L.P., Koduru, J.R., Dehghani, M.H., Khan, N.A., 2024. Carbon nanotubes for sustainable renewable energy applications. In: Water Treatment Using Engineered Carbon Nanotubes. Elsevier, pp. 433–456.

Karthikeyan, P., Ramkumar, K., Pandi, K., Fayyaz, A., Meenakshi, S., Park, C.M., 2021. Effective removal of Cr (VI) and methyl orange from the aqueous environment using two-dimensional (2D) Ti3C2Tx MXene nanosheets. Ceramics International 47 (3), 3692–3698.

Kemp, K., Griffiths, J., Campbell, S., Lovell, K., 2013. An exploration of the follow-up up needs of patients with inflammatory bowel disease. Journal of Crohn's and Colitis 7 (9), e386–e395.

Khan, A.R., Husnain, S.M., Shahzad, F., Mujtaba-ul-Hassan, S., Mehmood, M., Ahmad, J., Mehran, M.T., Rahman, S., 2019. Two-dimensional transition metal carbide (Ti 3 C 2 T x) as an efficient adsorbent to remove cesium (Cs+). Dalton Transactions 48 (31), 11803–11812.

Khan, F.S.A., Mubarak, N.M., Khalid, M., Tan, Y.H., Abdullah, E.C., Rahman, M.E., Karri, R.R., 2021. A comprehensive review on micropollutants removal using carbon nanotubes-based adsorbents and membranes. Journal of Environmental. Chemical Engineering 9 (6). https://doi.org/10.1016/j.jece.2021.106647.

Khan, F.S.A., Mubarak, N.M., Khalid, M., Khan, M.M., Tan, Y.H., Walvekar, R., Abdullah, E.C., Karri, R.R., Rahman, M.E., 2022. Comprehensive review on carbon nanotubes embedded in different metal and polymer matrix: fabrications and applications. Critical Reviews in Solid State and Materials Sciences 47 (6), 837–864. https://doi.org/10.1080/10408436.2021.1935713.

Khatami, M., Iravani, S., 2021. MXenes and MXene-based materials for the removal of water pollutants: challenges and opportunities. Comments on Inorganic Chemistry 41 (4), 213–248.

Kim, S., Gholamirad, F., Yu, M., Park, C.M., Jang, A., Jang, M., Taheri-Qazvini, N., Yoon, Y., 2021. Enhanced adsorption performance for selected pharmaceutical compounds by sonicated Ti3C2Tx MXene. Chemical Engineering Journal 406, 126789.

Kim, S., Nam, S.-N., Park, C.M., Jang, M., Taheri-Qazvini, N., Yoon, Y., 2022. Effect of single and multilayered Ti3C2TX MXene as a catalyst and adsorbent on enhanced sonodegradation of diclofenac and verapamil. Journal of Hazardous Materials 426, 128120.

Koduru, J.R., R.R. Karri, and N.M. Mubarak, Hybrid Nanomaterials for Sustainable Applications: Case Studies and Applications. Hybrid Nanomaterials for Sustainable Applications: Case Studies and Applications. 2023: Elsevier. 1-423.

Kong, A., Sun, Y., Peng, M., Gu, H., Fu, Y., Zhang, J., Li, W., 2021. Amino-functionalized MXenes for efficient removal of Cr (VI). Colloids and Surfaces a: Physicochemical and Engineering Aspects 617, 126388.

Kuang, P., Low, J., Cheng, B., Yu, J., Fan, J., 2020. MXene-based photocatalysts. Journal of Materials Science & Technology 56, 18–44.

Kulkarni, R., Lingamdinne, L.P., Koduru, J.R., Karri, R.R., Kailasa, S.K., Mubarak, N.M., Chang, Y.Y., Dehghani, M.H., 2024. Exploring the recent cutting-edge applications of CNTs in energy and environmental remediation: Mechanistic insights and remarkable performance advancements. Journal of Environmental. Chemical Engineering 12 (5). https://doi.org/10.1016/j.jece.2024.113251.

Kulkarni, R., Lingamdinne, L.P., Koduru, J.R., Chang, Y.Y., Somala, A.R., Karri, R.R., Mubarak, N.M., 2024. Graphene oxide nanocomposites for the removal of inorganic species. Comprehensive Analytical Chemistry 106, 533–566. https://doi.org/10.1016/bs.coac.2024.02.004.

Kumar, A., Raizada, P., Singh, P., Hosseini-Bandegharaei, A., Thakur, V.K., 2020. Facile synthesis and extended visible light activity of oxygen and sulphur co-doped carbon nitride quantum dots modified Bi2MoO6 for phenol degradation. Journal of Photochemistry and Photobiology a: Chemistry 397, 112588.

Lai, G., Lau, W., Goh, P., Ismail, A., Tan, Y., Chong, C., Krause-Rehberg, R., Awad, S., 2018. Tailor-made thin film nanocomposite membrane incorporated with graphene oxide using novel interfacial polymerization technique for enhanced water separation. Chemical Engineering Journal 344, 524–534.

Lee, P.-K., Choi, B.-Y., Kang, M.-J., 2015. Assessment of mobility and bio-availability of heavy metals in dry depositions of Asian dust and implications for environmental risk. Chemosphere 119, 1411–1421.

Lee, E., VahidMohammadi, A., Yoon, Y.S., Beidaghi, M., Kim, D.-J., 2019. Two-dimensional vanadium carbide MXene for gas sensors with ultrahigh sensitivity toward nonpolar gases. ACS Sensors 4 (6), 1603–1611.

Lei, J.-C., Zhang, X., Zhou, Z., 2015. Recent advances in MXene: Preparation, properties, and applications. Frontiers of Physics 10, 276–286.

Li, X., Bai, Y., Shi, X., Huang, J., Zhang, K., Wang, R., Ye, L., 2021. Mesoporous g-C3N4/MXene (Ti3C2Tx) heterojunction as a 2D electronic charge transfer for efficient photocatalytic CO2 reduction. Applied Surface Science 546, 149111. https://doi.org/10.1016/j.apsusc.2021.149111.

Li, M., Bai, Y., Zhuang, W., Liu, J., Wang, Z., Rao, Y., Li, M., Ying, H., Ouyang, P., 2023. Sandwich-like heterostructured nanomaterials immobilized laccase for the degradation of phenolic pollutants and boosted enzyme stability. Colloids and Surfaces a: Physicochemical and Engineering Aspects 660, 130820.

Li, D., Chen, X., Xiang, P., Du, H., Xiao, B., 2020. Chalcogenated-Ti3C2X2 MXene (x= o, s, Se and Te) as a High-Performance Anode Material for Li-Ion Batteries. Applied Surface Science 501, 144221.

Li, X., Huang, Z., Shuck, C.E., Liang, G., Gogotsi, Y., Zhi, C., 2022. MXene chemistry, electrochemistry and energy storage applications. Nature Reviews Chemistry 6 (6), 389–404.

Li, Z., Li, J., Tan, J., Jiang, M., Fu, S., Zhang, T., Wang, X., 2022. In situ synthesis of novel peroxo-functionalized Ti3C2Tx adsorbent for aqueous pollutants removal: Role of oxygen-containing terminal groups. Chemosphere 286, 131801.

Li, J., Wang, S., Du, Y., Liao, W., 2018. Enhanced photocatalytic performance of TiO2@C nanosheets derived from two-dimensional Ti2CTx. Ceramics International 44 (6), 7042–7046.

Li, S., Wang, L., Peng, J., Zhai, M., Shi, W., 2019. Efficient thorium (IV) removal by two-dimensional Ti2CTx MXene from aqueous solution. Chemical Engineering Journal 366, 192–199.

Li, S., Wang, Y., Wang, J., Liang, J., Li, Y., Li, P., 2022. Modifying g-C3N4 with oxidized Ti3C2 MXene for boosting photocatalytic U (VI) reduction performance. Journal of Molecular Liquids 346, 117937.

Li, S., Wang, Y., Wang, J., Liang, J., Li, Y., Li, P., 2022. Modifying g-C3N4 with oxidized Ti3C2 MXene for boosting photocatalytic U(VI) reduction performance. Journal of Molecular Liquids 346, 117937. https://doi.org/10.1016/j.molliq.2021.117937.

Li, Z.K., Wei, Y., Gao, X., Ding, L., Lu, Z., Deng, J., Yang, X., Caro, J., Wang, H., 2020. Antibiotics separation with MXene membranes based on regularly stacked high-aspect-ratio nanosheets. Angewandte Chemie International Edition 59 (24), 9751–9756.

Li, K., Xiong, T., Liao, J., Lei, Y., Zhang, Y., Zhu, W., 2022. Design of MXene/graphene oxide nanocomposites with micro-wrinkle structure for efficient separating uranium (VI) from wastewater. Chemical Engineering Journal 433, 134449.

Li, L., Yan, H.-T., Li, X.-H., 2023. Effect of preadsorbing gas molecules on the adsorption of SO2 molecule on Hf2CO2 MXene by first-principles study. Surfaces and Interfaces 36,102639.

Liang, Y., Zhang, B., Shi, Y., Jiang, R., Zhang, H.J.M., 2023. Research on Wide-Temperature Rechargeable Sodium-Sulfur Batteries: Features, Challenges and Solutions. Materials 16 (12), 4263.

Liao, D., Liu, Z., Huang, R., Yu, J., Jiang, X., 2022. In-situ construction of porous carbon on embedded N-doped MXene nanosheets composite for simultaneous determination of 4-aminophenol and acetaminophen. Microchemical Journal 175, 107067.

Lim, K.R.G., Shekhirev, M., Wyatt, B.C., Anasori, B., Gogotsi, Y., Seh, Z.W., 2022. Fundamentals of MXene synthesis. Nature Synthesis 1 (8), 601–614.

Lin, Q., Zeng, G., Yan, G., Luo, J., Cheng, X., Zhao, Z., Li, H., 2022. Self-cleaning photocatalytic MXene composite membrane for synergistically enhanced water treatment: Oil/water separation and dyes removal. Chemical Engineering Journal 427, 131668.

Liu, F., Hu, Z., Xiang, M., Hu, B., 2022. Magnetic amidoxime-functionalized MXenes for efficient adsorption and immobilization of U (VI) and Th (IV) from aqueous solution. Applied Surface Science 601, 154227.

Liu, F., Hu, J., Hu, B., 2022. Magnetic MXene-NH2 decorated with persimmon tannin for highly efficient elimination of U (VI) and Cr (VI) from aquatic environment. International Journal of Biological Macromolecules 219, 886–896.

Liu, A., Liang, X., Ren, X., Guan, W., Gao, M., Yang, Y., Yang, Q., Gao, L., Li, Y., Ma, T., 2020. Recent progress in MXene-based materials: potential high-performance electrocatalysts. Advanced Functional Materials 30 (38), 2003437.

Liu, T., Liu, X., Graham, N., Yu, W., Sun, K., 2020. Two-dimensional MXene incorporated graphene oxide composite membrane with enhanced water purification performance. Journal of Membrane Science 593, 117431.

Liu, M., Niu, B., Guo, H., Ying, S., Chen, Z., 2021. Simple preparation of g-C3N4@ Ni3C nanosheets and its application in supercapacitor electrode materials, hydrogengeneration via NaBH4 hydrolysis and reduction of p–nitrophenol. Inorganic Chemistry Communications 130, 108687.

Liu, W., Sun, M., Ding, Z., Gao, B., Ding, W., 2021. Ti3C2 MXene embellished g-C3N4 nanosheets for improving photocatalytic redox capacity. Journal of Alloys and Compounds 877, 160223.

Liu, Q., Tan, X., Wang, S., Ma, F., Znad, H., Shen, Z., Liu, L., Liu, S., 2019. MXene as a non-metal charge mediator in 2D layered CdS@ Ti 3 C 2@ TiO 2 composites with superior Z-scheme visible light-driven photocatalytic activity. Environmental Science: Nano 6 (10), 3158–3169.

Liu, Q., Han, X., Dou, Q., Xiong, P., Kang, Y., Kim, B.K., Park, H.S., 2022. NiFe-Layered Double Hydroxide Nanosheets Grafted onto Carbon Nanotubes for Functional Separator of Lithium Sulfur Batteries. International Journal of Energy Research 46 (7), 9634–9642.

Liu, Q., Luo, Y., Yang, S., Xiong, Y., Wang, R., Fu, X., Zhang, R., Hu, S., Bao, X., Xu, C., 2023. Transfer-free in-situ synthesis of high-performance polybenzimidazole grafted graphene oxide-based proton exchange membrane for high-temperature proton exchange membrane fuel cells. Journal of Power Sources 559, 232666. https://doi.org/10.1016/j.jpowsour.2023.232666.

Liu, F., Wang, S., Hu, B., 2023. Electrostatic self-assembly of nanoscale FeS onto MXenes with enhanced reductive immobilization capability for U (VI) and Cr (VI). Chemical Engineering Journal 456, 141100.

Liu, F., Wang, S., Hu, B., 2023. Electrostatic self-assembly of nanoscale FeS onto MXenes with enhanced reductive immobilization capability for U(VI) and Cr(VI). Chemical Engineering Journal 456, 141100. https://doi.org/10.1016/j.cej.2022.141100.

Liu, H., Yang, C., Jin, X., Zhong, J., Li, J., 2020. One-pot hydrothermal synthesis of MXene Ti3C2/TiO2/BiOCl ternary heterojunctions with improved separation of photoactivated carries and photocatalytic behavior toward elimination of contaminants. Colloids and Surfaces a: Physicochemical and Engineering Aspects 603, 125239.

Lu, Y., Yao, M., Zhou, A., Hu, Q., Wang, L., 2017. Preparation and photocatalytic performance of Ti3C2/TiO2/CuO ternary nanocomposites. Journal of Nanomaterials 2017.

Lu, C., Zhang, P., Jiang, S., Wu, X., Song, S., Zhu, M., Lou, Z., Li, Z., Liu, F., Liu, Y., 2017. Photocatalytic reduction elimination of UO22+ pollutant under visible light with metal-defect rich sulfur doped g-C3N4 photocatalyst. Applied Catalysis b: Environmental 200, 378–385.

Ma, Y., Xiong, D., Lv, X., Zhao, X., Meng, C., Xie, H., Zhang, Z., 2021. Rapid and long-lasting acceleration of zero-valent iron nanoparticles@ Ti 3 C 2-based MXene/peroxymonosulfate oxidation with bi-active centers toward ranitidine removal. Journal of Materials Chemistry A 9 (35), 19817–19833.

Mahar, I., Mahar, F.K., Mahar, N., Memon, A.A., Pirzado, A.A.A., Khatri, Z., Thebo, K.H., Ali, A., 2023. Fabrication and characterization of MXene/carbon composite-based nanofibers (MXene/CNFs) membrane: An efficient adsorbent material for removal of Pb+2 and As+3 ions from water. Chemical Engineering Research and Design 191, 462–471. https://doi.org/10.1016/j.cherd.2023.02.005.

Mashtalir, O., Cook, K.M., Mochalin, V.N., Crowe, M., Barsoum, M.W., Gogotsi, Y., 2014. Dye adsorption and decomposition on two-dimensional titanium carbide in aqueous media. Journal of Materials Chemistry A 2 (35), 14334–14338.

Meng, C., Gao, X., Zou, S., Na, B., Feng, W., Dai, Y., Yuan, D., Ming, B., 2022. Unraveling the adsorption behaviors of uranium and thorium on the hydroxylated titanium carbide MXene. Computational Materials Science 210, 111460.

Miao, Z., Wang, G., Zhang, X., Dong, X., 2020. Oxygen vacancies modified TiO2/Ti3C2 derived from MXenes for enhanced photocatalytic degradation of organic pollutants: The crucial role of oxygen vacancy to schottky junction. Applied Surface Science 528, 146929.

Miri-Jahromi, A., Didandeh, M., Shekarsokhan, S., 2022. Capability of MXene 2D material as an amoxicillin, ampicillin, and cloxacillin adsorbent in wastewater. Journal of Molecular Liquids 351, 118545.

Mu, W., Du, S., Yu, Q., Li, X., Wei, H., Yang, Y., 2018. Improving barium ion adsorption on two-dimensional titanium carbide by surface modification. Dalton Transactions 47 (25), 8375–8381.

Mubarak, N.M., Solangi, N.H., Karri, R.R., Tan, Y.H., Shams, S., Ruslan, K.N., Mazari, S.A., Khalid, M., 2024. Holistic Mechanism of Nanomaterials for Removal of Cd2+ from the Wastewater. Water, Air, and Soil Pollution 235 (4). https://doi.org/10.1007/s11270-024-07067-8.

Nasri, M.S.I., Samsudin, M.F.R., Tahir, A.A., Sufian, S., 2022. Effect of MXene Loaded on g-C3N4 Photocatalyst for the Photocatalytic Degradation of Methylene Blue. Energies 15 (3), 955.

Nie, X., Ji, Y., Ding, Y.-M., Li, Y.J.N., 2022. Layer-Stacking of Chalcogenide-Terminated MXenes Ti2CT2 (t= o, s, Se, Te) and Their Applications in Metal-Ion Batteries. Nanotechnology 34 (10), 105704.

Othman, Z., Sinopoli, A., Mackey, H.R., Mahmoud, K.A., 2021. Efficient Photocatalytic Degradation of Organic Dyes by AgNPs/TiO2/Ti3C2T x MXene Composites under UV and Solar Light. ACS Omega 6 (49), 33325–33338.

Pandey, R.P., Rasool, K., Madhavan, V.E., Aïssa, B., Gogotsi, Y., Mahmoud, K.A., 2018. Ultrahigh-flux and fouling-resistant membranes based on layered silver/MXene (Ti 3 C 2 T x) nanosheets. Journal of Materials Chemistry A 6 (8), 3522–3533.

Pandey, R.P., Rasheed, P.A., Gomez, T., Azam, R.S., Mahmoud, K.A., 2020. A fouling-resistant mixed-matrix nanofiltration membrane based on covalently cross-linked Ti3C2TX (MXene)/cellulose acetate. Journal of Membrane Science 607, 118139.

Park, S., Kim, S., Yea, Y., Saravanakumar, K., Lee, E., Yoon, Y., Park, C.M., 2023. Adsorptive and photocatalytic performance of cobalt-doped ZnTiO3/Ti3C2Tx MXene nanohybrids towards tetracycline: Kinetics and mechanistic insight. Journal of Hazardous Materials 443, 130165.

Parui, A., Srivastava, P., Singh, A.K., 2022. Selective Reduction of CO2 on Ti2C(OH)2 MXene through Spontaneous Crossing of Transition States. ACS Applied Materials and Interfaces14 (36),, 40913–40920.

Pazniak, H., Varezhnikov, A.S., Kolosov, D.A., Plugin, I.A., Vito, A.D., Glukhova, O.E., Sheverdyaeva, P.M., Spasova, M., Kaikov, I., Kolesnikov, E.A., 2021. 2D molybdenum carbide MXenes for enhanced selective detection of humidity in air. Advanced Materials 33 (52), 2104878.

Pérez-Álvarez, D.T., Brown, J., Elgohary, E.A., Mohamed, Y.M., El Nazer, H.A., Davies, P., Stafford, J., 2022. Challenges surrounding nanosheets and their application to solar-driven photocatalytic water treatment. Materials Advances 3 (10), 4103–4131.

Pouramini, Z., Mousavi, S.M., Babapoor, A., Hashemi, S.A., Pynadathu Rumjit, N., Garg, S., Ahmed, S., Chiang, W.-H., 2023. Recent Advances in MXene-Based Nanocomposites for Wastewater Purification and Water Treatment. A Review. Water 15 (7), 1267.

Raheem, I., Mubarak, N.M., Karri, R.R., Solangi, N.H., Jatoi, A.S., Mazari, S.A., Khalid, M., Tan, Y.H., Koduru, J.R., Malafaia, G., 2022. Rapid growth of MXene-based membranes for sustainable environmental pollution remediation. Chemosphere, 137056.

Raheem, I., Mubarak, N.M., Karri, R.R., Solangi, N.H., Jatoi, A.S., Mazari, S.A., Khalid, M., Tan, Y.H., Koduru, J.R., Malafaia, G., 2023. Rapid growth of MXene-based membranes for sustainable environmental pollution remediation. Chemosphere 311. https://doi.org/10.1016/j.chemosphere.2022.137056.

Rajendran, J., Kannan, T.S., Dhanasekaran, L.S., Murugan, P., Atchudan, R., ALOthman, Z.A., Ouladsmane, M., Sundramoorthy, A.K., 2022. Preparation of 2D Graphene/MXene nanocomposite for the electrochemical determination of hazardous bisphenol A in plastic products. Chemosphere 287, 132106.

Rana, D., Matsuura, T., Kassim, M., Ismail, A., 2013. Radioactive decontamination of water by membrane processes—a review. Desalination 321, 77–92.

Rana, A.G., Minceva, M., 2021. Analysis of photocatalytic degradation of phenol with exfoliated graphitic carbon nitride and light-emitting diodes using response surface methodology. Catalysts 11 (8), 898.

Ranjith, K.S., Vilian, A.E., Ghoreishian, S.M., Umapathi, R., Hwang, S.-K., Oh, C.W., Huh, Y.S., Han, Y.-K., 2022. Hybridized 1D–2D MnMoO4–MXene nanocomposites as high-performing electrochemical sensing platform for the sensitive detection of dihydroxybenzene isomers in wastewater samples. Journal of Hazardous Materials 421, 126775.

Rasheed, P.A., Pandey, R.P., Jabbar, K.A., Mahmoud, K.A., 2021. Platinum nanoparticles/Ti3C2Tx (MXene) composite for the effectual electrochemical sensing of Bisphenol A in aqueous media. Journal of Electroanalytical Chemistry 880, 114934.

Rasheed, P.A., Pandey, R.P., Jabbar, K.A., Mahmoud, K.A., 2022. Nb4C3Tx (MXene)/Au/DNA aptasensor for the ultraselective electrochemical detection of lead in water samples. Electroanalysis 34 (10), 1540–1546.

Rasool, K., Pandey, R.P., Rasheed, P.A., Buczek, S., Gogotsi, Y., Mahmoud, K.A., 2019. Water Treatment and Environmental Remediation Applications of Two-Dimensional Metal Carbides (MXenes). Materials Today 30, 80–102.

Ren, J., Zhu, Z., Qiu, Y., Yu, F., Zhou, T., Ma, J., Zhao, J., 2021. Enhanced adsorption performance of alginate/MXene/CoFe2O4 for antibiotic and heavy metal under rotating magnetic field. Chemosphere 284, 131284.

Rethinasabapathy, M., Hwang, S.K., Kang, S.-M., Roh, C., Huh, Y.S., 2021. Amino-functionalized POSS nanocage-intercalated titanium carbide (Ti3C2Tx) MXene stacks for efficient cesium and strontium radionuclide sequestration. Journal of Hazardous Materials 418, 126315.

Rethinasabapathy, M., Bhaskaran, G., Park, B., Shin, J.-Y., Kim, W.-S., Ryu, J., Huh, Y.S., 2022. Iron oxide (Fe3O4)-laden titanium carbide (Ti3C2Tx) MXene stacks for the efficient sequestration of cationic dyes from aqueous solution. Chemosphere 286, 131679.

Rizwan, K., Rahdar, A., Bilal, M., Iqbal, H.M., 2022. MXene-based electrochemical and biosensing platforms to detect toxic elements and pesticides pollutants from environmental matrices. Chemosphere 291, 132820.

Sani, Y.M., Solangi, N.H., Bello, T.K., Isa, M.T., 2023. Perovskite-based nanomaterials for CO2 conversion. In: Nanomaterials for Carbon Dioxide Capture and Conversion Technologies. Elsevier, pp. 181–209.

Sanko, V., Şenocak, A., Tümay, S.O., Orooji, Y., Demirbas, E., Khataee, A., 2022. An electrochemical sensor for detection of trace-level endocrine disruptor bisphenol A using Mo2Ti2AlC3 MAX phase/MWCNT composite modified electrode. Environmental Research 212, 113071.

Saravanakumar, K., Priya, V.S., Balakumar, V., Prabavathi, S.L., Muthuraj, V., 2022. Noble metal nanoparticles (Mx= Ag, Au, Pd) decorated graphitic carbon nitride nanosheets for ultrafast catalytic reduction of anthropogenic pollutant, 4-nitrophenol. Environmental Research 212, 113185.

Shahzad, A., Rasool, K., Miran, W., Nawaz, M., Jang, J., Mahmoud, K.A., Lee, D.S., 2017. Two-dimensional Ti3C2T x MXene nanosheets for efficient copper removal from water. ACS Sustainable Chemistry & Engineering 5 (12), 11481–11488.

Shahzad, A., Nawaz, M., Moztahida, M., Jang, J., Tahir, K., Kim, J., Lim, Y., Vassiliadis, V.S., Woo, S.H., Lee, D.S., 2019. Ti3C2Tx MXene core-shell spheres for ultrahigh removal of mercuric ions. Chemical Engineering Journal 368, 400–408.

Shahzad, A., Moztahida, M., Tahir, K., Kim, B., Jeon, H., Ghani, A.A., Maile, N., Jang, J., Lee, D.S., 2020. Highly effective prussian blue-coated MXene aerogel spheres for selective removal of cesium ions. Journal of Nuclear Materials 539, 152277.

Shahzad, A., Jang, J., Lim, S.-R., Lee, D.S., 2020. Unique selectivity and rapid uptake of molybdenum-disulfide-functionalized MXene nanocomposite for mercury adsorption. Environmental Research 182, 109005.

Shen, Z., Z. Wang, M. Zhang, M. Gao, J. Hu, F. Du, Y. Liu, and H. Pan, A novel solid-solution MXene (Ti0. 5V0. 5) 3C2 with high catalytic activity for hydrogen storage in MgH2. Materialia, 2018. 1: p. 114-120.

Sheth, Y., Dharaskar, S., Chaudhary, V., Khalid, M., Walvekar, R., 2022. Prospects of titanium carbide-based MXene in heavy metal ion and radionuclide adsorption for wastewater remediation: A review. Chemosphere, 133563.

Sinha, A., Ma, K., Zhao, H., 2021. 2D Ti3C2Tx flakes prepared by in-situ HF etchant for simultaneous screening of carbamate pesticides. Journal of Colloid and Interface Science 590, 365–374.

Solangi, N.H., Kumar, J., Mazari, S.A., Ahmed, S., Fatima, N., Mubarak, N.M., 2021. Development of fruit waste derived bio-adsorbents for wastewater treatment: A review. Journal of Hazardous Materials 416, 125848.

Solangi, N.H., Mubarak, N.M., Karri, R.R., Mazari, S.A., Jatoi, A.S., Koduru, J.R., Dehghani, M.H., 2022. MXene-based phase change materials for solar thermal energy storage. Energy Conversion and Management 273, 116432. https://doi.org/10.1016/j.enconman.2022.116432.

Solangi, N.H., Mubarak, N.M., Karri, R.R., Mazari, S.A., Kailasa, S.K., Alfantazi, A., 2023. Applications of advanced MXene-based composite membranes for sustainable water desalination. Chemosphere 314. https://doi.org/10.1016/j.chemosphere.2022.137643.

Solangi, N.H., Karri, R.R., Mubarak, N.M., Mazari, S.A., Jatoi, A.S., Koduru, J.R., 2023. Emerging 2D MXene-based adsorbents for hazardous pollutants removal. Desalination 549. https://doi.org/10.1016/j.desal.2022.116314.

Solangi, N.H., Mubarak, N.M., Karri, R.R., Mazari, S.A., Jatoi, A.S., 2023. Advanced growth of 2D MXene for electrochemical sensors. Environmental Research 222 (2), 115279. https://doi.org/10.1016/j.envres.2023.115279.

Solangi, N.H., Mazari, S.A., Mubarak, N.M., Karri, R.R., Rajamohan, N., Vo, D.-V.-N., 2023. Recent trends in MXene-based material for biomedical applications. Environmental Research 222. https://doi.org/10.1016/j.envres.2023.115337.

Solangi, N.H., Karri, R.R., Mazari, S.A., Mubarak, N.M., Jatoi, A.S., Malafaia, G., Azad, A. K., 2023. MXene as emerging material for photocatalytic degradation of environmental pollutants. Coordination Chemistry Reviews 477. https://doi.org/10.1016/j.ccr.2022.214965.

Solangi, N.H., Karri, R.R., Mubarak, N.M., Mazari, S.A., Azad, A.K., 2023. Emerging 2D MXenes as next-generation materials for energy storage applications. Journal of Energy Storage 70. https://doi.org/10.1016/j.est.2023.108004.

Solangi, N.H., Karri, R.R., Mubarak, N.M., Mazari, S.A., Jatoi, A.S., Koduru, J.R., 2023. Emerging 2D MXene-based adsorbents for hazardous pollutants removal. Desalination 549, 116314.

Solangi, N.H., Mubarak, N.M., Karri, R.R., Mazari, S.A., Koduru, J.R., 2023. Holistic mechanism of graphene oxide and MXene-based membrane for the desalination processes. Desalination 568. https://doi.org/10.1016/j.desal.2023.117035.

Solangi, N.H., Mubarak, N.M., Karri, R.R., Mazari, S.A., Koduru, J.R., 2024. Recent development of graphene and MXene-based nanomaterials for proton exchange membrane fuel cells. International Journal of Hydrogen Energy 73, 905–931. https://doi.org/10.1016/j.ijhydene.2024.06.034.

Solangi, N.H., Karri, R.R., Mubarak, N.M., Mazari, S.A., 2024. Mechanism of polymer composite-based nanomaterial for biomedical applications. Advanced Industrial and Engineering Polymer Research 7 (1), 1–19. https://doi.org/10.1016/j.aiepr.2023.09.002.

Solangi, N.H., Karri, R.R., Mubarak, N.M., Mazari, S.A., 2024. Comparative analysis of the carbon nanotubes and emerging MXene for CO2 capture and storage. Process Safety and Environmental Protection 185, 1012–1037. https://doi.org/10.1016/j.psep.2024.03.050.

Solangi, N.H., Abbas, A., Mubarak, N.M., Karri, R.R., Aleithan, S.H., Kazmi, J., Ahmad, W., Khan, K., 2024. Insight mechanism of MXene for the future generation of highly efficient energy storage device. Materials Today Sustainability 27. https://doi.org/10.1016/j.mtsust.2024.100896.

Song, D., Jiang, X., Li, Y., Lu, X., Luan, S., Wang, Y., Li, Y., Gao, F., 2019. Metal−organic frameworks-derived MnO2/Mn3O4 microcuboids with hierarchically ordered nanosheets and Ti3C2 MXene/Au NPs composites for electrochemical pesticide detection. Journal of Hazardous Materials 373, 367–376.

Su, S., Chen, S., Fan, C., 2018. Recent advances in two-dimensional nanomaterials-based electrochemical sensors for environmental analysis. Green Energy & Environment 3 (2), 97–106.

Sukidpaneenid, S., Chawengkijwanich, C., Pokhum, C., Isobe, T., Opaprakasit, P., Sreearunothai, P., 2023. Multi-function adsorbent-photocatalyst MXene-TiO2 composites for removal of enrofloxacin antibiotic from water. Journal of Environmental Sciences 124, 414–428.

Sumathi, S., Kavipriya, A., 2017. Structural, optical and photocatalytic activity of cerium doped zinc aluminate. Solid State Sciences 65, 52–60.

Sun, B., Tao, F., Huang, Z., Yan, W., Zhang, Y., Dong, X., Wu, Y., Zhou, G., 2021. Ti3C2 MXene-bridged Ag/Ag3PO4 hybrids toward enhanced visible-light-driven photocatalytic activity. Applied Surface Science 535, 147354.

Sun, B., Dong, X., Li, H., Shang, Y., Zhang, Y., Hu, F., Gu, S., Wu, Y., Gao, T., Zhou, G., 2021. Surface charge engineering for two-dimensional Ti2CTx MXene for highly efficient and selective removal of cationic dye from aqueous solution. Separation and Purification Technology 272, 118964.

Sun, Y., Yi, F., Li, R.H., Min, X., Qin, H., Cheng, S.Q., Liu, Y., 2022. Inorganic-Organic Hybrid Membrane Based on Pillararene-Intercalated MXene Nanosheets for Efficient Water Purification. Angewandte Chemie International Edition 61 (14), e202200482.

Sutariya, B., Sargaonkar, A., Raval, H., 2023. Methods of visualizing hydrodynamics and fouling in membrane filtration systems: recent trends. Separation Science and Technology 58 (1), 101–130.

Svoboda, L., Praus, P., Lima, M.J., Sampaio, M.J., Matýsek, D., Ritz, M., Dvorský, R., Faria, J.L., Silva, C.G., 2018. Graphitic carbon nitride nanosheets as highly efficient photocatalysts for phenol degradation under high-power visible LED irradiation. Materials Research Bulletin 100, 322–332.

Taghipour, S., Solangi, N.H., Anjum, A., Hussin, F., Mazari, S.A., Mubarak, N.M., Ataie-Ashtiani, B., Lee, U., Aroua, M.K., Moon, J-H., 2024. Catalytic conversion of CO2 using carbon nitride-based catalysts: Recent advances, opportunities. And Challenges. Coordination Chemistry Reviews 511, 215831.

Tang, Y., Yang, C., Que, W., 2018. A novel two-dimensional accordion-like titanium carbide (MXene) for adsorption of Cr (VI) from aqueous solution. Journal of Advanced Dielectrics 8 (05), 1850035.

Tong, X., Liu, S., Qu, D., Gao, H., Yan, L., Chen, Y., Crittenden, J., 2021. Tannic acid-metal complex modified MXene membrane for contaminants removal from water. Journal of Membrane Science 622, 119042.

Tran, N.M., Ta, Q.T.H., Noh, J.-S., 2021. Unusual synthesis of safflower-shaped TiO2/Ti3C2 heterostructures initiated from two-dimensional Ti3C2 MXene. Applied Surface Science 538, 148023.

Tu, X., Gao, F., Ma, X., Zou, J., Yu, Y., Li, M., Qu, F., Huang, X., Lu, L., 2020. Mxene/carbon nanohorn/β-cyclodextrin-Metal-organic frameworks as high-performance electrochemical sensing platform for sensitive detection of carbendazim pesticide. Journal of Hazardous Materials 396, 122776.

Tunesi, S., Le Dû, D., Gualano, G., Millet, J.-P., Skrahin, A., Bothamley, G., Casas, X., Goletti, D., Lange, C., Musso, M.J.J.o.I., 2022. Co-Administration of Treatment for Rifampicin-Resistant TB and Chronic HCV Infection: A TBnet and ESGMYC Study. 84 (6), 834–872.

Tunesi, M.M., Soomro, R.A., Han, X., Zhu, Q., Wei, Y., Xu, B., 2021. Application of MXenes in environmental remediation technologies. Nano Convergence 8 (1), 1–19.

Umapathi, R., Ghoreishian, S.M., Sonwal, S., Rani, G.M., Huh, Y.S., 2022. Portable electrochemical sensing methodologies for on-site detection of pesticide residues in fruits and vegetables. Coordination Chemistry Reviews 453, 214305.

Umar, W., M.Z. ur Rehman, M. Umair, M.A. Ayub, A. Naeem, M. Rizwan, H. Zia, and R.R. Karri, Use of nanotechnology for wastewater treatment: potential applications, advantages, and limitations, in Sustainable Nanotechnology for Environmental Remediation. 2022, Elsevier. p. 223-272.

Verger, L., C. Xu, V. Natu, H.-M. Cheng, W. Ren, Barsoum, M. Science, Overview of the synthesis of MXenes and other ultrathin 2D transition metal carbides and nitrides. Current Opinion in Solid State and Materials Science 2019. 23(3): p. 149-163.

Wang, F., Bian, Z., Zhang, W., Zheng, L., Zhang, Y., Wang, H., 2023. Fluorine-free MXene Activate Peroxymonosulfate to Remove Tetracyclic Antibiotics. Separation and Purification Technology, 123549.

Wang, R., Cao, H., Yao, C., Peng, C., Qiu, J., Dou, K., Tsidaeva, N., Wang, W., 2023. Construction of alkalized MXene-supported CoFe2O4/CS composites with super-strong adsorption capacity to remove toxic dyes from aqueous solution. Applied Surface Science 624, 157091. https://doi.org/10.1016/j.apsusc.2023.157091.

Wang, C., Cheng, R., Hou, P.-X., Ma, Y., Majeed, A., Wang, X., Liu, C., 2020. MXene-carbon nanotube hybrid membrane for robust recovery of Au from trace-level solution. ACS Applied Materials & Interfaces 12 (38), 43032–43041.

Wang, H., Cui, H., Song, X., Xu, R., Wei, N., Tian, J., Niu, H., 2020. Facile synthesis of heterojunction of MXenes/TiO2 nanoparticles towards enhanced hexavalent chromium removal. Journal of Colloid and Interface Science 561, 46–57.

Wang, X., Li, M., Yang, S., Bai, X., Shan, J., 2022. Self-assembled Ti3C2TX MXene/graphene composite for the electrochemical reduction and detection of p-nitrophenol. Microchemical Journal 179, 107473.

Wang, Y., Ma, S., Wang, L., Jiao, Z., 2019. A novel highly selective and sensitive NH3 gas sensor based on monolayer Hf2CO2. Applied Surface Science 492, 116–124.

Wang, L., Tao, W., Yuan, L., Liu, Z., Huang, Q., Chai, Z., Gibson, J.K., Shi, W., 2017. Rational control of the interlayer space inside two-dimensional titanium carbides for highly efficient uranium removal and imprisonment. Chemical Communications 53 (89), 12084–12087.

Wang, W., Wang, X., Cheng, N., Luo, Y., Lin, Y., Xu, W., Du, D., 2020. Recent advances in nanomaterials-based electrochemical (bio) sensors for pesticides detection. TrAC Trends in Analytical Chemistry 132, 116041.

Wang, S., Wang, L., Li, Z., Zhang, P., Du, K., Yuan, L., Ning, S., Wei, Y., Shi, W., 2021. Highly efficient adsorption and immobilization of U (VI) from aqueous solution by alkalized MXene-supported nanoscale zero-valent iron. Journal of Hazardous Materials 408, 124949.

Wang, S., Wang, F., Jin, Y., Meng, X., Meng, B., Yang, N., Sunarso, J., Liu, S., 2021. Removal of heavy metal cations and co-existing anions in simulated wastewater by two separated hydroxylated MXene membranes under an external voltage. Journal of Membrane Science 638, 119697. https://doi.org/10.1016/j.memsci.2021.119697.

Wang, Q., Xiong, Y., Xu, J., Dong, F., Xiong, Y., 2022. Oxidation-Resistant Cyclodextrin-Encapsulated-MXene/Poly (N-isopropylacrylamide) composite hydrogel as a thermosensitive adsorbent for phenols. Separation and Purification Technology 286, 120506.

Wang, Q., Yu, Z., Zhu, X., Xiang, Q., Chen, H., Pang, Y., 2022. ZIF-67 modified MXene/sepiolite composite membrane for oil–water separation and heavy metal removal. Journal of Industrial and Engineering Chemistry 115, 314–328. https://doi.org/10.1016/j.jiec.2022.08.014.

Wang, L., Yuan, L., Chen, K., Zhang, Y., Deng, Q., Du, S., Huang, Q., Zheng, L., Zhang, J., Chai, Z., 2016. Loading actinides in multilayered structures for nuclear waste treatment: the first case study of uranium capture with vanadium carbide MXene. ACS Applied Materials & Interfaces 8 (25), 16396–16403.

Wen, L., Dong, J., Yang, H., Zhao, J., Hu, Z., Han, H., Hou, C., Luo, X., Huo, D., 2022. A novel electrochemical sensor for simultaneous detection of Cd2+ and Pb2+ by MXene aerogel-CuO/carbon cloth flexible electrode based on oxygen vacancy and bismuth film. Science of the Total Environment 851, 158325.

Wu, Y., Li, X., Yang, Q., Wang, D., Yao, F., Cao, J., Chen, Z., Huang, X., Yang, Y., Li, X., 2020. Mxene-modulated dual-heterojunction generation on a metal-organic framework (MOF) via surface constitution reconstruction for enhanced photocatalytic activity. Chemical Engineering Journal 390, 124519.

Wu, Z., Liang, Y., Yuan, X., Zou, D., Fang, J., Jiang, L., Yang, H., Xiao, Z., 2020. MXene Ti3C2 derived Z–scheme photocatalyst of graphene layers anchored TiO2/g–C3N4 for visible light photocatalytic degradation of refractory organic pollutants. Chemical Engineering Journal 394, 124921.

Wu, Z., Liang, Y., Yuan, X., Zou, D., Fang, J., Jiang, L., Zhang, J., Yang, H., Xiao, Z., 2020. MXene Ti3C2 derived Z–scheme photocatalyst of graphene layers anchored TiO2/g–C3N4 for visible light photocatalytic degradation of refractory organic pollutants. Chemical Engineering Journal 394, 124921. https://doi.org/10.1016/j.cej.2020.124921.

Wu, X., Zhao, Q., Zhang, J., Li, S., Liu, H., Liu, K., Li, Y., Kong, D., Sun, H., Wu, M., 2023. 0D carbon dots intercalated Z-scheme CuO/g-C3N4 heterojunction with dual charge transfer pathways for synergetic visible-light-driven photo-Fenton-like catalysis. Journal of Colloid and Interface Science 634, 972–982.

Xiang, J., Wang, X., Ding, M., Tang, X., Zhang, S., Zhang, X., Xie, Z., 2022. The role of lateral size of MXene nanosheets in membrane filtration of dyeing wastewater: Membrane characteristic and performance. Chemosphere 294, 133728.

Xiao, B., Li, Y.-C., Yu, X.-F., Cheng, J.-B., 2016. MXenes: Reusable materials for NH3 sensor or capturer by controlling the charge injection. Sensors and Actuators b: Chemical 235, 103–109.

Xie, L., Yan, J., Liu, Z., Wen, H., Liu, P., Liu, H., 2022. Synthesis of a Two-Dimensional MXene Modified by Chloroacetic Acid and Its Adsorption of Uranium. ChemistrySelect 7 (1), e202103583.

Xu, L., Chen, Y., Su, W., Cui, J., Wei, S., 2023. Synergistic adsorption of U (VI) from seawater by MXene and amidoxime mixed matrix membrane with high efficiency. Separation and Purification Technology 309, 123024.

Xu, T., Wei, J., He, P., Wu, J., Chen, N., Shi, E., Pan, C., Zhao, X., Zhang, Y., 2022. CuS-doped Ti3C2 MXene nanosheets for highly efficient adsorption of elemental mercury in flue gas. Energy & Fuels 36 (5), 2503–2514.

Yan, Y., Han, H., Dai, Y., Zhu, H., Liu, W., Tang, X., Gan, W., Li, H., 2021. Nb2CT x MXene Nanosheets for Dye Adsorption. ACS Applied Nano Materials 4 (11), 11763–11769.

Yan, J., Liu, H.J., Xie, L., Liu, Z., Liu, P.F., Wen, H.X., 2022. Europium (III) removal from aqueous solution using citric acid modified alkalized Mxene as an adsorbent. Journal of Radioanalytical and Nuclear Chemistry 331 (2), 1063–1073.

Yang, G., Hu, X., Liang, J., Huang, Q., Dou, J., Tian, J., Deng, F., Liu, M., Zhang, X., Wei, Y., 2021. Surface functionalization of MXene with chitosan through in-situ formation of polyimidazoles and its adsorption properties. Journal of Hazardous Materials 419, 126220.

Yao, J., Chen, H., Jiang, F., Jiao, Z., Jin, M., 2017. Titanium dioxide and cadmium sulfide co-sensitized graphitic carbon nitride nanosheets composite photocatalysts with superior performance in phenol degradation under visible-light irradiation. Journal of Colloid and Interface Science 490, 154–162.

Yao, Z., Sun, H., Sui, H., Liu, X., 2020. Construction of BPQDs/Ti3C2@ TiO2 composites with favorable charge transfer channels for enhanced photocatalytic activity under visible light irradiation. Nanomaterials 10 (3), 452.

Yi, X., Yuan, J., Tang, H., Du, Y., Hassan, B., Yin, K., Chen, Y., Liu, X., 2020. Embedding few-layer Ti3C2Tx into alkalized g-C3N4 nanosheets for efficient photocatalytic degradation. Journal of Colloid and Interface Science 571, 297–306.

Yu, K., Jiang, P., Wei, J., Yuan, H., Xin, Y., He, R., Wang, L., Zhu, W., 2022. Enhanced uranium photoreduction on Ti3C2Tx MXene by modulation of surface functional groups and deposition of plasmonic metal nanoparticles. Journal of Hazardous Materials 426, 127823.

Yu, X.-F., Li, Y.-C., Cheng, J.-B., Liu, Z.-B., Li, Q.-Z., Li, W.-Z., Yang, X., Xiao, B., 2015. Monolayer Ti2CO2: a promising candidate for NH3 sensor or capturer with high sensitivity and selectivity. ACS Applied Materials & Interfaces 7 (24), 13707–13713.

Yu, T., Li, S., Zhang, L., Li, F., Wang, J., Pan, H., Zhang, D., 2023. In situ growth of ZIF-67-derived nickel-cobalt-manganese hydroxides on 2D V2CTx MXene for dual-functional orientation as high-performance asymmetric supercapacitor and electrochemical hydroquinone sensor. Journal of Colloid and Interface Science 629, 546–558.

Yu, S., Wang, X., Tan, X., Wang, X., 2015. Sorption of radionuclides from aqueous systems onto graphene oxide-based materials: a review. Inorganic Chemistry Frontiers 2 (7), 593–612. https://doi.org/10.1039/c4qi00221k.

Yu, S., Wei, D., Shi, L., Ai, Y., Zhang, P., Wang, X., 2019. Three-dimensional graphene/titanium dioxide composite for enhanced U (VI) capture: insights from batch experiments, XPS spectroscopy and DFT calculation. Environmental Pollution 251, 975–983.

Yue, R., Sun, X., 2021. A Self-cleaning, catalytic titanium carbide (MXene) membrane for efficient tetracycline degradation through peroxymonosulfate activation: Performance evaluation and mechanism study. Separation and Purification Technology 279, 119796.

Zhan, X., Si, C., Zhou, J., Sun, Z., 2020. MXene and MXene-based composites: synthesis, properties and environment-related applications. Nanoscale Horizons 5 (2), 235–258.

Zhang, X., Gu, P., Liu, Y., 2019. Decontamination of radioactive wastewater: State of the art and challenges forward. Chemosphere 215, 543–553.

Zhang, H., Guo, L.-H., Zhao, L., Wan, B., Yang, Y., 2015. Switching oxygen reduction pathway by exfoliating graphitic carbon nitride for enhanced photocatalytic phenol degradation. The Journal of Physical Chemistry Letters 6 (6), 958–963.

Zhang, Y.-J., Lan, J.-H., Wang, L., Wu, Q.-Y., Wang, C.-Z., Bo, T., Chai, Z.-F., Shi, W.-Q., 2016. Adsorption of uranyl species on hydroxylated titanium carbide nanosheet: A first-principles study. Journal of Hazardous Materials 308, 402–410.

Zhang, C., Li, C., Chen, G., Ji, F., Shen, Y., Peng, J., Zhang, J., 2021. In situ synthesis of a hybrid Fe (Co)/MXene/ZSM-5 catalyst for phenol abatement. New Journal of Chemistry 45 (36), 16862–16871.

Zhang, S., Liao, S., Qi, F., Liu, R., Xiao, T., Hu, J., Li, K., Wang, R., Min, Y., 2020. Direct deposition of two-dimensional MXene nanosheets on commercially available filter for fast and efficient dye removal. Journal of Hazardous Materials 384, 121367.

Zhang, D., Liu, L., Zhao, B., Wang, X., Pang, H., Yu, S., 2023. Highly efficient extraction of uranium from seawater by polyamide and amidoxime co-functionalized MXene. Environmental Pollution 317, 120826.

Zhang, Y., Wang, L., Zhang, N., Zhou, Z., 2018. Adsorptive environmental applications of MXene nanomaterials: a review. RSC Advances 8 (36), 19895–19905.

Zhang, X., Zhang, Z., Li, J., Zhao, X., Wu, D., Zhou, Z., 2017. Ti2CO2 MXene: a highly active and selective photocatalyst for CO2 reduction. Journal of Materials Chemistry A 5 (25), 12899–12903.

Zhang, X., Sun, H., Huang, J., Zheng, Q., Zhang, F., Li, H., Zhang, M., Zeng, J., Yan, Z., 2022. Alkalized MXene-supported nanoscale zero-valent iron in situ derived from NH2-MIL-88B (Fe) for the highly efficient catalytic reduction of 4-nitrophenol. Materials Today Sustainability 18, 100145.

Zhang, H., Tian, L., Han, J., Wei, Z., Wu, Z., Zhu, Y., Guo, Q., Tang, Y., Cao, Y., Zhang, Z. J.C., Physicochemical, S.A., Aspects, E., 2024:. Insights into the PMS Activation towards Phenol Removal Mechanism by a Ti3C2-MXene Doped BiVO4 Photocatalyst. Colloids and Surfaces A: Physicochemical and Engineering Aspects 698,, 134561.

Zhang, P., Wang, L., Du, K., Wang, S., Huang, Z., Yuan, L., Li, Z., Wang, H., Zheng, L., Chai, Z., 2020. Effective removal of U (VI) and Eu (III) by carboxyl functionalized MXene nanosheets. Journal of Hazardous Materials 396, 122731. https://doi.org/10.1016/j.jhazmat.2020.122731.

Zhang, G., Wang, T., Xu, Z., Liu, M., Shen, C., Meng, Q., 2020. Synthesis of amino-functionalized Ti 3 C 2 T x MXene by alkalization-grafting modification for efficient lead adsorption. Chemical Communications 56 (76), 11283–11286.

Zhang, K.-N., Wang, C.-Z., Lü, Q.-F., Chen, M.-H., 2022. Enzymatic hydrolysis lignin functionalized Ti3C2Tx nanosheets for effective removal of MB and Cu2+ ions. International Journal of Biological Macromolecules 209, 680–691.

Zhang, H., Zhao, L., Geng, F., Guo, L.-H., Wan, B., Yang, Y., 2016. Carbon dots decorated graphitic carbon nitride as an efficient metal-free photocatalyst for phenol degradation. Applied Catalysis b: Environmental 180, 656–662.

Zhao, D., Cai, C., 2020. Preparation of Bi 2 MoO 6/Ti 3 C 2 MXene heterojunction photocatalysts for fast tetracycline degradation and Cr (vi) reduction. Inorganic Chemistry Frontiers 7 (15), 2799–2808.

Zhao, S., Wang, R., Tian, T., Liu, H., Zhang, H., Tang, H., 2022. Self-Assembly-Cooperating in Situ Construction of MXene–CeO2 as Hybrid Membrane Coating for Durable and High-Performance Proton Exchange Membrane Fuel Cell. ACS Sustainable Chemistry & Engineering 10 (13), 4269–4278. https://doi.org/10.1021/acssuschemeng.2c00087.

Zhao, Y., Zhang, P., Liang, J., Xia, X., Ren, L., Song, L., Liu, W., Sun, X.J.A.M., 2022. Unlocking Layered Double Hydroxide as a High-Performance Cathode Material for Aqueous Zinc-Ion Batteries. 34 (37), 2204320.

Zhong, W., Gao, F., Zou, J., Liu, S., Li, M., Gao, Y., Yu, Y., Wang, X., Lu, L., 2021. MXene@ Ag-based ratiometric electrochemical sensing strategy for effective detection of carbendazim in vegetable samples. Food Chemistry 360, 130006.

Zhong, Q., Li, Y., Zhang, G., 2021. Two-dimensional MXene-based and MXene-derived photocatalysts: Recent developments and perspectives. Chemical Engineering Journal 409, 128099.

Zhong, W., Zou, J., Xie, Y., Yang, J., Li, M., Liu, S., Gao, Y., Wang, X., Lu, L., 2022. Three-dimensional nano-CuXO-MWCNTs-COOH/MXene heterostructure: An efficient electrochemical platform for highly sensitive and selective sensing of benomyl in fruit samples. Journal of Electroanalytical Chemistry 920, 116586.

Zhong, W., Zou, J., Yu, Q., Gao, Y., Qu, F., Liu, S., Zhou, H., Lu, L., 2023. Ultrasensitive indirect electrochemical sensing of thiabendazole in fruit and water by the anodic stripping voltammetry of Cu2+ with hierarchical Ti3C2Tx-TiO2 for signal amplification. Food Chemistry 402, 134379.

Zhu, X., Liu, B., Hou, H., Huang, Z., Zeinu, K.M., Huang, L., Yuan, X., Guo, D., Hu, J., Yang, J., 2017. Alkaline intercalation of Ti3C2 MXene for simultaneous electrochemical detection of Cd (II), Pb (II), Cu (II) and Hg (II). Electrochimica Acta 248, 46–57.

Zou, X., Zhao, X., Zhang, J., Lv, W., Qiu, L., Zhang, Z., 2021. Photocatalytic degradation of ranitidine and reduction of nitrosamine dimethylamine formation potential over MXene–Ti3C2/MoS2 under visible light irradiation. Journal of Hazardous Materials 413, 125424.